The Integrated Tile Concept in Space-Based Solar Power: Addressing Thermal and Energy Challenges

MSc Space Engineering

Ludovica Castronovo

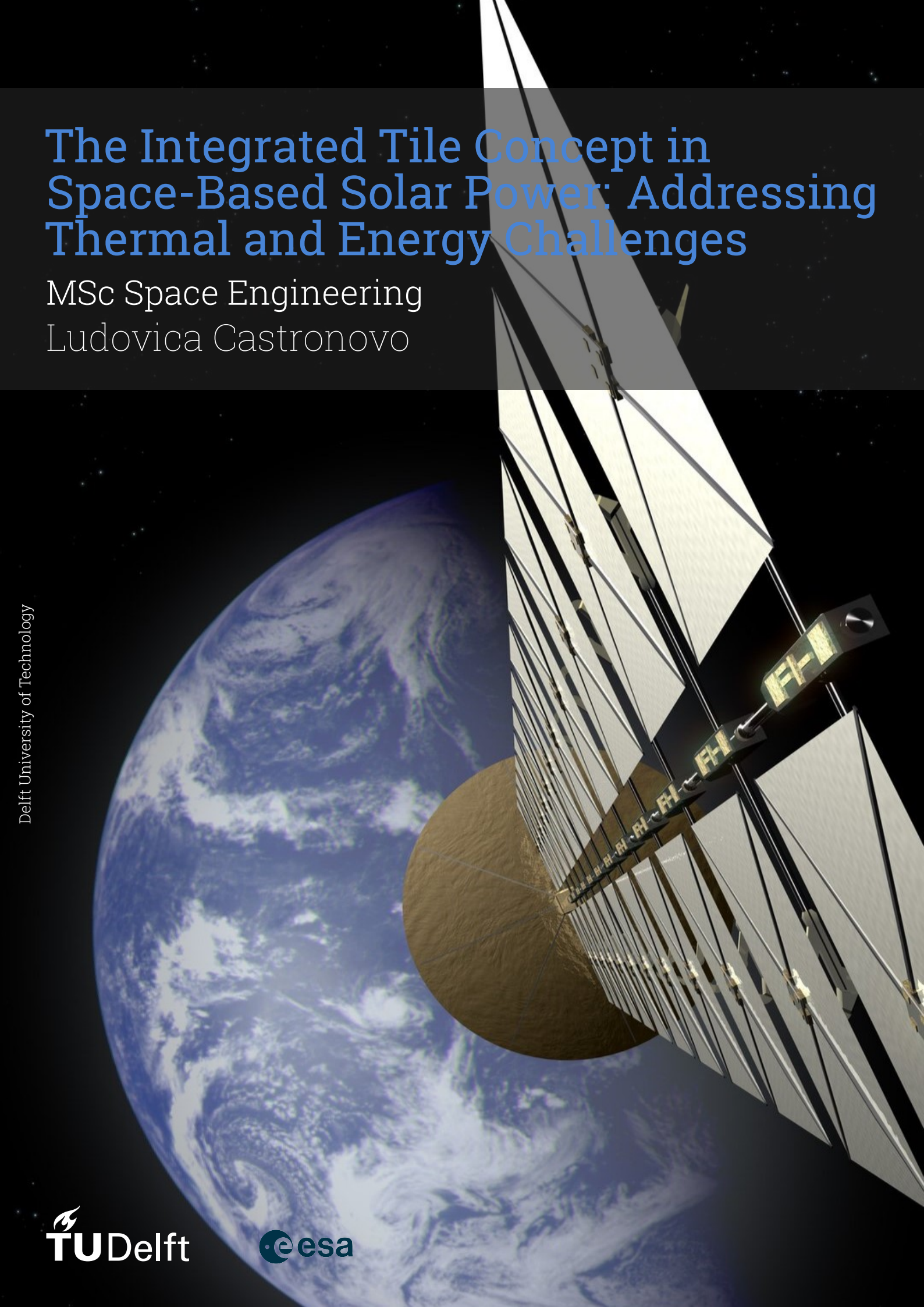

Delft University of Technology

TU Delft

esa

The Integrated Tile Concept in Space-Based Solar Power: Addressing Thermal and Energy Challenges

by

Ludovica Castronovo

Student Name	Student Number
Ludovica Castronovo	5763606

Instructor:	Dr. Angelo Cervone
Company Supervisor:	Dr. Sebastien Vincent-Bonnieu
Project Duration:	May, 2024 - April, 2025
Faculty:	Faculty of Aerospace Engineering, Delft
Company:	European Space Agency (ESA)

Style: TU Delft Report Style, with modifications by Daan Zwaneveld

TU Delft

Summary

This thesis investigates the energetic feasibility of Space-Based Solar Power (SBSP) systems by conducting a comprehensive Net Energy Analysis (NEA). While SBSP has gained renewed interest due to technological advancements and increasing global energy demands, its energetic performance remains largely underexplored. This work aims to fill that gap by assessing whether SBSP architectures can deliver a net energy surplus over their lifetime and how they compare to terrestrial photovoltaic solutions.

The analysis is carried out through a cradle-to-gate framework, considering all major energy inputs: raw material extraction, manufacturing, transportation, and launch to Geostationary Earth Orbit (GEO). The energy output is estimated based on system efficiency and degradation over a 30-year operational lifetime, accounting for eclipse-related downtimes.

A complete MATLAB-based parametric model is developed to evaluate different SBSP configurations. A specific case study is selected, based on an integrated modular concept with reflective concentration and microwave wireless power transmission. The system is fully dimensioned starting from the requirement to deliver 1 GW of continuous power to the grid, and all subsystems, including structural, power collection, and transmission components, are sized accordingly. Using Starship as the launch vehicle, the reference scenario yields an EROEI of 28.01 and an EPBT of 1.07 years. In comparison, a terrestrial multi-junction PV plant delivers an EROEI of 12.6.

To assess the robustness of these results, a sensitivity analysis is conducted on key parameters such as photovoltaic efficiency, wireless power transmission efficiency, system lifetime, degradation factor, and propulsion performance. Results indicate that the system lifetime and degradation rate have the highest influence on energy performance. Notably, even when using more conservative assumptions, such as lower efficiencies for PV and WPT, the SBSP case study still remains energetically competitive with respect to terrestrial solutions.

Nonetheless, several assumptions remain, especially regarding the simplification of subsystems. For this reason, this work also introduces a detailed thermal analysis, aimed at integrating the energetic cost of thermal control within the overall NEA framework. A dedicated sizing methodology is implemented to estimate the required radiator surface to maintain safe operating temperatures for all components, based on physical heat balance equations. This enables a progressive inclusion of thermal control contributions into the model. The methodology is developed within MATLAB and validated using key concepts and design practices typically implemented in professional thermal analysis software such as ESATAN-TMS. This step contributes to building a more realistic and complete energy assessment of SBSP architectures, and opens the path to progressively include additional subsystems such as power management, attitude control, and servicing in future work.

Contents

Nomenclature

Abbreviations

Abbreviation	Definition
ACT	Advanced Cooling Technologies
ADR	Active Debris Removal
AFRL	Air Force Research Laboratory
BOL	Beginning-of-Life
BOS	Balance of System
CCHP	Constant Conductivity Heat Pipes
CFRP	Carbon Fiber Reinforced Polymer
CPV	Concentrated Photovoltaics
CW	Continuous Wave
DC	Direct Current
DC-RF	Direct Current to Radio Frequency
DOE	Department of Energy
ELSA-d	End-of-Life Service
EPBT	Energy Payback Time
EROEI	Energy Return On Energy Investments
ESA	European Space Agency
ETB	Effective Temperature of the Beam
GEO	Geostationary Earth Orbit
GHG	Greenhouse Gas
GHI	Global Horizontal Irradiation
GPS	Ground Power Station
GTO	Geostationary Transfer Orbit
HLLV	Heavy-Lift Launch Vehicle
IOS	In Orbit Servicing
IEA	International Energy Agency
ISC	Integrated Symmetrical Concentrator
ISAM	In-space Servicing, Assembly, and Maintenance
ISS	International Space Station
ISP	Specific Impulse
JAXA	Japan Aerospace Exploration Agency
LEO	Low-Earth Orbit

Abbreviation	Definition
MEO	Medium-Earth Orbit
MRV	Mission Robotic Vehicle
MSC	Modular Symmetrical Concentrator
NASA	National Aeronautics and Space Administration
NEA	Net Energy Analysis
PMAD	Power Management and Distribution
PV	Photovoltaic
RE	Radiating Elements
RF	Radio Frequency
R/P	Reserve-to-Product
RPO	Rendezvous and Proximity Operations
SBSP	Space-Based Solar Power
SPS	Solar Power Satellite
SSPA	Solid State Power Amplifiers
SSPIDR	Space Solar Power Initiative and Demonstration Roadmap
TMS	Thermal Modeling System (used in ESATAN-TMS)
TRL	Technology Readiness Level
WPT	Wireless Power Transmission

Symbols

Symbol	Definition	Unit
CO_2	Carbon dioxide	–
$\approx$	Approximately (used for estimation)	–
TWh	Terawatt-hour, unit of energy	[TWh]
GW	Gigawatt, unit of power	[GW]
MW	Megawatt, unit of power	[MW]
kg	Kilogram, unit of mass	[kg]
km	Kilometre, unit of distance	[km]
GHz	Gigahertz, unit of frequency	[GHz]
A	Surface area	[m^2]
η_{sys}	Cumulative system efficiency	–
η_{pv}	Photovoltaic collection efficiency	–
η_{wpt}	Wireless power transmission efficiency	–
η_{gnd}	Ground conversion efficiency	–
η_{tot}	Total system efficiency	–
d	Annual degradation factor	–
N	System lifetime	[years]
t	Time (operational year index)	[years]
GHI	Global Horizontal Irradiation	[kWh/m^2/year]
E_0	Initial energy output	[MW]
T	Operational hours per year	[h/year]
E_{total}	Total energy output over lifetime	[GWh]

Symbol	Definition	Unit
E_{in}	Total energy input	[GWh]
$E_{\text{in, launch}}$	Energy input from launches	[GWh]
$E_{\text{in, orb}}$	Energy input from orbital transfer	[GWh]
$E_{\text{in, total}}$	Sum of all energy input contributions	[GWh]
E_{out}	Total energy output delivered to grid	[GWh]
$E_{\text{out, yearly}}$	Yearly average energy output	[GWh/year]
EROEI	Energy Return On Energy Investment	–
EPBT	Energy Payback Time	[years]
ΔV	Required orbital velocity increment	[m/s]
V	Velocity	[m/s]
Δi	Inclination change	[rad]
ρ	Density	[kg/m^3]
m_0	Initial launch mass	[t]
m_{prop}	Propellant mass	[t]
n_{launch}	Number of launches	–
m_{pv}	Mass of PV system	[t]
m_{wpt}	Mass of WPT subsystem	[t]
m_{str}	Mass of structural subsystem	[t]
m_{refl}	Mass of reflectors	[t]
m_{glass}	Mass of protective glass	[t]
m_{hb}	Mass of hexbus tiles	[t]
m_{tot}	Total system mass	[t]
Isp	Specific impulse	[s]

List of Figures

List of Tables

1

Introduction

1.1. Background and Problem Statement

The increasing global energy demand and the urgency to reduce greenhouse gas (GHG) emissions have made the transition to sustainable energy sources a critical priority. While fossil fuels remain the dominant energy source, their finite nature and environmental impact make them unsuitable for long-term energy security. Renewable energy sources such as solar, wind, and hydropower offer a low-carbon alternative, but their efficiency and capacity limitations, along with intermittency issues, question their ability to fully replace fossil fuels. In this context, Space-Based Solar Power (SBSP) emerges as a promising alternative, capable of providing continuous and predictable solar energy without being strongly affected by the Earth's atmosphere, seasonal variations, or the day-night cycle. With advancements in launch systems, wireless power transmission, and modular satellite architectures, SBSP is increasingly seen as a viable technology that could play a key role in achieving global energy goals. Although SBSP is a promising solution to the global energy challenge and an interesting subject for further exploration, it presents significant challenges, which can be broadly categorized into three areas: technical, economic, and energetic. From a technical perspective, many of the technologies required for the mission have a very low Technology Readiness Level (TRL) and require further development. Economic challenges primarily relate to the high costs associated with mission operations, including launches, production, and decommissioning, raising concerns about the cost competitiveness of space-based solutions.

However, while research efforts have largely focused on the technical and economic aspects of SBSP, there remains a significant gap in the literature regarding its energetic feasibility and efficiency. When excluding cost considerations, the key metrics for assessing the viability of SBSP projects are related to energy performance, which is crucial for evaluating whether SBSP is a more efficient alternative to terrestrial solar power.

One of the primary objections to SBSP is the concern that it may not offer a significant advantage over ground-based solar power plants. To address this, a comparative study from an energetic perspective is necessary, evaluating the energy inputs and outputs of both systems. The first objective of this study is to contribute to addressing this research gap by assessing the energetic performance of SBSP.

Moreover, at the core of the challenges surrounding SBSP is the impracticality of its large-scale deployment, given the immense size and weight of the system. With structures spanning several square kilometers, the complexity of launch, assembly, and deployment remains a major barrier.

An innovative concept that aims to address some of these issues is the sandwich module, or integrated tile, which consolidates the system's main functions within a single modular tile. This approach enhances modularity, optimizes launch packaging, and reduces mass and structural complexity. However, despite its potential advantages, this concept remains largely unexplored and presents a significant thermal management challenge, which has been largely overlooked in the literature.

Given its potential, this study places the integrated tile concept at the center of the analysis, incorporating it into energy assessments and conducting a detailed thermal study to evaluate its reliability in terms of energetic performance.

Despite its potential, SBSP still faces unresolved questions that prevent its advancement beyond the conceptual stage. In particular, there is a lack of comprehensive studies assessing whether it can outperform terrestrial solar technologies from an energy point of view, especially when considering realistic operational constraints. At the same time, while modular solutions like the integrated tile offer promising advantages in terms of mass, scalability, and packaging, their thermal behavior and overall feasibility remain largely unexplored.

This thesis aims to contribute to addressing these gaps by evaluating the energetic performance of SBSP systems in comparison to terrestrial alternatives and by using the integrated tile architecture as a case study to explore its potential and limitations.

2

Literature Review

In this chapter, a comprehensive literature review is conducted to define the project's context and address specific systems pertinent to the thesis. Following the background and motivation presented in chapter 1, this literature study is structured around clear objectives and guiding research questions, which provide the foundation for the development of the subsequent phases of the work. This review represents a critical step in formulating the overall research questions and research plan of the thesis.

The objectives of this literature review are as follows:

- Define the broader context in which the project of Space-Based Solar Power (SBSP) operates, outlining the motivations for its adoption as a potential solution to global energy challenges.
- Explore the historical evolution and recent advancements in SBSP technologies, with a focus on satellite architectures and their subsystems.
- Analyze the main subsystems that constitute a space solar satellite, identifying their most critical performance drivers and integration challenges.
- Develop a comprehensive understanding of the Integrated Tile concept, including its modular role within SBSP architectures, functional layout, enabling technologies, and unresolved technical limitations.

Based on these objectives, the chapter is guided by the following research questions:

1. What is the context in which Space-Based Solar Power (SBSP) operates, and which of its features make it unique among the diverse solutions for global energy supply?
2. What is the current state of development of space-based solar power concepts, and what are the main limitations and risks associated with their implementation? Among those concepts and applications, which specific mission is selected to be the case study?
3. What are the key subsystems of SBSP satellites, and which technologies present the most critical challenges in terms of performance, integration, and feasibility?
4. Which subsystem technologies are the most critical in terms of performance and integration challenges within a modular SBSP architecture?
5. What broader potentials and future applications could SBSP enable beyond its primary role in terrestrial energy supply?

The review begins by contextualizing space-based solar power (SBSP) as a promising solution to global energy challenges, highlighting its advantages over terrestrial alternatives and presenting its risks. This is followed by an overview of the historical development of SBSP concepts, from early proposals to recent initiatives and demonstrator projects, with a focus on how advances in launch systems, modularity, and in-space assembly have reshaped current approaches.

The chapter then provides a detailed analysis of the primary satellite subsystems that constitute an SBSP architecture, including solar energy collection, conversion, thermal management, and wireless power transmission. Special attention is given to the integrated and modular design approach exemplified by the Integrated Tile concept, which is discussed as a key architectural reference.

Finally, the review identifies critical knowledge gaps and areas of technological uncertainty that affect the feasibility and optimization of SBSP systems.

The literature review not only summarizes the current state of the art but also helps define and guide the research strategy for the rest of the thesis.

2.1. Global Energy Challenges and the role of Space Based Solar Power

In recent decades, the quest to meet energy needs and reduce green house gases (GHGs) emissions has become of utmost relevance on a global scale. The most widely used energy sources worldwide are fossil fuels, such as coal, oil, and natural gas; however, being non-renewable sources of energy, the use of fossil fuels represents a significant risk for maintaining livable conditions on Earth in the long term.
Although they have been the primary source of energy for many years, due to their high energy content and availability, characteristics such as their high environmental impact and finite nature make them unsuitable for continuously meeting global energy demands and emissions requirements.
Figure 2.1 shows the global use of fossil fuels, measured in TWh of primary energy consumption, from 1900 to 2022; it is clear from the graph that fossil fuels consumption has experienced a more significant rise in the last decades, linked to the increasing energy demands [86].

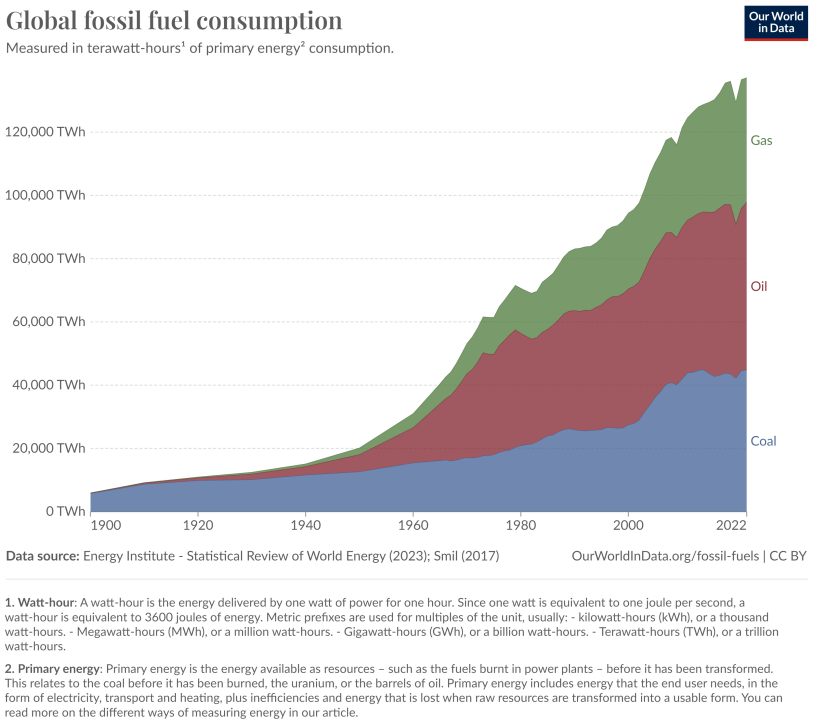

Figure 2.1: Global fossil fuel consumption, from 1900 to 2022 [86]

The Energy Institute published a prevision of the years of fossil fuel reserve left [103], reported as

the reserve-to-product ratio [1] and based on the production and consumption levels in year 2020; the respective output is depicted in Figure 2.2, from which it is clear how the limited supply of fossil fuels is a key factor why they cannot remain our principal energy source permanently.
Furthermore, the Global Carbon Project ([42]) finds that in 2021 91 % of GHG emissions came from fossil fuels, thus enhancing their impact on climate change issues ([37]).

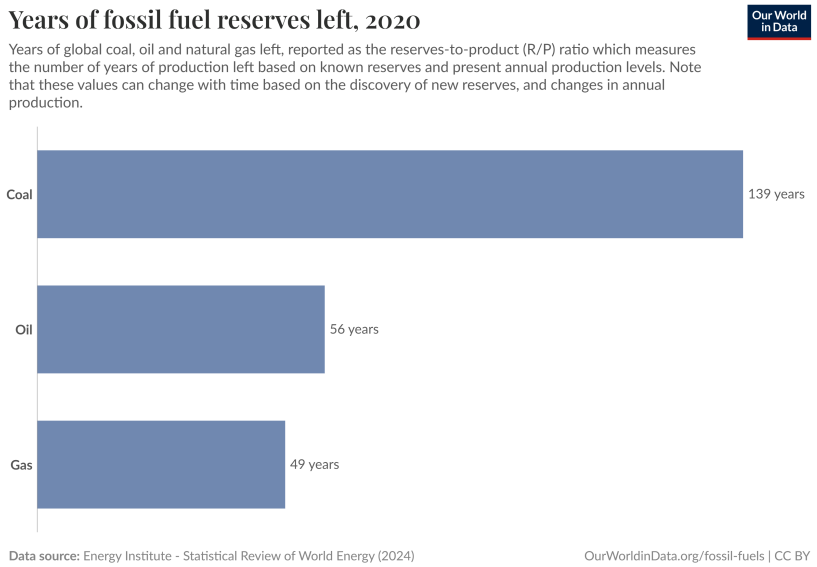

Figure 2.2: Years of fossil fuel reserves left, 2020 [103]

In contrast to fossil fuels, nuclear and renewable energy sources—such as hydropower, solar, wind, geothermal, wave, tidal, and modern biofuels—offer a low-carbon alternative and a powerful means to decarbonize energy production. While electricity is the primary focus, the energy mix also includes transport and heating, though these are more challenging to decarbonize [87]. Figure 2.3 illustrates the global energy consumption by source from 1965 to 2022, highlighting the significant increase and efforts in utilizing renewable energy sources over the past decade.

[1] The reserve-to-product (R/P) ratio defines the number of years of production left based on annual reserves and production levels [103]

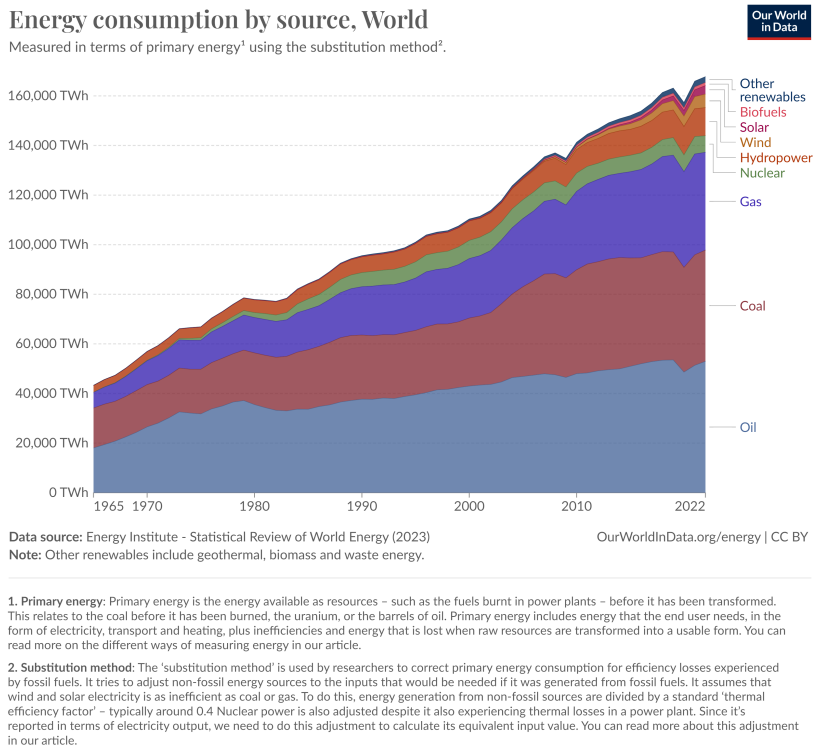

Figure 2.3: Evolution of global energy consumption by source, from 1965 to 2022 [85]

There is a global interest and effort in the use of green energy, embodied in the Net Zero by 2050 project, which has been signed by all countries in the International Energy Agency (IEA). The mission is to achieve a global energy framework with zero carbon emissions by 2050. To this end, various pathways are analyzed based on the current situation and future expectations [72]. One of the most significant findings from the IEA's studies is the forecast of energy demands for the coming decades. As shown in Figure 2.4, global electricity demand is projected to increase by 80% from 2020 to 2050. This forecast graph from the IEA highlights the expected increase in the use of renewable sources. Notably, the roadmap predicts that solar photovoltaics and wind energy will contribute around 50% to the growth in renewable supplies [72].

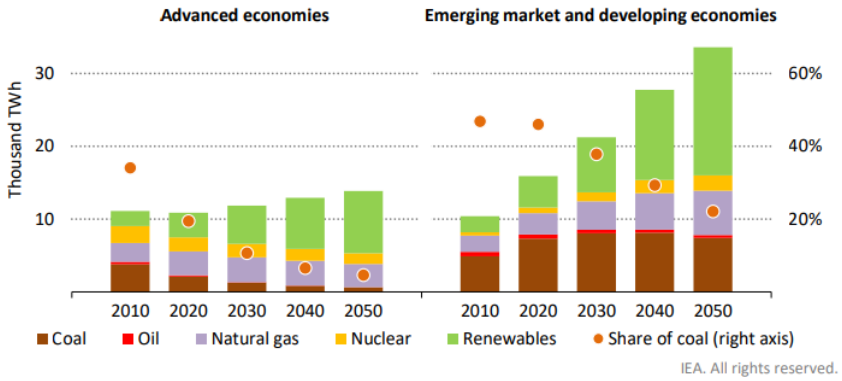

Figure 2.4: Expected levels of energy demand from various supply sources from IEA forecasts [72]

However, although the rising demand for renewable sources, the demand for non-renewable sources remains stable, thus not decreasing at a comparable rate. Despite their unlimited availability, conventional renewable sources (e.g., terrestrial solar PV technologies) are limited in efficiency and generating capacity. Therefore, their use alone might be insufficient to offset the reliance on non-renewable en-

ergy sources and achieve the net zero goal [5].
With these expectations and goals, a new kind of energy supply is strongly needed globally, with the fundamental requirements of being renewable, stable, flexible, and secure.
Space-based solar power has the potential to surpass the limitations of its terrestrial analog. By delivering solar energy from space, this technology can consistently provide clean, baseload energy, regardless of the Earth's location, season, or time of day. Nonetheless, it presents its risks and challenges.

2.1.1. Advantages of Space-Based Solar Power: A Comparison with Other Alternatives

Space-based solar power (SBSP) solutions have been contemplated since the mid to late 1900s and are seen as a promising contribution to solving the current global energy challenge, both in terms of low energy supply and high demand, as well as greenhouse gas emissions.
The current increasing interest in this project stems from recent advances in launch systems and more generally in technology, which have made SBSP more economically affordable and, despite its challenges, technologically feasible.
IEA's Net Zero Emission scenario [72] projects global electricity supply for the next 30 years, as depicted in Figure 2.5.

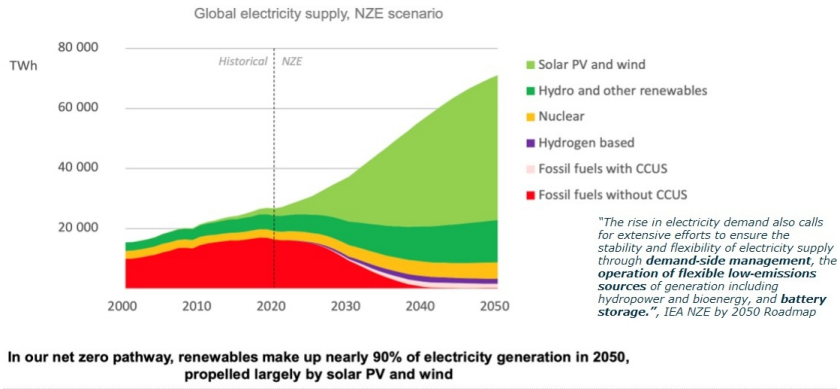

Figure 2.5: NZE scenario, global electricity supply [72]

In this pathway, 90 % of electricity generation is supplied by renewable sources, mostly solar PV and wind [72]. However, terrestrial PV technologies and wind energy are highly dependent on unpredictable natural variables, and would most likely create a supply gap given the predicted increase in energy demands, thus needing complex and big storage systems to provide the required energy.
Among other renewables, hydropower's large-scale operation is limited by its reliance on territorial conditions (altitude) [2]. Therefore, as mentioned in section 2.1, achieving the net zero target for 2050 is a significant challenge if only ground-based renewables are to be used.

In contrast, a space-based solar power system operating in orbit above the Earth's atmosphere would receive a continuous and predictable solar flux, undisturbed by the obscurations and variations in sunlight and the dependence on day-night cycles and weather conditions, thus providing a 24/7 base-load power source, approximately one order of magnitude higher than that of ground-based photovoltaic technologies currently implemented on Earth [2]. While the collected energy still needs to be transmitted to the ground—typically via radio frequency (RF) beams—it is worth noting that by selecting transmission frequencies below 10 GHz, atmospheric attenuation effects become minimal. This ensures high transmission reliability under most conditions, preserving the base-load nature of the power supply.

Another unique advantage of SBSP is that the energy can be transmitted wirelessly at frequencies that are almost transparent to the Earth's atmosphere, minimizing transmission losses due to atmospheric gases absorption. Finally, if the mission architecture allows for several receiving antennas to be placed

at different locations on Earth, the beam transmission could change from one place to another in a matter of minutes.

Space-based solar power could also offers an alternative to nuclear power. While nuclear power is currently one of the cleanest sources of energy with among the lowest greenhouse gas emissions, it presents significant downsides. The main public concerns regarding nuclear plants involve safety, nuclear weapon proliferation, and hazardous waste management. Unlike nuclear power plants, SBSP will not produce hazardous waste that needs to be stored and guarded for hundreds of years [100] and will not need fresh water consumption [124].
Moreover, with the latest advancements in space technology, SBSP could be competitive from a cost perspective compared to nuclear power [78]. Therefore, it could offer an alternative option for nations to limit or avoid future expansion of nuclear fission power to provide low-carbon energy.
Power beaming on Earth does not have to be seen just as a replacement for terrestrial renewable power sources, but more as a fundamental support to achieve the preset goals [1].

2.1.2. Other benefits of SBSP

Besides the pivotal contribution that Space-Based Solar Power (SBSP) can make in achieving the Net Zero goal by 2050, its development would bring numerous other advantages. A solar power station in orbit would enable the delivery of power to remote areas of the planet, where it is difficult to connect or distribute energy from terrestrial plants.
The implementation of such systems, along with the associated technologies required to deploy a solar power satellite, will lead to a technological and scientific revolution, not only within the space industry but also resulting in broader benefits.

The indirect impacts that research and development in the field of space-based solar power will have on other areas are referred to as 'spillover benefits'
Other terrestrial and space applications will benefit from the advancements in semiconductor and photovoltaic technologies driven by the development of SBSP. The ability to transmit high levels of power over long distances will impact several markets.
In addition to revolutionizing the space industry, researching and developing systems for autonomous robotic assembly will mitigate high risks in hazardous terrestrial environments. Finally, space-based solar power could facilitate international collaboration for shared energy generation and distribution to difficult geographic areas [99].

2.2. SBSP Overview

2.2.1. Introduction to space based solar power project

A Solar Power Satellite (SPS) is a massive satellite typically in a geostationary orbit ($\approx$ 36000 km altitude) intended for GW-scale energy generation [105]. Theoretically, an SPS can provide continuous baseload power throughout the year, except for short periods of eclipse; however, not every solar power satellite concept has been designed to deliver baseload power [20].
A typical space-based solar power system comprises a large area of lightweight solar panels that collect energy and distribute it to a transmitting antenna, where the electrical energy is converted to radio frequency waves (or laser beam) and wirelessly transmitted to Earth. A ground power system receives the energy in electromagnetic form, converts it back to DC electricity, and transforms it for distribution into the electrical grid [105], [99].

The system breakdown is shown in the scheme in Figure 2.6. The main elements of a Space-Based Solar Power system can be divided into three sections:

- Space segment: Solar power satellite
- Launch segment: Launch and transportation
- Ground segment: Receiving power station, control systems

In the design trade-off for the system, the main process to optimize in order to achieve higher efficiency is the energy chain, operated by the core power system and reported in Figure 2.6. It spans from collection to transmission in the space section, and from reception to distribution in the ground section. The connection between these two parts is achieved through wireless power transmission.
The core power system encompasses all the systems and operations directly associated with the main objective of the project: power generation. These components can be either in orbit, such as the systems of the solar power satellite, or part of the ground segment, including the receiving antenna and control system.
The enabling systems refer to all the systems and operations necessary for the development of an SBSP mission, but not part of the power system itself. These include space launch, in-orbit operations, manufacturing, maintenance, and decommissioning of space and ground components.

As will be seen in the following sections, several design solutions have been employed by different concepts to realize the project, encompassing all necessary systems and operations.

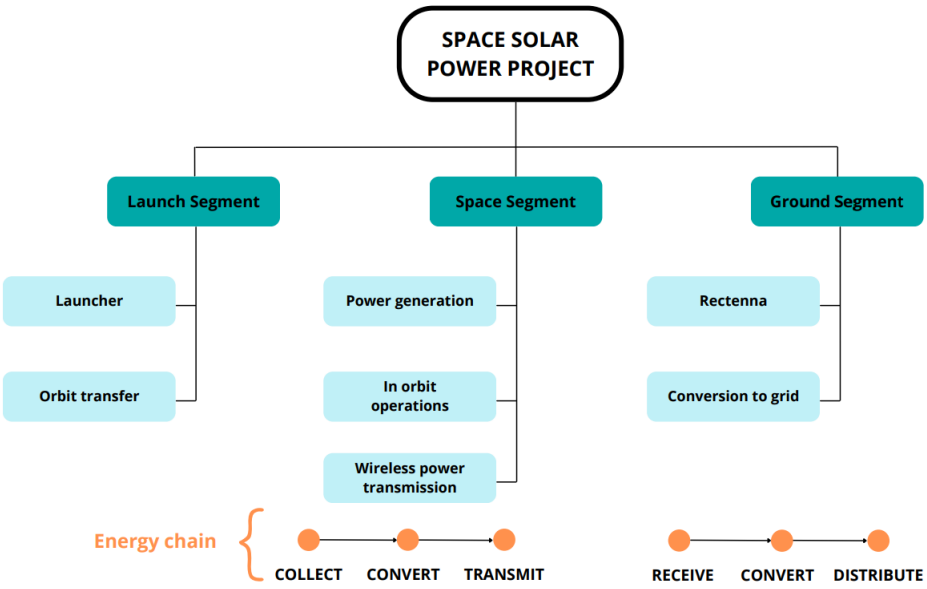

Figure 2.6: System breakdown for SBSP mission [99]

All space missions aimed at collecting solar energy in orbit and transmitting it to Earth share a common challenge: find a design solution to handle the orientation difference between the subsystems that point towards the Sun and those that point towards the Earth. This is crucial for the constant delivery of energy to Earth throughout the satellite's orbit. Cash (2019), [20] divides the solar satellites based on the design choices made to overcome this potential issue. Generally, the main ways to address this technical challenge are:

- **Electrical power transmission via articulated joints** (NASA 1979 Reference System [28], CAST Multi Rotary Joint (MRJ)):
  These systems use rotating joints to transfer power from the collecting PV area to the transmitting segment of the satellite. Managing losses and thermal dissipation is crucial in these systems since the cross-sectional area of the joints is much smaller than the collecting area and transmitter aperture. Additionally, the long power distribution path poses the risk of high resistive losses, necessitating high voltages to minimize them and increasing the overall mass of the system. Finally, if power is distributed along a single joint, the presence of a single point of failure is another aspect to consider.

- **Optical power transmission via articulated joints** (Modular Symmetrical Concentrator (MSC), SPS-ALPHA):
  These systems employ rotating solar reflectors to optically concentrate solar radiation onto the PV collecting area, thereby reducing power distribution losses. Moreover, the collection, conversion, and transmission of power occur on a layered module ("Sandwich module", section 2.2.4), which further reduces losses by shortening the distribution length. An issue with this concept could be the single point of failure associated with the rotating joint between the reflectors and the "sandwich" tile. As better explained in section 2.2.2, J. Mankins's SPS-ALPHA design avoids this obstacle by using multiple 2-axis sun-tracking reflector modules mounted on a framework that is essentially rigid relative to the sandwich panel.

- **Solid-state sytstems** (Tin Can SPS (with redundant PV systems), CASSIOPeiA SPS):
  These systems do not have movable parts. Some of them have redundant apparatus to cover in

case of failure. By employing a solid-state design concept, these systems increase their reliability while lowering the complexity of the design. However, some convoluted architectures, like the helical structure of CASSIOPeiA (Section 2.2.2), may be necessary to achieve the absence of rotating parts.

Collection	Pointing	Existing concept
Direct	Electrical	MR-SPS
Direct	Transmission	Abacus [97]
Direct	Solid State	No extant designs(similar to CASSIOPeiA but no reflectors)
Reflect	Electrical	No extant designs
Reflect	Optical	SPS-Alpha
Reflect	Transmission	No extant designs
Reflect	Solid State	CASSIOPeiA

Table 2.1: Classification of SBSP concepts by collection and pointing method, adapted from [20].

In the following section, a historical overview of space-based solar power satellites is presented, tracing their evolution from early concepts to current developments

2.2.2. Historical context of Space-Based Solar Power

Basic technologies necessary to develop the idea of using solar power in space, such as solar cell technology and wireless power transmission, date back to the early 1900s [67]. However, it was not until 1968 that the first concept of a satellite orbiting Earth to collect energy from the sun and transmit it back to Earth was proposed by Peter Glaser [41], who advocated the potential revolution in energy production that could have been achieved by transmitting continuous solar power to Earth in microwave bands [79]. Nevertheless, the general context of those years included lower oil prices and a global population approximately half the size of today's, which did not create an urgency for developing the idea. Moreover, the state of space technologies and high launch costs at the time made it unfeasible.

In the 1970s, NASA supported the US Department of Energy and proposed the first detailed study on the concept of space solar power (Reference model, see Table 2.2), which entailed an architecture of 60 solar space satellites into GEO. Although certain systems and technologies needed improvement or development, no insurmountable technological barriers were identified, but the project was deemed economically and programmatically unachievable [63]. In the same years, wireless power transmission experiments were also conducted, yielding positive results [2].

In the past couple of decades, global interest in space-based solar power projects has grown, driven by the urgent need for new energy sources, concern for CO_2 emissions and advancements in space launch and technology, which have made these projects more feasible. In Table 2.2 the models for SBSP developed over the years are summarized, with details on the proposed mission and system.

Year	Concept	Organization	Power	Orbit	Mass (MT)	Frequency (GHz)	Rotary Joints
1979	Reference Model	NASA	5 GW	GEO	30,000–50,000	2.45	Yes
1993	SPS 2000	ISAS	10 GW	LEO	–	2.45	Yes
1995	Sun Tower	NASA	100–300 MW	MEO	2,000–7,000	5.8	Yes
1997	SOLAR DISC	NASA	1–10 GW	GEO	8,000–70,000	5.8	–
1998	ISC	NASA	1.2 GW	GEO	22,463	2.45	No
1999	Sail Tower	ESA	450 MW	GEO	2,100	2.45	Yes
2015	MR-SPS	CAST	2 GW	GEO	10,000	5.8	Yes
2017	SPS-ALPHA Mk-II	Mankins Space Technology	1–2 GW	GEO	9,200	2.45/5.8	Yes
2017	CASSIOPeiA	IECL	2 GW	GEO	2,000	2.45	No
2024	SPS-ALPHA Mk-IV	Mankins Space Technology	1 GW	GEO	3,200	5.8	–

Table 2.2: History of proposed SBSP models [5].

As can be seen in Table 2.2, the range of power transmission frequencies is consistently within the microwave spectrum, with no proposed concepts employing laser frequencies. This is because, in the trade-off involved in selecting the operating frequency, lasers present significant disadvantages in terms of efficiency. A more detailed explanation will be provided in Section 2.3.2.

NASA "Fresh Look" study, 1995-97

In the late 1990s, NASA published a ”Fresh Look” study on the development of concepts and missions for Space Solar satellites. Mankins reports the main results of the study in [63]. In particular, the research consisted of examining the ”technologies, systems concepts and terrestrial markets that might be involved in future space solar power (SSP) systems” ([63]). The objective was to assess whether solar power satellites and the related systems could have made a good option for providing energy worldwide in a cost-efficient way, analyzing the associated risks and challenges. Three scenarios in particular were considered for examination: a sun-synchronous low Earth orbit (LEO), a middle Earth orbit (MEO) constellation, and one or more geostationary Earth orbit (GEO) satellites serving single, dedicated ground sites [63].
The study focused on analyzing the space segment, ground segment, space infrastructure and transportation aspects, from which two major system concepts emerged: the ”Sun Tower”and the ”Solar Disc”. One of the main concerns of of this study was to avoid heavy lift launch vehicles (HLLV), which brought to the modularization of solar power satellites [60].

The ”Sun Tower” consisted of a single modular space segment, for which the components could be launched in pre-packaged elements (self-assembling later in orbit). To meet power generation requirements, technologies such as thin film structures and multiple band gap PV arrays were employed. Wireless power transmission was achieved using electronic beam-steering and surpassing the past concept of mechanical pointing [60]. The architecture of the satellite is displayed in Figure 2.7, with multiple solar collectors and a central power transmitting structure.

Despite the advancements made in this NASA study, several technological improvements and gaps were identified that needed to be overcome to enable the realization of the SunTower concept. These included: the development of low-mass and low-cost PV arrays, efficient RF beam generation and thermal management systems, high-performance electric propulsion systems, robust protection against space debris, the creation of specific materials, low-cost launch options, robotic maintenance, and self-deploying mechanisms [60]. Since the concept was first developed, significant progress has been made in these areas, making the realization of SBSP more feasible today.

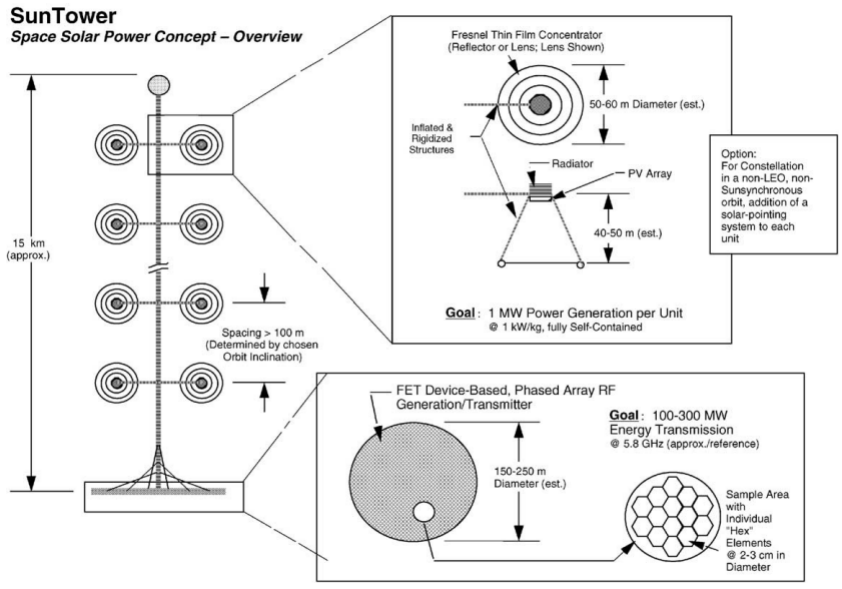

Figure 2.7: ”Sun Tower” solar power satellite concept [60]

The other concept that emerged from this study was the ”SolarDisc,” which leveraged modularity to address development and cost challenges. The design included small modular components to launch and assemble in geostationary Earth orbit (GEO), facilitating the use of various launch systems and

easing management. The system started with a basic version at the first launch, generating and transmitting low power, and became more powerful as assembly progressed.
The fully assembled disc was 3 to 6 kilometers in diameter, always sun-facing, and incorporated advanced photovoltaic (PV) arrays that convert sunlight into electrical energy. The power generated by the PV arrays was transmitted through redundant structures to an Earth-facing phased array at the base of the disc. This phased array, approximately 1 kilometer in diameter, transmitted power to Earth using radio frequency (RF) at 5.8 GHz.
The system featured beam steering, allowing the transmission beam to be directed within a 10-degree range for precise targeting of ground receivers [63].

ESA Sail Tower, 1998/1999

Compared to other SPS projects developed during the same period, the ESA Sail Tower introduced a novel approach utilizing advanced solar sail technology. This design originated from a study conducted by ESA and DLR in 1998/1999 focused on solar sail development. The SPS concept architecture involved deploying twin sail modules in LEO, which were then transferred via electric propulsion to GEO, where they were assembled into a tower-like system with a total length of 15 km [94]. Each twin module consisted of two 150 m x 150 m square sails connected by a carbon fiber arm and a 250 m long central tether, serving as connection with the other modules, forming the main 15 km-long structure. Additionally, ten ion thrusters with tanks were included to facilitate the transfer from LEO to GEO and provide attitude control.

Each solar sail was composed of four triangular sail segments, deployed by four CFRP (carbon fiber reinforced polymer) booms from a central deployment module. The innovative aspect laid in the use of lightweight sails coated with thin-film solar cells. To enhance overall system efficiency, the thin solar panels were capable of tracking the sun about two axes, reducing losses when sunlight was not perpendicularly incident on the PV sail, and mitigating instances where sunlight was parallel, resulting in no power generation.

Once assembled in GEO, the PV sails would collect solar power, which would then be transferred to the transmitting antenna via the central tether, functioning as both the structural connector and power conduit. The antenna would generate microwaves at 2.45 GHz in magnetrons and transmit them to Earth, achieving a total power generation of approximately 450 MW and a mass-specific power of 150 W/kg [94]. An artist's impression of the deployed Sail Tower in orbit is shown in Figure 2.8, highlighting the central tether connecting all twin modules of solar sails and the final antenna at the structure's end, directed towards Earth.

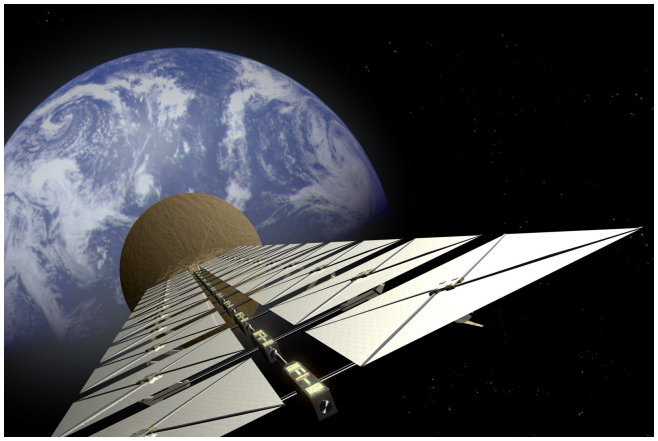

Figure 2.8: Artist's impression of Sail Tower SPS concept [31]

Multi-rotary solar power satellite (MR-SPS), 2015

The concept of the Multi-Rotary SPS was developed in 2015 at the China Academy of Space Technology in Beijing. Unlike traditional designs that rely on mirrors or solar concentrators, this satellite

employs a structure of photovoltaic panels that can rotate to continuously face the sun. A large scaffold connects these panels to the central microwave transmitter, which is permanently oriented towards Earth to beam the energy collected and converted into RF signals [101]. Each solar panel is supported by a rotary joint, with the collected power transmitted to the antenna through these spinning joints [5]. This rotational design presents significant technological challenges [21]. The current plan envisions a 1 GW, 11.8-kilometer-wide, 10,000-tonne structure in geostationary orbit (GEO) [5].

SPS-ALPHA (Arbitrarily Large PHased Array), 2012-2024

The first Solar Power Satellite via Arbitrarily Large PHased Array (SPS-ALPHA) is based on a highly modular architecture with no single points of failure, composed of small elements that are assembled together to build the satellite. The mission's chosen orbit is a geosynchronous Earth orbit, with the flexibility to change and explore other mission scenarios, such as Moon or Mars explorations. The large non-rotating structure of reflectors utilizes thin-film reflector technology to concentrate sunlight; the geometric arrangement of these reflectors allows for continuous solar radiation incidence. The power generation, conversion, and transmission modules are integrated into a "sandwich module." Deployable beams connect the reflector array to the power generation and transmitting segment. An interesting aspect of the SPS-ALPHA design is the use of a retrodirective phased array, an array of antennas that can be controlled to change the direction of the transmitted beam using the pilot signal [62], [61]. Figure 2.9a, Figure 2.9b and Figure 2.9c display three different versions of SPS-ALPHA.
The main differences among the successive SPS-ALPHA architectures lie in the structural design and arrangement of components, to reduce overall system mass and enhance modularity. However, the available literature does not provide detailed technical specifications regarding these design iterations.

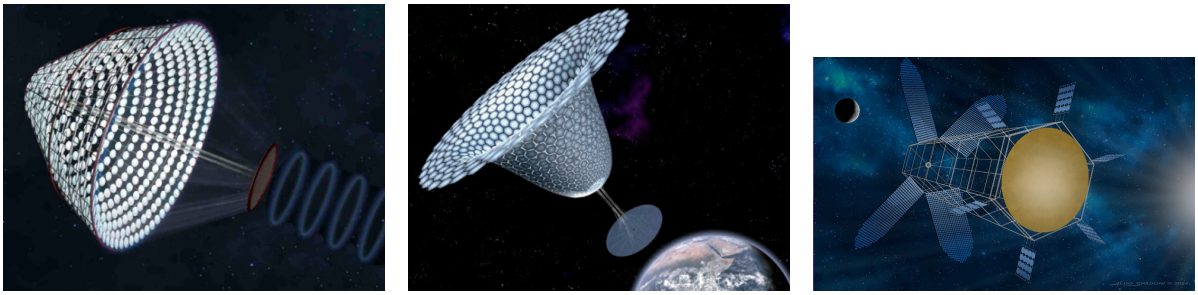

(a) SPS-ALPHA concept I **(b)** SPS-ALPHA concept II **(c)** SPS-ALPHA concept IV

Figure 2.9: Evolution of SPS-ALPHA concepts: version I (a), version II (b), and version IV (c). Adapted from [61].

CASSIOPeiA (Constant Aperture, Solid State, Integrated, Orbital Phased Array), 2017

The CASSIOPeiA Solar Power Satellite, developed by Ian Cash at International Electric Company Limited in the UK, addresses the challenge of rotational alignment between the sun-facing solar collectors and the Earth-facing transmitting side by utilizing a helical structure. Importantly, this design does not depend on moving or rotating parts, nor does it require specific redundancy, thus simplifying the system and reducing its overall mass. Relying on solid-state modules, the design is intended to increase reliability, minimize power distribution over distances and the thermal challenges.
The solar collection area remains constant, and the issue of limited beam steering in planar phased arrays is resolved by allowing for 360-degree beam steering while maintaining a consistent orientation towards the sun [21].

The primary helical structure accommodates a sun-facing array of high concentration photovoltaic cells and integrates a retrodirective microwave helical phased array transmitter, which includes a set of pilot beam receivers. Figure 2.10b depicts a detail of the CASSIOPeiA's helical structure, where the phased array is situated on a plane perpendicular to the plane of the high concentration panels and the power management and distribution system (PMAD). Two fixed pairs of solar concentrators are rigidly attached to each end of the helical structure at a 45-degree angle, see Figure 2.10a.

When deployed in geostationary orbit (GEO) near the equatorial plane, each 1.43 km satellite would weigh between 400 and 900 tonnes and deliver 430 MW to a rectenna with a 3.16 km diameter, [21],

[20].

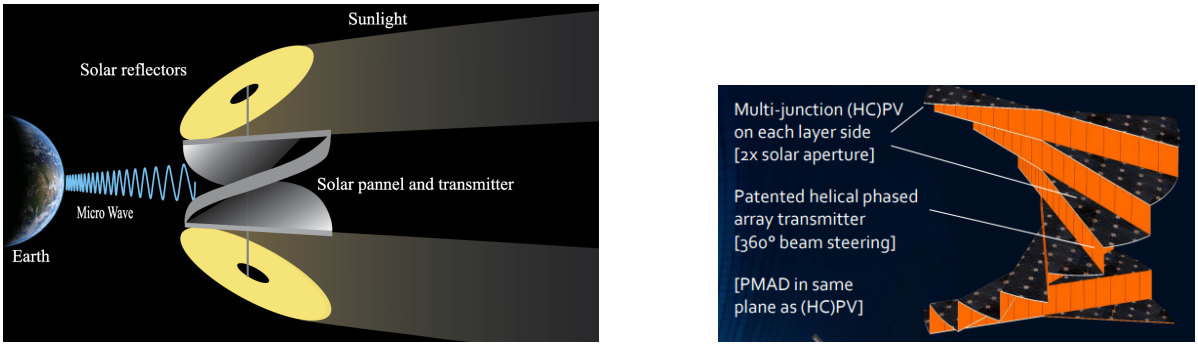

(a) (b)

Figure 2.10: CASSIOPeiA SPS Concept (a) [5], detail of helical structure of CASSIOPeiA (b) [21]

NASA initiatives

NASA is working on developing technologies and capabilities that would enable space-based solar power missions, such as in-space servicing, assembly, and manufacturing [89]. At the beginning of 2024, an analysis was conducted on two reference designs of solar power satellites, focusing on their life-cycle costs and greenhouse gas (GHG) emissions, and performing a sensitivity analysis to determine the conditions that would make space solar power competitive with terrestrial alternatives. The study applied to two reference designs, RD1 and RD2, respectively ”Innovative Heliostat Swarm” and ”Mature Planar Array.” These designs were based on historical concepts, SPS-ALPHA and Tethered-SPS (JAXA) [91], because these concepts provide enough data for the necessary analysis. NASA updated some systems with recent technical data and scaled both designs to generate 2 GW of power. Both systems were studied to be launched to low Earth orbit (LEO), then transported and assembled in GEO, where they would operate. The analysis considered the lifecycle of the systems: development, assembly, operation, maintenance, and disposal. Results showed that the most influential factors for making space-based solar power competitive in terms of GHG emissions are the efficiency of the solar cells and the lifetime of the system [89].

ESA activities

The European Space Agency (ESA) has shown a strong interest in space solar power research by launching the SOLARIS project in 2022 [3]. The aim of this initiative is to lay the groundwork for developing a Space-Based Solar Power mission in the near future. To achieve this, several research activities are underway, including cost-benefit and risk assessment analyses, as well as the research and development of the latest advancements in technologies necessary for the project.

The most recent work produced for the SOLARIS project is a comprehensive system study of a Commercial-Scale Space-Based Solar Power (SBSP) System for terrestrial applications, conducted in collaboration with Thales Alenia Space in 2023. This study encompasses state-of-the-art research activities from the European Space Agency, providing a detailed trade-off analysis for most mission systems. It offers valuable insights into the advanced technologies that can be utilized to realize the mission. The trade-off results in the selection of an architecture for the solar power satellite and mission parameters: a satellite with rotating electric interfaces is chosen, injected in LEO and transported to GEO, collecting energy with conventional photovoltaic technologies and transmitting it at a frequency of 5.8GHz [34]. Section 2.3 includes some results of the study, presenting a detailed overview of the subsystems of a space power satellite mission.

Moreover, the European Space Agency commissioned two cost-benefit studies of Space Based Solar Power for terrestrial energy needs: one by Fraser-Nash in the UK and another by Roland Berger in

Germany ([105], [23]).
The 2022 ESA Fraser-Nash study uses the CASSIOPeiA satellite architecture as a reference to conduct an in-depth analysis of costs and benefits, technological feasibility, risks, and limitations of the project, with some modifications to the design. The study focuses on the development, deployment, and operation of the SPS in geostationary orbit (GEO) [17].

Roland Berger's analysis is based on the SPS-ALPHA design and focuses on assessing the risks, costs, and benefits of using space-based solar power to achieve net zero [93]. The reports provide valuable insights into the technological readiness levels (TRL) of the main subsystems that constitute a space solar satellite and the challenges that need to be overcome to make a project of this kind more efficient and reliable [108]. A comprehensive overview is given of the components of the three segments of an SBSP project: Launch, Space, and Ground; this data will be prove useful for the present dissertation to conduct a trade-off analysis and determine a case study. Generally, results from both European studies show promising prospects for space power to contribute to the de-carbonization of Earth and are positive in terms of benefits over costs [9], [107]. From a technical perspective, the study identifies key areas where technological advancements are necessary to increase the project's feasibility. These areas will be examined in depth in the next section.

All the concepts developed over the years, along with the experiments and research activities, present a range of options for operational orbits and a wide range of values for operating frequency and satellite mass, which serve as the foundation and starting point for the next section, where a trade-off among all these possibilities is presented.. Table 2.2 illustrates these values.

2.2.3. Current Research

Some of the early SPS architectures described in previous sections faced several technical challenges that made them economically non-viable. The required technology had not yet reached a sufficient level of maturity. The weight of most systems, especially those for power management and distribution, was excessively high. The aerospace industry had not met the need for heavy-lift reusable launchers, and the necessity for in-orbit assembly made those concepts unfeasible given the lack of advanced space robotics technology.
In recent years, global efforts have been dedicated to research and development of space solar power projects and their enabling technologies.
Current SPS design activities are primarily based on the SPS-ALPHA and CASSIOPeiA architectures.

2.2.4. Sandwich Module (or integrated tile)

The ”sandwich module” was first studied by NASA and the DOE in their reference model in the 1970s. Notably, concepts such as the Integrated Symmetrical Concentrator (ISC) and Modular Symmetrical Concentrator (MSC), as discussed by Jaffe et al. (2011) [51], build upon the principles of the sandwich module. Both concepts rely on the use of lightweight solar reflectors spanning a large area to concentrate sunlight onto a smaller photovoltaic surface, thereby minimizing the need for high-density PV components and reducing the overall mass required for launch.

The sandwich panel is a critical component in these concepts, functioning as a three-layered module that integrates solar power collection, DC to RF conversion, and RF emission functionalities. This design eliminates the need for mechanical joints, simplifying construction and enhancing reliability. However, despite efficiency gains achieved through solar concentration via reflectors, challenges arise during certain orbital phases when direct sunlight may reach the transmission layer, leading to undesirable thermal loads. Figure 2.11a illustrates a representation of this concept, while a detailed view of the sandwich module is depicted in Figure 2.11b.

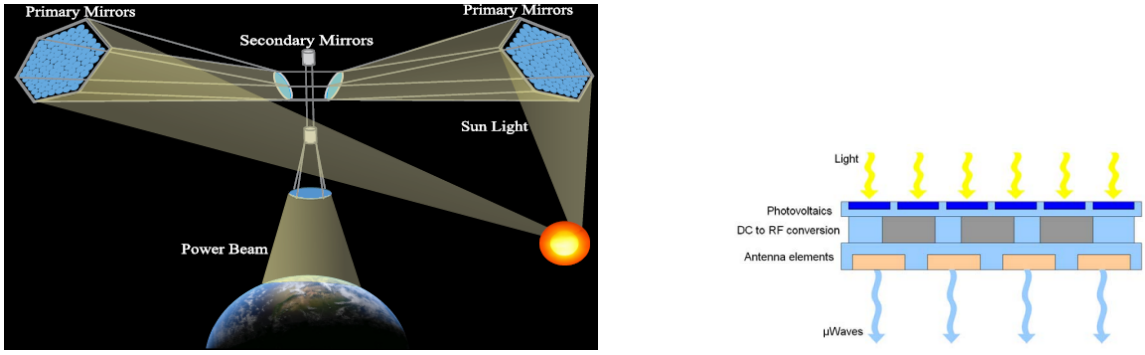

(a) (b)

Figure 2.11: MSC-SPS concept based on the sandwich module (a) [5], and detail of the sandwich module layers (b) [124].

Although the sandwich module concept has been explored in the literature, there remains a significant gap in detailed research and analysis. Apart from the Air Force Research Laboratory (AFRL), which has developed a prototype and plans to launch it in 2025, and a conceptual study by Caltech [18] [33], there has been limited investigation into the practical implementation of this architecture. While some research papers discuss the concept, many key issues and subsystems remain unexplored.

One of the primary challenges associated with the sandwich tile concept is thermal management. This architecture is exposed to higher solar radiation concentrations than conventional space-based solar panels, leading to extreme power densities that are difficult to manage. Without effective heat dissipation strategies, thermal buildup could significantly degrade system performance and efficiency. Several studies, including those by Jaffe et al. [51], highlight the thermal constraints inherent in such high-power-density designs, yet a comprehensive solution has not been established.

Another major issue in the Modular Symmetrical Concentrator (MSC) architecture (Figure 2.11a) concerns its mechanical bearing, which poses a risk of failure. To address this, John Mankins' SPS-ALPHA concept replaced the primary and secondary mirrors of the MSC with multiple heliostatic reflectors arranged in a conical structure, eliminating single points of failure and enhancing system robustness.

However, the details and performance of the integrated tile concept remain largely unexplored, leaving a gap in understanding whether this design is truly more effective than conventional architectures. While promising, this approach presents several limitations and unresolved questions. Concentrating solar energy onto a small photovoltaic area leads to significantly high temperatures, and the compact design results in high power density with limited surface area for heat dissipation. If not properly managed, this could lead to severe thermal inefficiencies or even component failure.

As mentioned earlier, research on the integrated tile for SBSP is still in its early stages, with studies conducted at a high level and lacking detailed assessments. Jaffe et al. [51] performed preliminary

trade studies on the layers and architecture of the module based on the technological development available at the time. Their work later progressed to the implementation of a prototype [52] and the planning of an experimental test [49]. However, since these studies were conducted, the efficiencies of the technologies involved in the architecture have improved, making it necessary to revisit these analyses with updated performance parameters.

Additionally, Jaffe et al. [51] and [52] noted a key reason for not selecting magnetrons and klystrons as power conversion devices: these components are difficult to manage in the space environment and require high-voltage power converters. Since they operate at high voltages, they introduce an additional conversion stage, reducing overall efficiency. This trade-off is another important factor in determining the viability of the integrated tile concept.

Despite the progress made in early studies, there is still a substantial knowledge gap regarding the key subsystems and challenges of the sandwich module architecture. Future research should focus on addressing the thermal limitations, optimizing power conversion strategies, and validating the concept through experimental demonstrations.

Today, research efforts in Space-Based Solar Power (SBSP) are increasingly focusing on turning theoretical architectures into technologically feasible solutions. Among the most promising current concepts, the CASSIOPeiA system developed by Ian Cash and IECL stands out for its innovative solid-state, helical structure that eliminates moving parts and enhances reliability—particularly attractive for minimizing complexity in high-power orbital systems. Parallel to this, the SPS-ALPHA architecture, originally proposed by John Mankins, is undergoing continued refinement, with newer modular versions aiming to reduce system mass and improve deployment efficiency. Recent updates to SPS-ALPHA (e.g., Mk-IV) integrate advanced materials, autonomous robotic assembly, and more compact retrodirective antenna designs, pointing toward a more scalable and realistic path to deployment.

Beyond full-system architectures, a growing portion of research is also dedicated to developing enabling technologies for SBSP, including high-efficiency photovoltaic materials, lightweight structural components, advanced heat rejection systems, and in-space manufacturing and servicing capabilities. Agencies and defense research labs such as AFRL, are now actively testing prototype components—such as modular sandwich tiles, power beaming systems, and autonomous assembly units—which represent critical building blocks for future SBSP implementation.

Despite recent progress and increasing interest from both institutional and private actors, the development of SBSP remains a highly complex challenge. Concepts like CASSIOPeiA and the evolving SPS-ALPHA architectures show promising directions, and key enabling technologies are advancing. However, the step from theoretical viability to practical implementation is far from straightforward. The realization of space-based power systems will require deep integration of multiple subsystems, each with its own constraints and trade-offs.

2.3. System Breakdown

This section aims to provide a comprehensive overview of the various subsystems relevant to the mission of a Space based solar power station for Earth applications. The breakdown of the project in subsystems can be found in Figure 2.6.

In this section, each subsystem will be presented with a detailed description, highlighting the different available options and their key characteristics. To ensure a clear and organized structure, each subsystem will be outlined as follows:

- **Overview**: A brief introduction to the subsystem, outlining its importance and role in the mission.
- **Different configurations**: A presentation of the various implementation options available for the system, for subsequent comparison.
- **Important criteria and characteristics**: Identification of the critical features of the system and criteria that need to be taken into account for its assessment.
- **Latest advancements and current gaps**: A summary of the latest technological developments essential for advancing the space-based solar power project, and identification of any existing gaps in the research or limitations in the technology related to the system.

The purpose of this section is to prepare the basis for the trade-off analysis that will be conducted in the second phase of the thesis, which will identify the most suitable mission case study by using specifically selected criteria.

2.3.1. Launch segment

Orbit selection

When designing a space mission, one of the primary considerations is the choice of orbital location. This decision is typically driven by specific mission requirements or, more broadly, by the overall features and objectives of the mission.
Based on a review of the literature and previous projects, the orbits considered for the subsequent trade-off are Low Earth Orbits (LEO), Medium Earth Orbits (MEO), Geostationary Earth Orbits (GEO), and Molniya Orbits. Most previous studies have selected geostationary orbit for space solar power missions.

Low Earth Orbits are circular or quasi-circular orbits around Earth with an altitude below 2000 km [19]. While they allow for higher payload capacity of a launcher compared to higher orbits, operating in those altitudes poses challenges related to atmospheric drag, space debris, and orbital decay.

Geo-synchronous orbits have a very low eccentricity and an altitude of approximately 35,786 km, so their period coincides with the Earth's rotation. A circular equatorial orbit at this altitude is called a geostationary orbit, and a spacecraft in this orbit always has the same zenith with respect to a certain location on the Earth's surface. Although at this altitude atmospheric drag is not a concern, perturbations linked to the Moon's influence and solar radiation pressure become more influential [19].

Medium Earth Orbits are all the orbits with an altitude between LEO and GEO. An important consideration for these orbits is their location within the Van Allen radiation belts, which necessitates additional attention to the radiative environment.

Table 2.3 outlines the advantages and disadvantages of each orbit for space-based solar power missions. The assessment focuses on power beaming efficiency, insertion into orbit, presence of eclipses, system complexity (including launch and attitude control), and incoming solar radiation levels. These are preliminary considerations, and a more detailed trade-off analysis, based on specific criteria, will be conducted to select the optimal orbit for the mission [6].

Orbit	PROs	CONs
LEO	• Shortest transmission distance, thus smaller transmitting/receiving antenna dimensions* • Lowest launch cost • Highest launcher payload capacity • Easiest and cheapest in-orbit assembly • No orbital transfer needed	• Lowest incoming solar radiation • Atmospheric drag (<800 km) causes orbital decay and requires complex station-keeping systems [75] • Regular eclipses • High presence of space debris • Multiple satellites needed • Complex SPS operations due to power-beaming switching
MEO	• Shorter transmission distance than GEO/Molniya → smaller transmitting/receiving antennas • Lower launch cost than GEO/Molniya • Higher launcher payload capacity than GEO/Molniya • Easier and cheaper in-orbit assembly than GEO/Molniya	• Multiple satellites needed • Complex SPS operations due to power-beaming switching
GEO	• Single satellite provides continuous power delivery • Very brief eclipses throughout the year • High solar incoming radiation • No switching needed among satellites • Always pointed at same Earth location – no steerable antenna needed	• Larger antenna size • Highest launch cost • Complex and expensive in-orbit assembly • Requires multiple in-orbit services
Molniya	• Fewer satellites needed than LEO/MEO (but more than GEO) • Lower launch cost than GEO • Cheaper in-orbit assembly than GEO	• Complex SPS operations due to power-beaming switching • Complex launch and orbital injection • High radiation (Van Allen belts) • Orbital perturbations (J2 effects)

Table 2.3: Comparison of orbital options for SBSP systems

* The required size of the transmitting and receiving antennas depends on the distance between them. For a given frequency, the product of the areas of the two antennas is proportional to the square of the separation distance. Therefore, shorter transmission distances allow for smaller antenna sizes.

Launcher

Recent advancements in launcher technology are facilitating the development of space-based solar power projects. Given the significant mass and large dimensions of a space solar power station, its deployment requires multiple launches and the use of heavy-lift vehicles.

Different scenarios are possible depending on the selected operational orbit. For a Low Earth Orbit (LEO) deployment, the payload would be injected directly into LEO. However, if a Geostationary Orbit (GEO) is chosen, a significantly higher Delta V is required to inject the payload directly into GEO. Thus, the launch may initially place the payload into LEO or a Geosynchronous Transfer Orbit (GTO), followed by transfer to GEO using its propulsion system or with the assistance of orbital transfer vehicles.

In the past decade, significant developments in the launcher industry have represented a pivotal moment both economically and technologically. In 2011, SpaceX introduced a project for the first reusable

launch system, Falcon 9, and in 2015 it achieved the first successful landing of a reusable first stage. Introducing reusability in launch systems has significantly reduced launch costs, addressing a critical barrier for space projects that require multiple launches, such as SBSP.
Additionally, the substantial mass of a solar power satellite (approximately 10,000 tons [89]) necessitates the use of heavy lift launchers. Currently available options include the Falcon 9, Falcon Heavy, Ariane 5, and Ariane 6.

SpaceX's latest innovation, Starship, represents a significant advancement in the launch industry, potentially crucial for enabling SBSP. Offering high payload capacity and full reusability, Starship could revolutionize transportation services for ambitious space missions. Many companies are now developing reusable launchers capable of handling payloads in the range of hundreds of metric tons. This trend is expected to continue in the coming decades, further reducing the unit cost per kilogram of rocket launches and enabling rapid reusability of launch vehicles.

Table 2.4 summarizes the characteristics of suitable launch vehicles that are currently in use or under development.

Launcher	Payload to LEO [t]	Payload to GTO [t]	Fairing dimensions (diam x height) [m]	Reusability
Ariane 5	20	10	5.4 x 17	None
Ariane 6	21.6	11.5	5.4 x 20	None
Falcon 9	22.8 (17.5)	8.3 (5.5)	5.2 x 13.1	First stage and fairing
Falcon Heavy	63.8 (33)	26.7	5.2 x 13.1	First stage (boosters) and fairing
Starship	100-150	21 (150 orbitally refilled)	8 x 17 (1000 m^3)	Fully reusable

Table 2.4: Characteristic of suitable launcher systems, [108]

Key characteristics for evaluating and selecting the optimal launcher system include payload capacity, reusability, fairing dimensions, and considerations of the launch site to compute the required Delta V for orbital transfers, thus energy expenditure.

The selection of the appropriate launcher depends on advancements anticipated in the coming years, the chosen operational orbit, and the specifications of the payload. It is reasonable to assume that in the next few years, progress in launcher systems will focus on increased reusability and enhanced payload capacity.

Orbital transport

An important consideration in the design of the mission is the transport to the operational orbit. The method of achieving this depends directly on the selected operational orbit.

If a Low Earth Orbit (LEO) is selected as the best option, direct injection by the launcher can be realized into LEO, with by multiple launches and subsequent orbital assembly of the modules.

For higher orbits, such as Geostationary Orbit (GEO), spacecraft typically need to execute impulsive maneuvers to reach the target orbit. For instance, a Geostationary Transfer Orbit (GTO) is an elliptical orbit with a low perigee (sometimes as low as 200 km) and an apogee at the altitude of the GEO. At apogee, the spacecraft's propulsion system performs a maneuver to transfer the spacecraft into the geostationary orbit. Several options are available for injection into orbit, either with or without requiring additional orbital transportation.:

1. Direct injection into orbit

2. Injection into LEO/GTO followed by transport to the target orbit using orbital transfer vehicles
3. Injection into LEO/GTO and orbit raising of the segments using their own propulsion system
4. In the case of selecting Starship as the launcher: injection into LEO, refueling Starship, and orbit raising using the refueled Starship

Once the target orbit for SPS deployment and operation is selected, the main criteria for assessing the best method for orbital transportation include the energy required for transport (ΔV), scalability, and complexity (for module deployment and subsequent in-orbit operations). These criteria will be further elaborated and reviewed in the next chapter during the trade-off analysis.

If orbital transport is achieved through the propulsion system of the launched modules, two alternatives require attention for comparison: chemical and electrical propulsion.

Chemical propulsion offers higher thrust, allowing for rapid transfer times. However, compared to electrical propulsion, it requires more propellant due to its lower specific impulse (typically 200-300 seconds versus 2000-5000 seconds for electrical propulsion), which negatively impacts the mission in terms of mass.

Electrical propulsion, on the other hand, involves low-thrust transfers (typically in the order of millinewtons to newtons versus newtons to kilonewtons for chemical thrusters), which could take years instead of days for the transfer. Additionally, this type of transfer would pass through the Van Allen radiation belts, which can seriously affect the performance of the space solar satellite components, such as solar cells and electronics.

Orbital transfer vehicles
A significant interest of the latest times for relocation activities relates to space tugs, or orbital transfer vehicles. These can have the objective of transporting a payload to its final orbit after separation from the launch vehicle, or orbital change, refueling, satellites constellation management, decommissioning and debris removal. European Spaceflight LTD [29] posted an index of the latest developed or in development orbital transfer vehicles (see Table 2.5).

Company	Vehicle	Function	Servicing	Launch	Payload Capacity [kg]
ClearSpace	Clearspace-1	Debris removal	LEO	2026	>225
D-Orbit	ION	Multirole	LEO	2020	160
Dark	Orbital Stage	Multirole	LEO	2026	300
ESA / ArianeGroup	ASTRIS	Payload deployment	Multi	2024	–
Exolaunch	Reliant Pro	Multirole	Multi	–	260
Exolaunch	Reliant Standard	Payload deployment	Multi	2021	200
Exotrail	SpaceVan	Payload deployment	LEO	2023	400
Hybrogines	Hyscab	Payload deployment	LEO	2027	100
Lúnasa Space	VIA	Multirole	LEO	2024	200
MaiaSpace	Colibri	Multirole	LEO	2026	–
RFA	Redshift	Multirole	LEO	2024	–
Skyrora	Space Tug	Multirole	LEO	–	–
UARX Space	OSSIE	Payload deployment	LEO	2025	–
UARX Space	Lucas	Payload deployment	Lunar Orbit	–	100

Table 2.5: Index of Orbital Transfer Vehicles in Europe [29]

Most technologies are being designed to operate in Low Earth Orbits; for applications related to space solar power stations, space tugs can be useful to transfer modules from LEO to GEO (or operational orbit), thus future advancements should focus on systems to enable this transfer.

2.3.2. Space segment

For each subsystem, further considerations can be made regarding design choices and specific characteristics, such as the type of solar cells or antenna design for wireless power transmission (WPT). Figure 2.12 summarizes the primary trade-off options. For power collection, reflectors can concentrate sunlight onto photovoltaic cells, or power can be collected directly through solar cells. As noted in section 2.2, addressing the alignment mismatch between collection and transmission segments is a common challenge across solar power designs. This can be managed by rotating one of the interfaces or using a solid-state solution like the helical structure of CASSIOPeiA. For power transmission, the options considered are microwave and laser transmission.

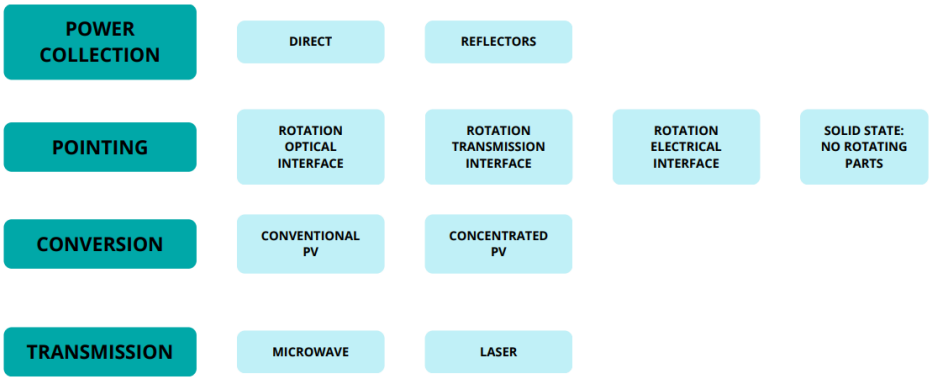

Figure 2.12: High level trade-off options for Space segment of SPS

Power generation

The power generation system represents the first step of the energy chain to optimize. Therefore, achieving the highest efficiency in this process is critical for the overall mission's performance. It is essential to select the most appropriate technologies to perform the two main functions of the system: collecting solar energy and converting it into electrical power [92]. For solar power collection, the choice to make is whether to implement a system of reflectors to point at the conversion interface, or to directly convert solar power. For power conversion, photovoltaic cells represent the most reliable and efficient technology, widely used in space applications [114], [92].

The use of solar cells in space requires special attention compared to terrestrial applications. This is due to the extreme thermal cycles and high radiation levels to which they are subjected, which can significantly influence the performance of the PV system.

Key characteristics to consider when selecting the technology to employ include efficiency, specific power, radiation hardness, and resistance to extreme thermal conditions. It is important to evaluate not only the efficiency at beginning-of-life (BOL), but also its end-of-life (EOL) value, which accounts for degradation due to exposure to extreme environments. Additionally, an analysis of the necessary cooling systems to manage high temperatures during the satellite's orbit is needed. Current research focuses on finding lightweight, high-efficiency, low-cost photovoltaic cells.

Space environment

Solar cells operating in space experience several challenges, and it is fundamental to address and study the effects that these have on cells' performance.

Firstly, the levels of solar irradiance that cells experience are higher than terrestrial standards due to the absence of atmospheric attenuation. The Air Mass standard in space is AM0, whereas on Earth's surface, it is typically AM1 or AM1.5[2]. The absence of atmospheric attenuation in space results in a different solar flux spectrum, particularly in the short wavelength region, which is otherwise absorbed by O_3 and O_2 in the atmosphere (see Figure 2.13). This necessitates a different classification for space solar cells compared to those used on Earth. Higher levels of solar irradiance can negatively affect the conversion efficiency of the cell, since most of the additional light energy in the AM0 spectrum is in the infrared and ultraviolet regions, where the cell's spectral response is low.
Woodyard and Landis suggest a correction factor, which depends on the cell's spectral response, to apply to the efficiency in the AM1.5 spectrum and approximate its value in the AM0 spectrum [119].

[2]The Air Mass standard value refers to the length of the path that the solar beam takes through Earth's atmosphere relative to the shortest possible path.

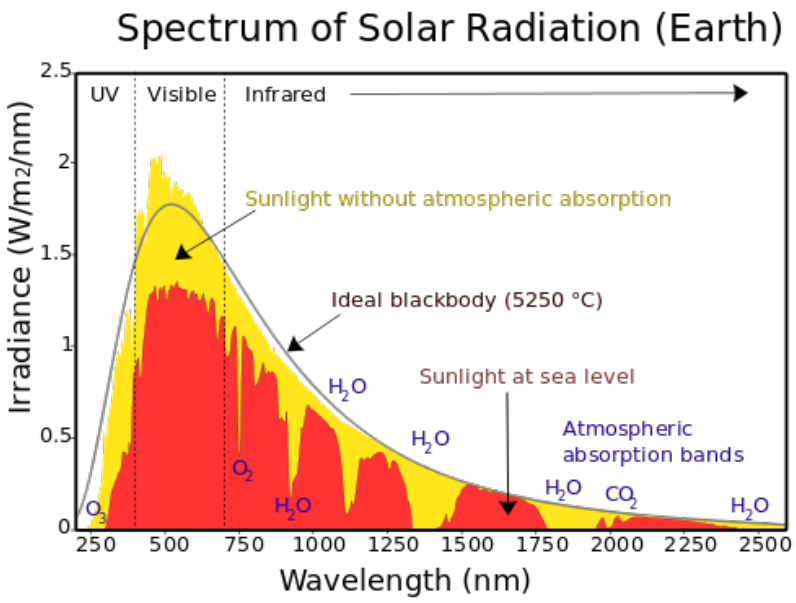

Figure 2.13: Spectrum of solar radiation, at sea level, and without atmospheric absorption [117].

Another challenge is the high concentration of radiative particles, which varies depending on the satellite's orbit. Research and testing have shown that performance degradation in solar cells due to radiative particles primarily depends on the differential flux of the particles and the total ionizing dose (cumulative dose from various sources such as electrons, protons, heavy ions, X-rays, gamma rays, etc.) [119], [44]. Once the operative orbit is selected for the mission, the specific radiation environment should be studied to predict or simulate its effects on the solar cells.

The negative effect that radiation has on conversion efficiency is more evident in cells with higher efficiency, since lower efficiency is linked to defects in the lattice, which are "healed" upon interaction with charged particles, thus masking the detrimental effects of radiation [44].

Lastly, space devices experience extreme thermal cycles, inducing stresses, efficiency degradation, and delamination. Banik et al. [11] propose a silicon-oxycarbonitride coating with high transparency at UV-VIS frequencies, allowing for high efficiency of the cell, and high emissivity in the MIR region, functioning as radiative cooling. This coating demonstrates positive effects on a CIGS (Copper indium gallium diselenide) solar cell in lab-experiments conducted by the DLR, for the GoSolAr (Gossamer Solar Array) power sail mission. A single layer of coating increases cell emissivity from 0.3 to 0.72 and reduces the maximum temperature by 30°C, resulting in a 27% increase in output power under maximum irradiance conditions [11]; however, it has not been demonstrated in space yet. These flexible, lightweight, high-emissivity coatings are promising options for radiative cooling of solar cells in space.

Types of solar cells

In the last decade, significant advancements have been made in the use of solar cells in space, particularly in terms of power collection efficiency[3], cost, mass, and resistance to the space environment.

The state-of-the-art in space solar cells is represented by multi-junction (MJ) cells, typically III-V MJ cells grown on germanium (Ge) or gallium arsenide (GaAs) substrates [44]. These cells offer high power conversion efficiency (PCE) in the AM0 spectrum (exceeding 30%), a favorable efficiency-to-cost ratio, and excellent stability in orbit [71]. Advancements are ongoing with the development of four-junction, five-junction, and six-junction cells. However, many missions still opt for lower-efficiency silicon-based solar cells to minimize operational costs.

[3] Power conversion efficiency (PCE) is defined as the ratio of the electrical power produced by the cell to the incident power [114]

Recent research and development efforts focus on lightweight, flexible, thin-film solar cells, such as those based on $Cu(In,Ga)Se_2$ (CIGS) and hybrid organic-inorganic perovskite cells. These technologies are promising for space applications, offering high radiation hardness, specific power (approximately 3 W/g for CIGS cells, 23 W/g for perovskite), and lower production costs [114].

Thin-film solar cells consist of a thin (nm-µm thickness) layer of amorphous or polycrystalline material on a lightweight, flexible substrate. With the exception of groups II-III V MJ thin cells (AM0 PCE ≈ 25%), this technology currently presents low conversion efficiency values for AM0 conditions [44].

In Table 2.6 a preliminary comparison among different photovoltaic cells technology is presented; the needed areas of research are also indicated.
The state-of-the-art efficiencies of commercial solar cells, updated in June 2024, presents III-V four-junction concentrator PV cell from the Fraunhofer Institute for Solar Energy Systems achieving an efficiency of 47.6%.

	Silicon	**Multijunction**	**Cu(In,Ga)Se_2**	**Perovskite**
Efficiency	Medium	High	Medium	Medium
Lab-scale record	26.1%	47.1%	23.4%	25.5%
In space application	≈ 17%	Up to 32%	Not available	Not available
Radiation hardness	High	High	Excellent	High
Specific power	0.38 W/g	0.4–3.8 W/g	3 W/g	23 W/g
Flexibility	Low	Low	High	High
Fabrication cost	High	High	Low	Low
Research areas (gaps)	Enhance efficiency	Bandgap and current matching in subcells	Space demonstration, scalability, efficiency	Radiation resistance validation

Table 2.6: Comparison of technological and performance parameters of different types of PV cells [114]

Concentrated Photovoltaics (CPV)

Concentrator arrays are used to improve performance and reduce the cost of solar power generation in space. These arrays operate by using reflective and refractive optics to concentrate sunlight onto a smaller area of photovoltaic (PV) cells, resulting in a much higher sunlight intensity compared to conventional PV systems without concentrators. This is typically achieved with the help of Fresnel lenses or mirrors [44]. However, a critical consideration is that the solar cells will receive a higher power density (measured in KW/m^2), necessitating a proper cooling system to prevent the PV cells from overheating [76], [115].

An essential aspect of maintaining the efficiency of these cells is to keep their temperature stable. Any temperature variation can cause issues in the cell's performance, especially given the high power density due to the reduced area of the PV cells.

State-of-the-art concentrator photovoltaic (CPV) systems typically utilize Fresnel lenses, multi-junction (MJ) cells, and a graphene-based radiative cooling system. The primary advantage of using CPV systems lies not only in the potential increase in efficiency but also in the significant reduction in mass, cost, and complexity of the overall system. Figures 2.14a and 2.14b illustrate the basic layout of a concentrated PV system, in the case of primary and secondary mirror (Fig 2.14a) and Fresnel lens (2.14b).

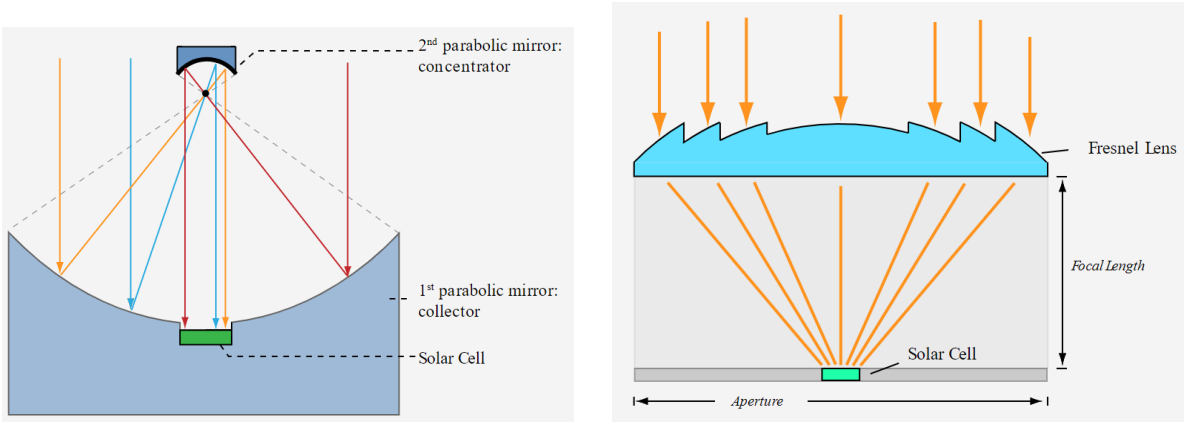

(a) CPV **(b)** CPV2

Figure 2.14: Concentrated PV with parabolic mirrors **(a)** and Fresnel lens **(b)**

Wireless Power Transmission

The concept of wireless power transmission dates back to the late nineteenth century, pioneered by Nikola Tesla. In recent years, significant advancements have been made, particularly in far-field and high-power wireless transmission systems, which are crucial for the feasibility of Space-Based Solar Power (SBSP). The two primary categories of wireless power transmission (WPT) capable of long-distance delivery are microwave and laser beaming. Both face challenges with low efficiency, but recent experiments and advancements in materials and technology have shown potential for improved long-distance performance [58].

Microwave power transmission requires larger transmitting and receiving antennas to achieve higher efficiencies. However, antenna dimensions are often limited by mission or system requirements. Laser technology, while offering precise beam targeting, suffers from very low efficiency and raises safety and health concerns.

One of the earliest demonstrations of enhanced microwave WPT performance was conducted in 1964 by William Brown, who used silicon diodes as rectifiers in the receiving antenna to improve transmission efficiency. Brown's team successfully beamed 30 kW of power over a distance of 1.4 km, achieving a rectenna efficiency (power converted to DC/power received) greater than 80%, which powered a small helicopter for 14 hours of flight [15], [58].

Numerous experiments have since been conducted to demonstrate wireless power transfer. The longest transmission distance for microwave power transfer to date is 148 km, achieved through a collaboration between the University of Kobe in Japan, Texas A&M University, and Managed Energy Technologies. However, the efficiency was extremely low due to the small sizes of the transmitting and receiving antennas [104].

Japan has shown a strong interest in developing WPT technologies. The Japan Aerospace Exploration Agency (JAXA) has conducted an experiment that allowed for the transmission of guiding signals from the receiving antenna back to the transmitting array using reverse guidance techniques, achieving precise beam control [64].

The California Institute of Technology (Caltech) is also actively researching and developing space solar power through its Space Solar Power Project (SSPP). This effort led to the launch of a solar power satellite demonstrator (SSPD-1) in 2023 [18]. The SSPD-1 demonstrated three key technologies:

- MAPLE (Microwave Array for Power-transfer Low-orbit Experiment)
- DOLCE (Deployable on-Orbit ultraLight Composite Experiment) to demonstrate the building, packing, and deployment of a modular structure
- ALBA, a collection of 32 different types of photovoltaic cells to assess the most effective cells in the space environment [18].

MAPLE successfully demonstrated wireless power transmission in space for the first time. Two arrays were positioned 30 cm from the transmitter, converting the energy to DC and lighting up a pair of LEDs. Additionally, the experiment showed the capability of beaming energy to Earth, with researchers detecting transmitted energy at a receiver station on the roof of the university laboratory.

Laser power transmission experiments have been conducted by NASA, LaserMotive, and the US Naval Research Laboratory, with the primary limitation being low system efficiency. LaserMotive experiments reached a laser power of 1 kW over 1 km, with an overall efficiency of 10 %. The maximum efficiency achieved was 15% during an experiment involving a spacecraft, where a 28W laser beam with an 810nm wavelength was transmitted over a distance of 200 meters [58].

As of today, wireless power transmission technologies are categorized based on their functioning mechanisms and the frequencies at which they operate. Magnetic field coupling (MC-WPT) and electric field coupling (EC-WPT) are near-field technologies, whereas microwave (M-WPT) and laser (L-WPT) are considered far-field technologies [58]. Figure 2.15 provides an overview of all these systems, along with application examples and the frequencies used. For space-based solar power applications, only far-field technologies will be considered as options to be employed [38].

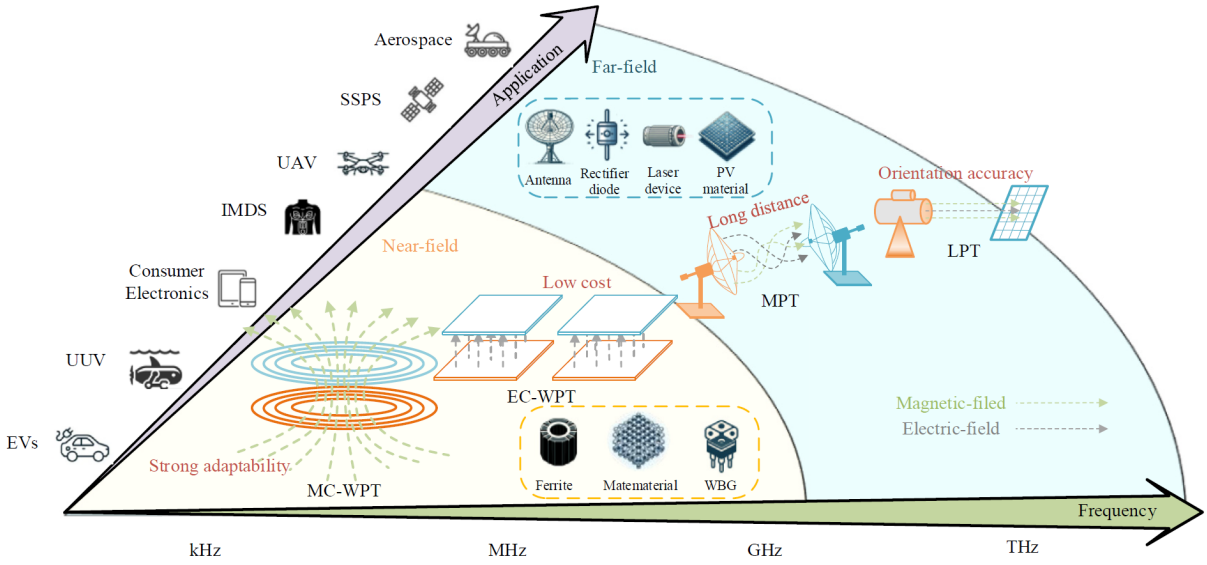

Figure 2.15: Overview of existing WPT technologies [58]

The system handling power is the most critical part of the entire project. The primary aim and challenge are to maximize the efficiency of power generation, focusing mainly on the energy chain of the process (see Figure 2.6). The power collected through reflectors or photovoltaic cells needs to be transferred to the power bus management system and then distributed to the transmitting antenna to be beamed to Earth. The detailed architecture and components of the power bus management (e.g., power conditioning, DC-DC converter) are beyond the scope of this review. The level of detail maintained is reflected in dividing the power chain process into the blocks reported in Figure 2.6 , where the selection of each subsystem is based on optimizing the total efficiency of the process. The power transmission efficiency is the most important specification to evaluate the system performance, and maximizing this efficiency is the key focus for improving the system design.

An overview of the functional blocks of microwave and laser wireless transmission architectures is depicted in Figures 2.16 and 2.17, respectively.

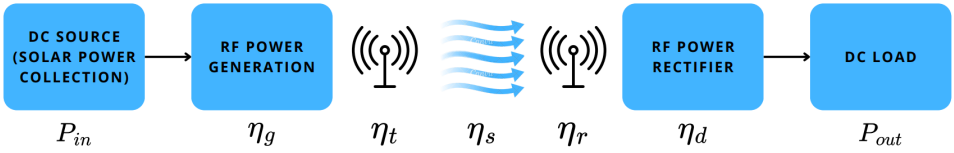

Figure 2.16: Components of a Microwave Wireless Power Transmission System

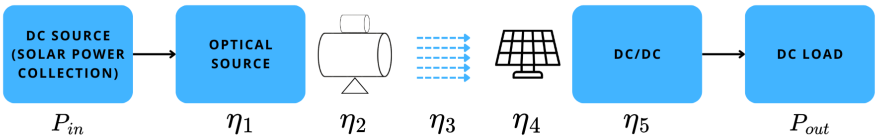

Figure 2.17: Components of a Laser Power Transmission System

Microwave beaming employs frequencies from 300 MHz to 300 GHz, and the used transmitting antennas are categorized into phased array and directional antennas [58]. As already stated, efficiency is the key parameter to optimize, and the total efficiency of the microwave wireless power transmission process can be defined as:

$$\eta_{MPT} = \frac{P_{out}}{P_{in}} = \eta_g \eta_t \eta_s \eta_r \eta_d$$

η_g = DC-RF conversion efficiency
η_t = transmitting antenna efficiency
η_s = free space transmission efficiency
η_r = receiving antenna efficiency
η_d = rectifying circuit conversion efficiency

The phases of receiving the beam and converting RF to DC are part of the ground segment, discussed in section 2.3.3. Currently, the main limitation hindering the development of microwave power transmission is the low efficiency of the transfer and the lack of demonstrations for long-distance transmission and high power levels [58].

Laser power transmission operates at higher frequencies, usually in the order of hundreds of THz. The electrical energy collected is converted into a laser beam through a laser power source, then transmitted with an optical system and received by a PV system, where the laser beam is converted back into electrical energy. Similar to microwave power transmission, the total efficiency of the process is obtained by the product of the efficiencies of all these steps [58].

Although laser-based wireless power transmission offers high beam directionality and potentially smaller receiver sizes, it currently presents significant limitations for large-scale SBSP applications. The main drawbacks lie in its overall energy transfer efficiency and atmospheric attenuation. As highlighted in [109], state-of-the-art laser systems typically achieve an end-to-end efficiency (including conversion from electricity to laser and back to electricity) of about 1–10%, with highly optimized systems approaching 15% in laboratory settings. In contrast, microwave-based systems can achieve total transmission efficiencies ranging from 35% to 55% [81]. Moreover, laser beams are significantly affected by weather conditions such as cloud cover, rain, and atmospheric scattering, making them less reliable for consistent terrestrial energy delivery. For these reasons, while laser WPT may be suitable for point-to-point

applications (e.g., satellites, drones, or lunar surface operations), it is currently not viable for large-scale, ground-based SBSP implementations.

Multiple choices have to be made for the system regarding power transmission:

- Microwave or Laser transmission
- Operating frequency
- Transmitting antenna design

These will be developed in detail during the trade-off analysis, assessing their validity based on selected criteria, which should include process efficiency, design and deployment complexity, mass, safety, and environmental impact.

The main research areas requiring focused investigation include improving efficiency, demonstrating long-distance power beaming, and reducing system mass. An interesting development is the “sandwich” panel, explained in Section 2.2.4, which aims to minimize power losses during distribution and reduce system mass.

System	Research Areas
Microwave power transmission	• Safety systems for beam detection and cut-off systems [126] • Balancing increased transmission efficiency with the aperture sizes of antennas and transmission distance. • Precise beam targeting and alignment. • No studies exist on the biological effect of beaming frequency greater than 1GHz at high power density.
Rectenna	• Rectifier device nonlinearity causes impedance changes due to power, frequency, and load variations, negatively impacting efficiency. • Low efficiency of high power rectification
Laser transmission	• **Laser Emitter Optimization** – Enhance pump beam efficiency. – Develop high-efficiency heat sinks and high thermal conductivity packaging. • **Transmission Efficiency** – Customize optical paths for wavelength, beam quality, and medium. – Use Adaptive Optics for real-time beam quality correction. – Implement active tracking systems. – Use power sphere receivers and Fresnel lenses for better power reception. • **Laser Receiving Efficiency** – Develop high-efficiency LPCs matching the laser wavelength. – Select materials suited for specific environments (e.g., GaAs for space, chalcogenides for underwater). – Design efficient heat dissipation structures for stability in high-power applications [125].

Table 2.7: Key research areas for improving WPT systems

In-orbit operations

Operations involving contact of proximity between space vehicles are referred to as In Orbit Servicing (IOS) [77].
One of the latest directions in the space industry is the development of large structures to deploy in space, such as space-based solar power stations, that require to be broken down into modular elements and to be assembled in orbit, in order to comply with the current launchers' limitations. This has increased attention and research in the field of robotics in space, enabling operations such as in-orbit manufacturing, assembling, refueling, repairing, updating, and transferring [56].
Moreover, in-space servicing, assembly, and maintenance (ISAM) operations promote a sustainable paradigm shift in space exploration around Earth. This new approach establishes a dynamic environment where objects in orbit are managed throughout their entire lifecycle, from deployment to disposal, thanks to in-orbit operating vehicles. This would address the space debris challenge, extend the lifetime of satellites, reduce launch costs, and make payload requirements less prohibitive, even for large-scale structures [8], [77].

The project of harnessing solar power in orbit necessitates extensive and complex in-orbit operations, given the large dimensions of the structure, making manual assembly by astronauts unfeasible for practical, economic and risk-related reasons.
For in-orbit assembly, large space structures require a process that is flexible, scalable, and precise, and the level of autonomy of the operation is the most critical criterion and goal for all in-orbit services involved in the mission. In-orbit manufacturing can significantly reduce the costs and complexity of space missions by launching raw materials that are then manufactured and assembled by robots in space. Routine checks for maintenance and in orbit repair are necessary. Therefore, Space-based solar power projects require avdanced technologies to operate multiple complex robots in space.

Space robotics has been utilized since the early 1980s and has undergone significant advancements to date. While technologies for in-orbit services like rendezvous, docking, and robotic manipulations have been successfully flight demonstrated and implemented in several missions (mainly operating in the International Space Station), other capabilities such as autonomous in-orbit assembly of modular structures are currently under research and require further experimentation.

As part of the Horizon 2020 program initiated in 2014, the European Commission funded the "Space Robotic Technologies" Strategic Research Cluster (SRC) with the objective of studying and developing new technologies for space robotics to enhance Europe's competitiveness [31]. The program aimed to explore new frontiers in space robotics is called PER ASPERA and is coordinated by ESA.
Urbina et al., (2023) [112] analyze and simulate the in-orbit assembly process of a solar power satellite based on the SPS-ALPHA architecture, utilizing European technologies.
These include:

- **HOTDOCK**: Standardized interface for robotic manipulation, allowing for in orbit assembly. It is capable of supporting mechanical loads, electrical power, data and thermal loads through a single interface.
- **Multi-Arm Robot (MAR)**: First introduced in ESA MIRROR program [27], it allows for self assembly and self-maintenance of the client satellite. Two robotic arms are attached to a central torso, to enable the assembly of solar reflectors (or any other modular unit) in SPS-ALPHA architecture. The interface between the robotic system and the modules is realized using HOTDOCK

Figure 2.18 shows a demonstration of MAR operating on a modular structure. The two arms, central torso are visible, and it connects to the main structure through HOTDOCK interfaces.

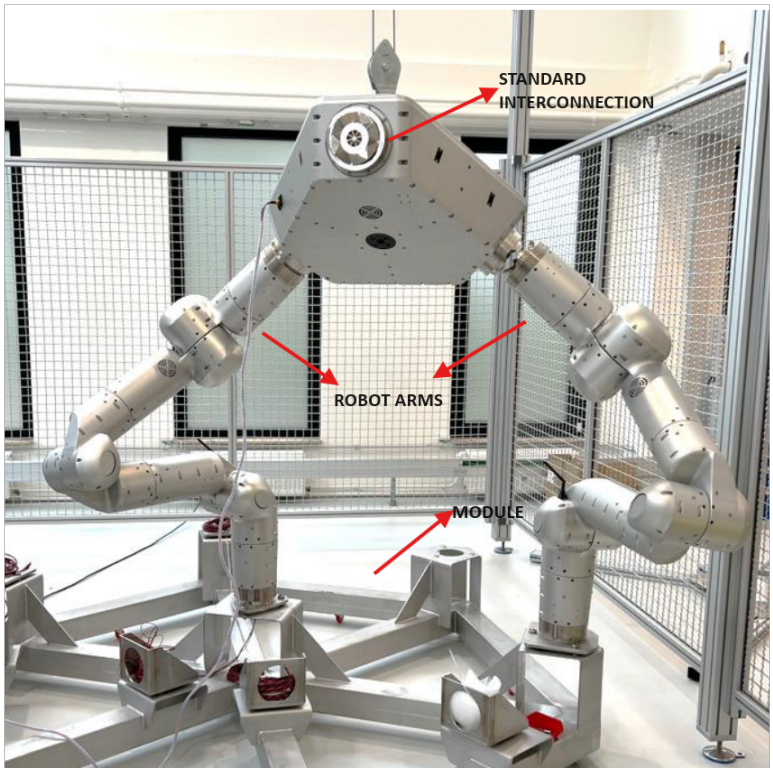

Figure 2.18: Multi-Arm Robot demonstration of operation, [27]

Arney et al. (2023) [8] published a report for NASA, presenting the state-of-the-art of ISAM activities in 2023. The work distinguished 11 categories of applications for space robotics, and summarized the ongoing and past activities in every field, including flight demonstrations, enabling activities or ground experiments. In Table 2.8, the original 11 capability areas have been consolidated into 7 by merging related ones. Each area is briefly described and its potential applications in an SBSP project are highlighted.

Capability	Description	SBSP application
Robotic Manipulation	Manipulate parts of spacecraft, assemble, weld, facilitate integration of large structures	Assist the assembly of structures or other operations
Rendezvous & Proximity Operations, Capture, Docking, and Mating	Interaction between spacecrafts, from docking to be joined in space (mating)	Necessary to perform any interaction between two space vehicles (refueling, orbital transfer, ...)
Relocation	Ability of a space vehicle to change orbital parameters of another spacecraft	Transfer modules from LEO to higher energy orbit (e.g. GEO)
Repair, Maintenance, and Installation	Service a target spacecraft, planned before launch or not prepared	Various
Refueling and Fluid Transfer	Move storable fluids between spacecrafts	Orbital transfer
Structural Manufacturing and Assembly	Produce structures and assemble modules. Produce elements from raw materials delivered from Earth	Assemble deployed modules in space
Recycling, Reuse, & Repurposing	Employ elements in space for new purposes	
Surface Construction	Design and build structures or infrastructures on non-terrestrial surfaces	Non-terrestrial applications of SBSP
Inspection and Metrology	Observation of objects in space to assess their features of interest	Control the state of systems, e.g. solar cells

Table 2.8: Areas for in-orbit operations and potential applications for a SBSP mission

Figure 2.19 displays the activities related to the actualization of ISAM operations, indicating the state of each technology: operational in a mission, flight demonstrated or planned to be demonstrated.

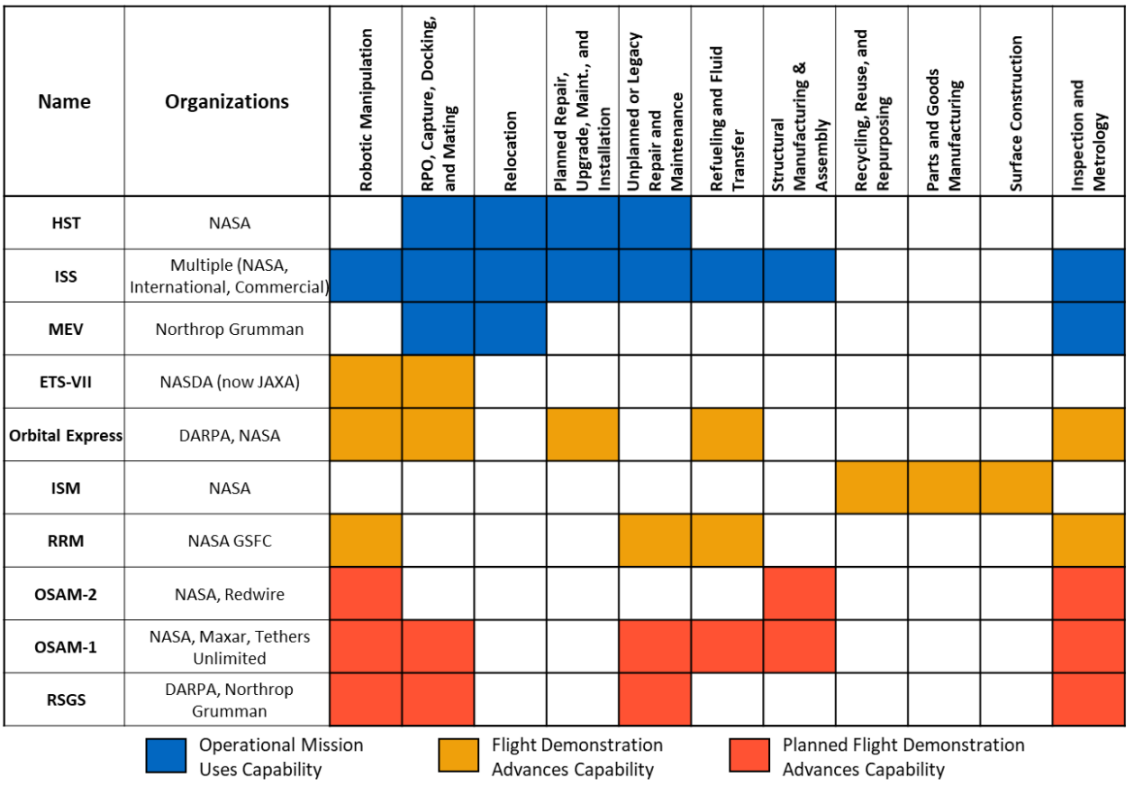

Figure 2.19: ISAM capabilities used in operational missions or demonstrations [8].

Most in-orbit activities are successfully conducted on the International Space Station (ISS), providing an ideal environment for applying ISAM technologies and advancing space robotics.

Robotic Manipulation
Robotic manipulation operations have been used in space since the 1980s, supporting activities in the ISS and Space Shuttle, such as on landers and rovers for Mars exploration, to assist with complex tasks. The current direction in robotic manipulation is to reduce costs, increase capability and flexibility, with the objective of substituting manual operations by astronauts, deemed risky and expensive.

RPO, Capture, Docking and Mating
Interaction between two or more spacecraft is a fundamental capability required for conducting almost every orbital operation. Many space missions have successfully undertaken these activities since the 1960s, with the International Space Station (ISS) playing a critical role in advancing and developing related technologies. State-of-the-art advancements are focused on achieving full autonomy and flexibility, such as developing capture mechanisms capable of adapting to various target objects.

Recent advancements include:

- **Mission Extension Vehicle (MEV-1,2)**: Led by Northrop Grumman, MEV-1 successfully demonstrated in-orbit servicing (IOS) in Earth orbit for in 2020 [73]. The mission aims to extend the lifetime of geostationary orbit (GEO) satellites by docking with nearly depleted satellites and using onboard thrusters and fuel to keep them operational [77].
- **Shijian-21 Satellite Mission**: Designed by the China Academy of Space Technology, the Shijian-21 satellite mission focuses on space debris mitigation. In 2022, the satellite docked with a defunct satellite and towed it 3,000 km above its original orbit [77], [95].
- **End-of-Life Service (ELSA-d)**: Developed by Astroscale and Surrey Technologies, the ELSA project, with its first satellite launched in 2021, demonstrated key technologies for space debris docking and removal.

- **Clear-Space 1**: In 2019, ESA partnered with ClearSpace to develop a satellite for active debris removal (ADR), targeting the VESPA satellite launched in 2013 and orbiting in a slightly eccentric orbit [13].
- **Mission Robotic Vehicle (MRV)**: Following the success of MEV-1 and MEV-2, Northrop Grumman is currently advancing its Mission Robotic Vehicle (MRV), which integrates cutting-edge robotic arm technologies with rendezvous, proximity operations, and docking capabilities inherited from its predecessors. The primary objective is to install mission extension pods on target vehicles—small augmentation propulsion systems that subsequently become owned and controlled by the customer. This capability opens up multiple potential applications including relocation, active debris removal, repair, refueling, and more. MRV capability to dock with non-standard spacecraft expands its flexibility in performing Rendezvous and Proximity Operations (RPO) [73].

This set of operations, from rendezvous to mating, could prove essential for deploying a space solar satellite in orbit, facilitating all necessary on-orbit activities.

Relocation
Orbital transfer of space objects serves various purposes, including the relocation of retired satellites from active orbits for space debris management, changing orbital parameters for mission requirements (e.g., LEO-GEO transfer), and extending satellite lifespans. China's Along-1 mission demonstrated space debris removal for the first time in 2016. Similarly, the Elsa-d mission has contributed significantly to advancing technologies for debris removal. Relocation activities can also prolong satellite life, as in the case of Mission Extension Pods transferred to customer satellites by the MRV.

Repair, upgrade, maintenance, installation
Repair and other forms of intervention on target spacecraft can be planned pre-launch by co-designing both the "client" spacecraft and the servicing vehicles. Interfaces must be installed to facilitate ISAM activities whenever necessary. For instance, the Hubble Space Telescope was specifically designed for servicing operations, which were conducted multiple times during space shuttle missions, with astronauts performing manual operations on the telescope.

Unplanned in-orbit services pose different challenges, as the servicing vehicle must be equipped with flexible interfaces capable of interacting with a wide range of target spacecraft not initially prepared for servicing. The Special Purpose Dexterous Manipulator, known as Dextre, has been serving the ISS since 2008, performing tasks such as maintenance, installation, replacement of small equipment or components, and testing new tools and technologies for future advancements in space robotics [66]. Dextre has also been utilized to interact with legacy spacecraft components that were not originally designed for servicing operations.
Hotdock is an example of a standardized interface for robotic interactions and manipulations in space [112].

Refueling
Refueling a spacecraft in orbit represents an interesting capability to use to extend its lifetime, or enable reusable transfer vehicles.
Orbitfab, a company based in Colorado, has designed, built, tested the first flight-qualified refueling system to operate in space. Rapidly Attachable Fluid Transfer Interface (RAFTI) is a refueling interface with built-in docking capabilities. It has been designed to serve also in geostationary orbits and beyond, and with the function of replacing the fill and drain valves and allow for refueling in orbit, compatible with all main propulsion systems. Its architecture supports the transfer of two independent fluids, and it can store various kinds of propellants (Xenon, High-Test Peroxide, Hydrazine, Water, Kripton, Propene, Ethane) [90].
SpaceX's Starship is designed to enable refueling in low Earth orbit for future Mars missions. SpaceX plans to test on-orbit refueling next year by launching a "target" Starship, followed by a "chaser" Starship a few days later. The chaser will dock with the target to transfer propellant.

In space assembly and manufacturing
Assembly of modules or structures and manufacturing of components in space is the most critical in orbit operation activity that needs to be developed for space-based solar power missions, reducing costs, launch and design complexity.

Jiang et al. ([53]) in their survey of intelligent robotic systems for space applications, classify space intelligent robots based on their applications: space stations, satellites, and large space structures. This study focuses particularly on robotic intelligent systems for in-orbit manufacture, assembly, and maintenance, which are crucial for large-scale structures.

The Skyworker (2001) is the first generation of modular robotic systems designed for in-orbit assembly, detection, and maintenance. Developed by Carnegie Mellon University, Skyworker is a mobile robot that uses reaction forces with other objects to perform its functions. When manipulating an object in space, the robot attaches to the object with a gripper and performs the desired activity with another gripper. It can transport payloads up to several tons over distances of up to half a kilometer [53], [102].

In 2017, NASA's Dragonfly successfully completed its ground demonstration, showcasing its capability for self-robotic assembly of structures in space. The robotic system can install satellite antennas and assemble multiple modular segments of a satellite. Future plans include integrating 3D printing functionality to replace damaged components and build new ones on the target satellite [69].

The SpiderFab project, developed by Tethers Unlimited, Inc., uses 3D printing to construct trusses and assemble them, enabling the modular construction of large structures [53].

Among other projects, NASA worked on OSAM-1 (On-Orbit Servicing, Assembly, and Manufacturing), to demonstrate automated service technologies for refueling and assembling spacecrafts in orbit. Despite its cancellation, OSAM-1 represents a significant step in IOS technologies, including autonomous relative navigation, robotics for spacecraft refueling, and propellant transfer systems [77].

Finally, coordinated by Thales Alenia Space with European partners, EROSS IOD (European Robotic Orbital Support Services In Orbit Demonstrator) aims to demonstrate in-orbit services, with a planned launch in 2026 [116].

In general, increasing attention is being given to all in-orbit operations, with current research emphasizing enhanced autonomy, dexterity, flexibility, and scalability of systems. There is also significant focus on orbital transfer vehicles and technologies for active debris removal, which are being developed by numerous companies worldwide.

2.3.3. Ground segment

The ground segment of the project comprises two main systems: one controls the satellite and manages communications, while the other is dedicated to energy collection, conversion, and distribution — a ground power station. The focus will be directed towards the latter system, as the former is conventional and does not necessitate a unique implementation beyond standard communication and control systems. For a geostationary orbit, one ground power station suffices since the beam remains fixed over a specific location on Earth. In contrast, when other orbit types are selected, multiple receiving stations are necessary to maximize energy collection potential.

Rectifying antenna

The term *rectenna* refers to an antenna integrated with a rectifier circuit. RF waves are captured by the antenna and converted to DC through the rectifier. Subsequently, the DC energy is inverted to AC for distribution to the grid and utilization as electrical power.
For SPS applications involving high levels of power, the receiving station requires large dimensions and is typically composed of an array of multiple rectenna receiving elements, as illustrated in Figure 2.20.

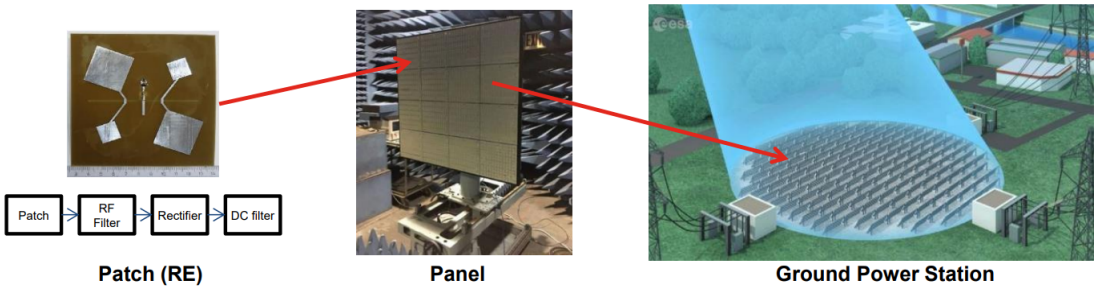

Figure 2.20: Rectenna array components for large scale applications, [92]

A single module of the rectenna array comprises several functional components: an impedance matching network designed to optimize power transfer from the antenna to the rectifier circuit, a rectifying circuit (RF-DC converter) typically utilizing a Schottky diode, and a DC-AC inverter.
The system must be sized to capture the maximum possible energy and designed to optimize conversion efficiency while minimizing power losses [36]. The apertures of the transmitting and receiving antennas are linked through diffraction physics and sized to maximize beam collection efficiency. This efficiency is defined as the percentage of power radiated by the transmitter that arrives at the receiving surface [88]. Rodenbeck et al. [88] present a plot showing beam collection efficiency as a function of τ a parameter dependent on the transmitter aperture (A_{TX}), receiver aperture (A_{RX}), power beam wavelength (λ), and distance between transmitter and receiver (d_{TRX}). Increasing the operational frequency reduces the required antenna apertures to achieve a certain collection efficiency. As expected, transmitting over longer distances necessitates larger antennas.

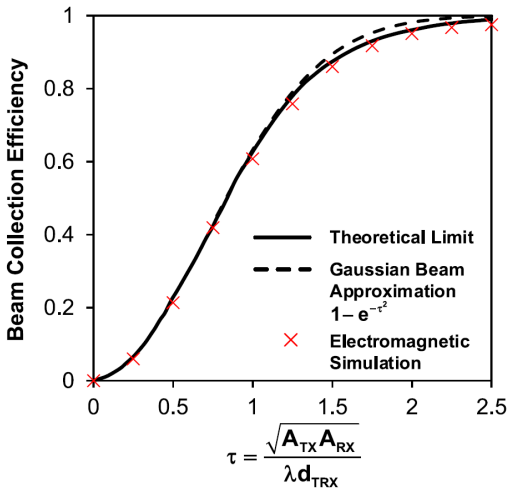

Figure 2.21: Beam collection efficiency as a funcion of τ, where $\tau = \frac{\sqrt{A_{TX} \cdot A_{RX}}}{\lambda \cdot d_{TRX}}$

RF-DC rectifier circuit

The primary criterion driving rectenna design is the conversion efficiency from RF to DC:

$$\eta_{PC} = \frac{P_{OUT}}{P_{IN} - P_{REF}}$$

where P_{REF} is the reflected power due to impedance mismatch between the antenna and rectifying circuit.
Several key losses can occur in the circuit:

- **Threshold and reverse breakdown voltage of the diode**: The threshold voltage of a diode acts as a barrier, limiting the minimum incoming power required to activate the circuit and thereby affecting efficiency at low power levels. Schottky diodes are advantageous in Solar Power Satellite (SPS) systems for low power harvesting due to their low threshold voltage, enabling higher efficiency at low power levels, and their low junction capacitance, which supports operation at higher frequencies. Conversely, the reverse breakdown voltage limits efficiency at high levels of incoming power [113]. On the other side, the reverse-breakdown voltage limits the efficiency at high levels of incoming power [113].
- **Impedance matching**: To mitigate impedance mismatch—where part of the incoming power is reflected, reducing efficiency—an impedance matching system is crucial.
- **Device Parasitics**: General losses in the diode circuit, including junction resistance and power dissipation.
- **Harmonic generation**: Diode-generated frequency harmonics can result in the loss of power that needs conversion, with these losses increasing at higher incoming voltages [113].

Figure 2.22 from [111] illustrates the state-of-the-art efficiencies of rectifiers and rectennas across different operating frequencies as a function of incoming power, expressed in dBm (decibel-milliwatts) [4]. It is important to consider that most designs depicted in Figure 2.22 represent individual rectenna cells rather than arrays, thus total array efficiency must be carefully evaluated and compared.

Efficiency decreases with increasing frequencies due to diode junction resistance and capacitance. Conversely, efficiency improves with higher levels of incoming power, moving away from the risk posed by the threshold voltage.

[4] One dBm expresses power in the logarithmic decibel scale respective to milliwatss. dBm $= 10 \log_{10} \left(\frac{P_{\text{mW}}}{1} \right)$

Designing an RF-frequency rectifying antenna involves balancing the operating frequency, which impacts efficiency and losses through the atmosphere, with antenna aperture size and the choice of rectifier circuit—specifically its threshold and reverse breakdown voltages. These considerations vary depending on the application. Note that the plot extends up to 40 dBm of incoming power, equivalent to 10 W.
Initial demonstration systems for space-to-Earth power beaming typically operate at lower incoming power levels to align with operational feasibility (designing a GW-scale demonstrator initially is impractical).

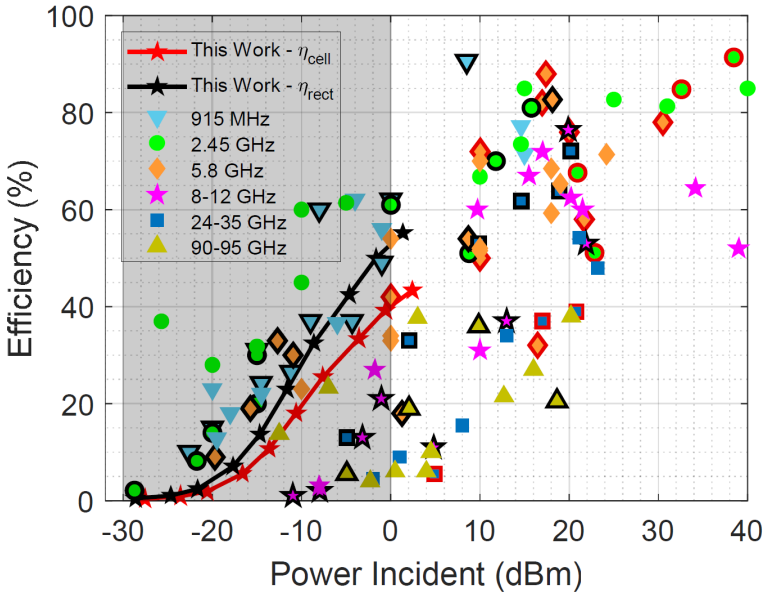

Figure 2.22: Rectifier and rectenna efficiencies as a function of incoming power for various operating frequencies. Markers outlined in red denote rectenna efficiencies plotted against power incident into a rectenna cell. Markers outlined in black represent rectifier efficiencies estimated from rectenna measurements. The shaded area indicates estimated rectifier power levels for the power densities specified by the SSPIDR program. η_{rect} = rectifier efficiency. η_{cell}= rectenna efficiency [111]

Latest Developments in Rectenna Technology

Rectifying antennas for receiving microwave power have been studied for the last 60 years. One of the main challenges in rectenna design is managing high incoming power.
In 2015, researchers at Sichuan University built a rectenna array for an input power of 41 dBm, achieving 68% RF-DC conversion efficiency using half-wavelength branches to avoid overheating. In 2018, researchers from Korea developed a rectenna capable of handling and converting 100 W of incoming power.

The Air Force Research Laboratory (AFRL) is currently working on the SSPIDR (Space Solar Power Incremental Demonstration and Research) project. Among the initiatives, Arachne will demonstrate space-to-Earth power beaming and optimize in situ beam formation. This will involve developing a ground power station, with the launch planned for no earlier than 2025.

Tierney et al. [111] present the first rectenna-array prototype developed for the SSPIDR project. This modular, scalable X-band rectenna is designed to receive power beaming at an RF frequency of 10 GHz. The incident power density ranges from 1 mW/m^2 to 1 W/m^2; the SSPIDR demonstration will not achieve higher incident power levels. Arachne, the main flight experiment of the SSPIDR project, will play a fundamental role in advancing the enabling technologies for SBSP.
Arachne will test aspects of power collection, conversion, and transmission for various spacecraft orientations relative to the Sun and Earth, gathering data for the design of a large-scale system. Sanwich tiles will be used to collect, convert and beam solar power, allowng for a flight demonstration of this promising technology. The energy will be captured on Earth by a rectifying antenna, which will convert the RF into usable power [55].

Laser power receiver

In the case of laser power beaming to Earth, the ground receiving station collects the laser source, converts it to usable electrical energy, then distributed to the grid.
On the receiving end of a laser power system, either photovoltaic panels or heat-based conversion systems are present [106].

Laser converters have a power conversion efficiency that depends on the material used and wavelength of the laser beam: Zheng et al. [125] presented a survey of the recent progress in laser power transmission, with a peak of PCE for laser converters at wavelengths of 850nm and 950nm, reaching values of 75 %. Nonetheless, the state-of-the-art overall efficiency of a laser power transmission system is between 10% and 25%.

2.3.4. Key limitations and gaps

Although a space-based solar power (SBSP) project is currently deemed conceptually feasible, it remains technologically immature and unproven at scale: several critical advancements and systemic developments are necessary before any large-scale demonstration or implementation can occur [107]. These include repeated heavy-lift launches, autonomous in-orbit assembly, extreme thermal regulation, and long-distance high-efficiency wireless power transmission. These complexities imply that the energy generated must not only be reliable but also cost-competitive with terrestrial alternatives, setting a high bar for both performance and efficiency.

In recent years, technological progress in photovoltaics, space robotics, and microwave transmission has brought SBSP closer to reality, as discussed in Section 2.3. However, substantial challenges remain. This section highlights current limitations, research gaps, and systemic drawbacks that must be addressed. The overview in Table 2.9 outlines Technology Readiness Levels (TRLs), based on the European Space Agency classification [4], and identifies key research domains.

Importantly, while SBSP offers the promise of uninterrupted, space-based renewable energy, it also presents a number of disadvantages and risks that must be considered:

- High initial investment and cost uncertainty: SBSP requires massive upfront capital for launch vehicles, orbital infrastructure, and maintenance technologies. The cost recovery model remains speculative, especially when compared to ever-cheaper terrestrial renewables like solar and wind.
- Space debris and congestion: The deployment of large structures in orbit raises concerns about collisions with existing satellites or debris. The absence of standardized decommissioning protocols (TRL 2) for such structures compounds this risk.
- Thermal management: Maintaining the temperature of high-density solar panels in the harsh thermal environment of space is still an unresolved issue (TRL 5). This is crucial, as excessive heat reduces photovoltaic efficiency and can damage equipment.
- Regulatory and geopolitical challenges: The use of geostationary orbits for large energy satellites could lead to diplomatic and legal disputes regarding spectrum allocation, orbital slots, and energy beaming rights across borders.
- Public perception and safety concerns: Beaming energy via microwaves or lasers, even if tightly focused, raises safety concerns, which could become a barrier to societal acceptance.

The summary of existing TRLs and research areas is provided in Table 2.9. Further granularity for subsystems like solar cells and power transmission technologies is presented in Tables 2.6 and 2.7, respectively. These layered insights are essential for identifying research opportunities and guiding future SBSP system architecture.

System	TRL	Research Areas
Large solar reflectors in space	2-3	Develop and deploy large scale mirrors in space. Today limited dimensions
High efficiency PV cells	7	Improve efficiency, study cooling techniques for high power intensity. See Table 2.6
Sandwich module concept	3	Simulate functioning. Test in relevant environment
CPV in space	3	Demonstration in space, need for cooling techniques
Wireless Power Transmission	2-3	Develop and simulate systems for long distances and high power, increase efficiency. Balance size and efficiency of antennas. See Table 2.7
Thermal management	5	Management of high power on PV panels in space not demonstrated
In orbit assembly	3	Ground test or demonstration of large structure assembly in space
Satellite decommissioning	2	No technique defined for decommissioning of large scale structures in space

Table 2.9: Summary of Research Areas and TRLs [93]

2.4. Non-terrestrial applications of SBSP

The context and background of space-based solar power (SBSP) for Earth applications have been extensively discussed, with the challenges that it poses and its importance as potential solution to the global energy challenge. However, the project of collecting available solar power in space offers interesting opportunities and could enable new frontiers for space exploration missions, where a continuous supply of energy is required.
First, having solar power stations in orbit could power satellites and allow them to maintain their functions for longer periods without relying on limited onboard power reserves, extending their operational lifetimes.

Space missions currently rely on photovoltaic (PV) arrays or radioisotope thermoelectric generators (RTGs) for power. RTGs are typically used for missions to the outer planets of the solar system, where solar irradiance is insufficient to meet energy demands. However, these power sources have limitations that SBSP could address.
The researches on the topic of solar power in space for interplanetary mission are focused on Moon and Mars applications.

It is important to consider that non-terrestrial applications of SBSP have different characteristics and face other challenges compared to Earth-based power beaming. For Moon missions, laser power transmission may be the most effective method for power beaming. The Moon's lack of atmosphere reduces the challenges associated with laser transmission, and the ability to easily direct and focus the beam allows for precise power delivery to specific locations [12].

Current trend in the space industry include the research to colonize Mars, building a permanent base station. In view of this, Space-X's Starship has been designed to transport 100 tonnes to Mars, after refueling on orbit. On Mars, the average solar irradiance is 590 W/m^2 and sandstorms affect solar collection on the surface of the planet, making it less efficient. Therefore, most missions are powered by RTGs, which supply the needed energy to run avionics on landers or rovers.
The project of a permanent base station requires advanced power solutions, able to provide continuous and high energy supply. Among the alternatives, RTGs, while reliable, are limited in power output and cannot fulfil the energy demands of the project, and nuclear power plants, which could meet the power requirements, pose an excessive risk. Here, SBSP could provide a viable solution by positioning power stations in orbit or deploying constellations of satellites to deliver energy [12].

Significant interest is also given to new concepts for moon missions, where space solar power could facilitate the development of new projects, such as in-situ resource utilization (ISRU) and establishing habitat base stations for further interplanetary travel.
After decades of researches on the surface of the Moon, the Moon Mineralogy Mapper (M3) on Chandrayaan-1 provided the first mineralogical map of the its surface, and in 2009 showed concentrations of OH/H_2O in the polar regions and craters, redefining perspectives for future projects on the celestial body [80]. These regions, although promising for habitation, suffer from limited sunlight and low temperatures. To support continuous operations in these areas, a lunar-based SBSP system could be deployed in orbit to provide reliable energy.
Moreover, the Lunar Crater Observation and Sensing Satellite (LCROSS) mission, designed to detect hydrogen concentrations over the permanently shaded craters in the Moon [65], showed that the highest presence of hydrogen is in the south polar region, opening a new possibility for in situ resource utilization, extracting water in the form of ice present in the substrates of the Moon. This kind of operations would require continuous power delivery, which, given the low temperatures and level of sunlight of the region, cannot be provided by PV arrays on the ground.

Orbiters, which require continuous power for avionics and payloads, currently depend on solar panels or RTGs. However, these power management systems can account for 10-25% of a satellite's mass. An SBSP system could alleviate these issues by offering continuous, mobile power, thus increasing payload capacity and enhancing the effectiveness of interplanetary missions [12].

Baraskar et al. [12] propose a concept involving small solar power satellites, known as E-sats, each capable of generating 10 kW of power. These E-sats would demonstrate the feasibility and efficiency of SBSP in space. By deploying multiple E-sat constellations, continuous power could be delivered to various remote locations such as landers, rovers, orbiters, or surface base stations. This approach would mitigate launch challenges, as the smaller size of E-sats facilitates easier deployment and operation. An illustrative example is displayed in Figure 2.23.

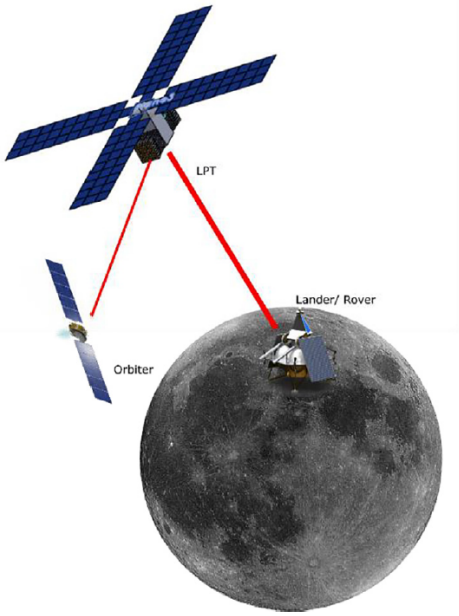

Figure 2.23: SPS concept design for Moon mission [12].

A project commissioned by the European Space Agency and conducted by a group of students at Delft University of Technology, developed a conceptual design for a space power system to deliver energy to the South pole of the moon. The design consist in a constellation of 110 satellites deployed in a highly-elliptic frozen lunar orbit. 77 satellites are in view at any time, each of them delivering 117 KW of power, transmitted via laser beaming.

Finally, Tekbıyık et al. [110] in their study look into the option of transmitting power wirelessly to the surface of Mars, to power zero-energy (ZE) devices, namely those devices with ultra low power receivers. The performance of the system are investigated and the effects of pointing errors and dust storm on the efficiency of various designs is analyzed, with the development of a simulation tool.

2.5. Conclusions of the Literature Review

This chapter has provided a comprehensive overview of space-based solar power (SBSP) systems, highlighting their unique characteristics, technical development, and associated challenges. SBSP emerges as a promising long-term solution for global energy supply due to its operation in an orbital environment, where access to solar radiation is continuous and uninterrupted by atmospheric or diurnal variations.

Throughout the evolution of SBSP concepts, several architectural proposals have been developed, including the SPS-ALPHA design. Despite this progress, the implementation of SBSP still faces significant technological and economic challenges. Key limitations include the efficiency and feasibility of wireless power transmission, thermal regulation in the space environment, the complexity of in-orbit assembly, and the substantial costs associated with launching and deploying large-scale infrastructure in space.

The main subsystems that compose SBSP satellites, such as solar collectors, power conversion units, thermal management systems, and transmitting antennas, have been examined in detail. Among them, thermal control and wireless power transmission present the most critical challenges. These subsystems are exposed to intense solar fluxes and operate under extreme environmental conditions, demanding advanced materials, efficient control strategies, and integrated design approaches to ensure reliable operation.

In addition to these technical considerations, the literature has revealed several knowledge gaps that limit the further development and implementation of SBSP systems. Notably, there is a lack of experimental validation for proposed architectures and limited performance data on integrated subsystems (particularly regarding thermal behavior). These uncertainties underscore the importance of continued research in subsystem modeling, technology demonstration, and comparative performance analysis.

Beyond terrestrial applications, SBSP has also been proposed as a potential energy source for future lunar or Martian habitats, as well as for space-based infrastructure and mobile platforms such as drones or aircraft. Although these applications remain largely speculative, they represent exciting directions for future investigation and technological evolution.

The insights gained through this literature study directly inform the development of the thesis research plan, which is presented in the following chapter. In particular, the need to evaluate the energy performance of SBSP systems and address the thermal challenges associated with modular designs such as the integrated tile architecture has emerged as a central focus. Among the three primary domains in which SBSP faces major challenges, technological feasibility, economic viability, and energy performance, the first two have received considerable attention in the literature, with several studies proposing advanced design solutions and economic assessments. In contrast, the energetic dimension of SBSP, including a comprehensive understanding of its efficiency and sustainability as a power generation concept, remains underexplored. This lack of focused energy analysis is particularly critical given the scale and ambition of SBSP systems, which must ultimately prove not only technically feasible and economically viable, but also energetically justified. Addressing this gap is a core motivation of this thesis. The next phase of this work is therefore dedicated to a detailed assessment of the energy performance of SBSP systems, with specific attention to the integrated tile concept and the influence of thermal constraints on its operation and overall efficiency.

3

Research Plan

Building upon the findings and gaps identified in the literature review, this chapter outlines the research plan that structures the remainder of this thesis. While space-based solar power (SBSP) has been explored from technological and economic standpoints, a key insight from the literature study is the relative lack of dedicated energy performance analyses. As discussed in Chapter 2, this gap is especially evident in the context of novel modular architectures such as the integrated tile. Addressing this lack of energetic evaluation, and particularly how thermal constraints influence it, constitutes the central objective of this research.

This chapter presents the motivations, research questions, and methodological approach adopted to carry out the study. The plan is designed to assess and compare the energy performance of SBSP architectures, especially the integrated tile concept, by considering both life-cycle metrics and thermal behavior.

3.1. Research Objectives and Questions

The primary objective of this thesis is to evaluate the energy performance of a modular SBSP architecture based on the integrated tile concept and to understand the role of thermal management in shaping its feasibility. The work aims to:

- Assess the energy performance of SBSP systems relative to terrestrial PV systems.
- Compare the performance of a conventional SBSP architecture with that of an integrated tile-based concept.
- Analyze the thermal challenges posed by the integrated tile and evaluate their impact on overall energy performance.

These objectives give rise to the following research questions:

- **RQ1:** How does the life-cycle energy performance of space-based solar power systems compare to terrestrial solar power systems in terms of lifetime energy efficiency, considering variations in architecture?
  - **RQ1.1:** What are the differences in energy performance between terrestrial solar power systems and space-based systems, for a defined baseline architecture?
  - **RQ1.2:** How does the integrated tile architecture affect the net energy performance compared to the baseline?
- **RQ2:** What are the main thermal challenges of the tile component in a SBSP system, and how do they impact the system's overall energy performance?
  - **RQ2.1:** How does heat accumulation in the integrated tile affect system efficiency, and what are the consequences for its energetic performance?

- **RQ2.2:** What thermal management strategies can be implemented to meet thermal requirements, and what is their impact on the energy performance of the system?

The methodology followed in this thesis is designed to address the defined research questions. The first step involves the definition of a case study focused on the integrated tile architecture, a modular concept that serves as the central design reference for the study. In this phase, the system is sized according to orbital parameters and mission requirements, and two additional configurations are introduced for comparison: a conventional SBSP architecture based on ESA's trade-off study, and a terrestrial photovoltaic (PV) power station. These cases establish the baseline for a comparative analysis that evaluates the energy performance of space-based systems in relation to a ground-based alternative. The energy analysis is developed from a life-cycle perspective, with the goal of assessing, through specific metrics, the net efficiency of the different configurations, while also addressing a key gap in the literature regarding the energetic competitiveness of SBSP architectures.

However, due to the harsh thermal environment in space and the high energy fluxes involved, thermal behavior becomes a critical factor in determining whether the theoretical energy output of a system can actually be harvested and used efficiently. In particular, the integrated tile architecture poses unique thermal challenges, as its compact and modular nature makes it more susceptible to heat accumulation. For this reason, the energy analysis must be coupled with a detailed thermal analysis to obtain more reliable performance metrics.

Accordingly, a dedicated thermal model of the integrated tile is developed using ESATAN-TMS. This model captures the thermal behavior of the component in orbit, quantifying the extent of heat accumulation and evaluating the effectiveness of passive thermal control strategies, such as radiators and surface coatings. By understanding how thermal limitations constrain power production, the thermal study directly informs the energy model. In the final phase of the methodology, the outcomes of the thermal analysis are integrated into the energy performance framework, enabling a refined re-evaluation of system efficiency. This approach ensures that the thesis does not treat energy and thermal analyses as isolated tasks, but as mutually dependent components of the same performance-driven assessment.

This structure ensures a logical progression from contextual foundation to technical analysis, with each chapter building upon the insights and data of the previous ones. The overall aim is to provide a holistic feasibility assessment of SBSP systems, with a focus on energetic performance and the influence of thermal constraints in modular architectures.

4

Mission cases definition

As outlined in Chapter 1, the purpose of the energy analysis is to establish a framework for assessing the efficiency of an SBSP mission, to allow for comparisons among different space-based designs and a terrestrial solution over their operational lifetime. To achieve this, specific mission architectures must be selected to estimate energy demand and production, as these depend on defined specifications, including materials, orbit, and system configuration.

For this reason, a scenario describing a ground-based solar plant is presented, and a baseline reference architecture for SBSP is adopted, based on a Commercial study conducted by ESA and Thales Alenia Space ([32], [34], [92], [6]), which is available in ESA's official repository [30]. These, will be compared to the case study of a SBSP architecture based on the concept of the integrated tile.

The integrated tile concept architecture is also included in the energy analysis, allowing for a direct comparison with alternative designs and a quantitative estimation of its performance. While the first reference architecture is derived from an existing trade-off study, a preliminary component selection and sizing is necessary for the integrated tile concept to ensure a valuable evaluation.

This chapter presents the selected architectures, providing the necessary technical details required for the subsequent energy analysis and comparison.

4.1. Case 1: Ground-based solar power station

4.1.1. Plant Specifications

The first case presented is a very large-scale ground-based photovoltaic plant. The study carried out by Ito et al. [47] is taken as a reference for some aspects.

Carpentras, France, is selected as plant location because reliable, location-specific data for this region is already available. The plant consists of photovoltaic modules, and balance of System (BOS) components (supporting structures, inverters, trackers, electrical wiring, etc.).
The data needed for sizing is taken from the Global Solar Atlas [120].

The platform relies on Solargis data [98], updated to the current year, to provide key metrics such as Global Horizontal Irradiance (GHI)[1] and Photovoltaic Power Potential[2] (annual averages). These values help estimate the total energy output of the PV plant, supporting feasibility studies and project planning.

[1] Total amount of solar radiation received per unit area by a horizontal surface. It encompasses both direct sunlight and diffuse sky radiation

[2] Estimated annual energy output per unit of installed photovoltaic (PV) capacity, typically measured in kilowatt-hours per kilowatt peak (kWh/kWp).

Table 4.1 presents the site-specific data, while Figure 4.1a and Figure 4.1 display maps showing the global horizontal irradiance and photovoltaic power potential, respectively, as provided by [120].

Parameter	Value
Longitude [°]	4.73 E
Latitude [°]	44.58 N
Altitude [m]	74
Specific Photovoltaic Power Output	1581.9 kWh/kWp
Global Horizontal Irradiation (GHI)	1598.2 kWh/m²/year 4.379 kWh/m²/day

Table 4.1: Annual Averages for the PV System **cite atlas and solargis**

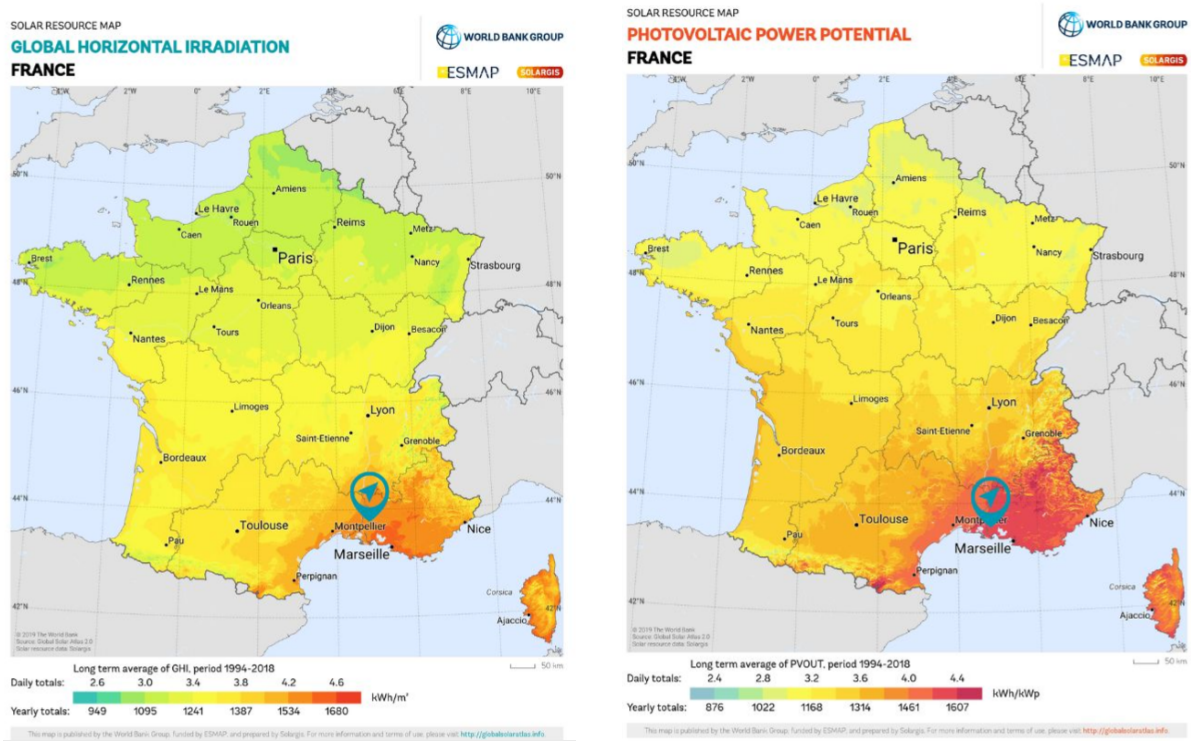

(a) Global Horizontal Irradiation (GHI) for Carpentras, France

(b) Photovoltaic power potential for Carpentras, France

Figure 4.1: Solar resource data for the selected location [120], [98]

4.1.2. Sizing the Ground PV Plant

The design of the plant is driven by the requirement for average daily energy production. This approach ensures consistency in the comparative analysis with the space-based counterpart, which is also designed to deliver a specific amount of energy to the grid (1 GW of continuous power, i.e., 24 GWh on average per day). Sizing the ground-based system solely based on nominal (or peak) power[3]—1 GW in this particular case—would be inaccurate, as its actual output is affected by several factors, including geographic location, atmospheric conditions, surface reflectivity, and system-specific technical losses. Designing the system to meet a specific daily energy target, instead, inherently accounts for these losses, as they are all included in the concept of capacity factor. This factor is already embedded in

[3]Power that the system would generate under Standard Test Conditions (solar irradiance of 1000 W/m², air mass of 1.5, representing sunlight at 35°N latitude in summer, and cell temperature of 25°C) [7]

the Global Horizontal Irradiance (GHI) value used to size the system, providing a more accurate and robust design basis. Although this results in a larger required surface area, it provides a meaningful basis for comparison.

To estimate the area required for the PV plant, two key factors are considered: the available solar irradiance and the system's overall efficiency. The Global Horizontal Irradiance (GHI) values from Table 4.1 serve as the reference for incoming solar energy, with particular focus on the daily average.

The plant is sized starting from the average daily energy output expected from the space-based solar station. By dividing this energy value by the average GHI at the selected location and by the total system efficiency, the required solar cell area is calculated. However, since additional spacing between modules is necessary to prevent shading and allow for maintenance, the total land requirement exceeds the calculated active cell area.

The technology considered is modern multijunction Gallium Arsenide (GaAs) solar cells. The specific module values are taken from recent technology surveys, although the efficiency for MJ cells has been updated from an outdated study ([47]) to 36%, ensuring consistency with the assumptions made for space-based solar cells.

The requirement for daily energy production is derived from the space-based system delivering 1 GW of continuous power—equivalent to 24 GWh per day (neglecting eclipse periods). Dividing this value by the GHI from Table 4.1 and the system's total efficiency yields a required solar cell area of 21,922,813 m².

The total efficiency factor (see Table 4.2) accounts for losses due to electrical conversion, cabling, temperature effects, and other system inefficiencies (details are provided in [47]).
To account for the performance degradation of the solar cells and other plant components, a yearly linear degradation rate of 0.7% is applied throughout the system lifetime, which is estimated to be 30 years. The degradation factor and system lifetime are based on current industry data and findings from net energy analyses available in the literature for ground-based PV plants [25], [26], [82], [83]. The impact of these parameters on the overall energy performance, specifically the Energy Returned on Energy Invested (EROEI), will be explored through a sensitivity analysis.

All key results and system details are summarized in Table 4.2.

System Characteristic	Specification
Technology	Multijunction GaAs/InGaAs
Efficiency	0.36 (solar cells), 0.25 (system)
Solar cells area	21,922,813 m²
Estimated Annual Energy (no degradation)	8,760 GWh
Materials*	6700 tons (steel), 40000 tons (concrete)
Yearly degradation factor	0.7%
System lifetime	30 years

Table 4.2: Sizing and Material Estimates for the Ground-Based PV System

*The material estimates for steel and concrete are based on the computations in [47] and [72].

4.2. Baseline SBSP Architecture from ESA Trade-Off Study

The selection of this baseline SBSP design as reference architecture for the energy analysis conducted in this study, is justified by the fact that it was developed recently (2023) using up-to-date data, detailed insights into the advantages and disadvantages of different designs and solutions, and a comprehensive evaluation of both generic and technical aspects across major mission subsystems. The selection of SBSP architectures was based on a structured trade-off evaluation considering both general and technical factors, as summarized in Table 4.3. Thus, building upon this trade-off study ensures consistency in methodology and evaluation criteria, while providing a solid baseline for further analyses. The trade-off methodology and details can be found in [6].

Criteria	Description
General Criteria	
Cost	Relative cost of the proposed solution
Energy expenditure	Energy Returned on Energy Invested across the system lifetime
Social acceptance	Public acceptance of the proposed solutions
Environmental impact	Carbon footprint of the proposed solutions
Technical Criteria	
Mass / Area / Volume	Physical dimensions of the analyzed solutions will be assessed and quoted
Design Complexity	Degree of structural and functional intricacy in the system architecture
Deployment Complexity	Difficulty in launching and assembling the SBSP system
Operational Complexity	Difficulty in operating, maintaining, and decommissioning the SBSP system
Failure Tolerance	Capability of the solution to withstand failures and performance degradation
Capacity Factor	Amount of power the solution can provide
Modularity	Capability of the analyzed solution to be realized with separate parts that, when combined, form a complete whole
Scalability	Capability of the analyzed solution to be scalable in performance
TRL / Heritage	Technology maturity of the proposed solution
Lifetime	Capability of the analyzed solution to comply with the specified functionalities for the entire lifetime while minimizing maintenance

Table 4.3: Trade-off Evaluation Criteria, [6]

4.2.1. Trade-off summarized

Launch segment: operational orbit and transfer

The first design decision concerned the operational orbit, with geostationary orbit (GEO) and eccentric orbits being the primary options considered. By applying the defined trade-off criteria, GEO was selected as the most suitable orbit for the mission. As for orbital transport to the final destination, the system is first launched into Low Earth Orbit (LEO) and then transferred to Geostationary Orbit (GEO) via a Geostationary Transfer Orbit (GTO).

Space segment: power collection and pointing

For the solar power satellite architecture, the first systems to be selected were the power collection system and a pointing solution to address the challenge of simultaneously:

1. Pointing the transmission interface towards Earth
2. Orienting the power collection system towards the Sun

Specifically, for the power collection system, the options included the use of reflectors/solar mirrors or direct conversion through solar cells; for the pointing system, the options included rotation across the electrical, optical, or transmission interface, or a geometric solid-state solution.

Following the selection of the power collection and pointing system, further trade-off assessments were conducted for:

- **Solar cells technology**: Choosing between concentrated and conventional photovoltaics and selecting the appropriate solar cell type.
- **Transmission system**: Evaluating options for DC-to-RF conversion, determining the operating frequency, and selecting the antenna architecture.

Since a detailed breakdown of the trade-off methodology is beyond the scope of this study, only the final selected architecture is presented, focusing on the key characteristics relevant to the upcoming analyses.

4.2.2. Selected architecture

Applying the evaluation criteria to the various options, the outcome of the trade-off analysis has led to the definition of the reference architecture, which includes the following key selections:

System Component	Value/Selection	Justification
Orbit	Geostationary Orbit (GEO)	Chosen for its continuous Earth coverage and optimal power transmission conditions.
In-Space Transportation	LEO to GEO Transfer	Injection in Low Earth Orbit (LEO), followed by orbital transfer to GEO through an intermediate transfer orbit.
Solar Cell Technology	Perovskite Cells	Chosen for their high power/-mass coefficient.
DC to RF Power Conversion	Solid State Power Amplifiers (SSPA)	Selected for their reliability and efficiency.
Wireless Power Transmission Frequency	5.8 GHz	Selected based on efficiency and regulatory considerations.
Ground Power Station (GPS) Location	On-shore, Spain	Strategically positioned for efficient power distribution.

Table 4.4: Key System Components and Their Justifications

The selected architecture, depicted in Figure 4.2, will serve as one of the case scenarios for the energy analysis, forming the basis of the study. It will then be compared with the case study of the integrated tile, which will be defined and preliminarily sized in the next section.

The key values relevant to the analysis are presented below and summarized in Table 4.5.

Parameter	Value
Area PV	6 km²
Mass PV	1870 tons (density 0.3 kg/m² for PV assembly)
Phased array antenna area	0.75 km²
Phased array antenna mass	250 tons (density 0.5 kg/m²)
Estimate Annual Energy	8760 GWh

Table 4.5: Baseline SBSP system specifications

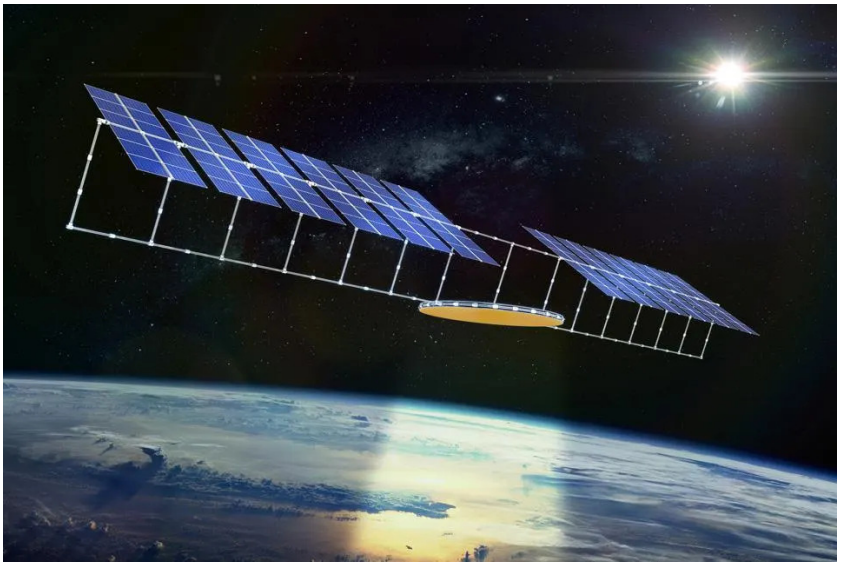

Figure 4.2: Baseline SBSP architecture from trade-off

4.3. Alternative SBSP Architecture: Integrated Tile Concept

Regarding the alternative solution, case study at the center of the present work, it is based on the concept of an integrated tile architecture, which consolidates power collection, conversion, and transmission within a modular structure and lies at the core of the present work. Current SBSP concepts, such as SPS-Alpha and CASSIOPeiA, already incorporate this component in their design, as described in Chapter 2.
This architecture is of particular interest in this study because certain design characteristics make it a highly promising yet underexplored solution for mass and cost savings concerns, and therefore energetic optimization of the mission.

Designing a solar power satellite architecture in full detail is beyond the scope of this study. Instead, the focus is primarily set on the thermal and energetic processes affecting the tile component.
For other subsystems, details regarding sizing and components are taken from an existing reference architecture, SPS-Alpha, developed by John Mankins ([62], [61], [108]) This architecture has a comprehensive dataset available, with information on components, materials and efficiencies. For such a novel and largely unexplored concept, having a well-documented reference architecture is particularly valuable, especially for secondary systems.

Incorporating the three main functions of the mission (power collection, DC to RF conversion, and phased array transmission), this component offers high compactness and modularity. The tile architecture significantly reduces the power distribution and transmission paths and avoids the use of large conductive rotating joints, hence the losses in the distribution of power through cables over long distances from the PV system to the power conversion section. At the same time, it has the potential to reduce mass and design complexity. Integrating three subsystems in one component also offers potential for a reduction in mass and an easier deployment of the modules in space.

4.3.1. Trade-off procedure

To construct the case study and carry out the analyses, the main systems of the mission are defined. These choices are primarily informed by the literature; however, as previously mentioned, only a limited number of studies have addressed this topic, and many are outdated. Consequently, some of the considerations on efficiency or components need to be revised.

For most systems and segments of the mission, the results from trade-offs performed by Thales Alenia and ESA remain applicable and valid. However, the architecture of an integrated tile introduces new challenges, requiring revised criteria and weighting. For subsystems outside the scope of this study, such as structural elements or reflectors, the architecture and design are entirely inherited from the reference architecture provided in [62],[61]. For other subsystems, architecture selection is based on dedicated trade-off analyses.
Using tools from systems engineering, different options are assessed for each relevant subsystem. The set of evaluation criteria is presented in Table 4.7, with their significance level indicated as a weight factor from 1 (low significance) to 5 (high significance), based on mission requirements and key performance factors. While not all criteria apply to every subsystem, the unified framework ensures consistency and comparability across trade-offs. To facilitate the evaluation process, each option is scored on a qualitative scale from 1 (very poor) to 5 (very good).
Where calculations require a reference mass, for instance, when mass impacts cost or launch constraints, a nominal mass of 1000 tons is assumed. This value serves only as a consistent baseline to guide comparisons and does not affect the relative outcome of the trade-off.

Criterion	Description	Weight	Rationale
Cost	Cost of developing, testing, and deploying the analyzed solution.	3	In space missions, cost is a major constraint. However, in the SBSP context, high initial investments may be acceptable if balanced by long-term energy delivery benefits.
Deployment Complexity	Difficulty and risks in deploying the system in orbit.	4	One of the most critical aspects of SBSP, due to the scale of structures involved. Deployment feasibility is currently a major technological challenge.
Operational Complexity	Difficulty in operating and maintaining the system once deployed.	4	Due to the system's scale and remote operation, minimizing operational complexity is key to mission reliability and longevity.
Mass	Weight of the subsystem, affecting launch cost, deployment, and system integration.	4	Mass is a key factor in space design. It directly impacts feasibility and is one of the first parameters to optimize.
Output Power	Electrical power delivered to Earth. Measures the efficiency and performance of subsystems.	5	Central to mission success. Maximizing output power is the primary driver in subsystem selection and optimization.
TRL	Technology Readiness Level: maturity of the technology from concept to operational status.	3	Though usually critical, in SBSP the TRL is moderately weighted since many technologies are still emerging and projections are made with assumed future development.
Failure Tolerance	Ability to withstand and recover from failures.	4	In large, complex space systems, failure tolerance ensures continuity and mitigates mission-critical risks. Redundancy and robustness are vital.

Table 4.6: Evaluation criteria and weights used for subsystem trade-offs

Energy Consumption	Amount of power to deploy and operate the system, or the solution (e.g. for the orbit selection, energy required to reach that orbit).	4	It is a critical criterion because it directly affects the efficiency of the project, thus the mission viability.
Lifetime	Duration for which the system is expected to remain operative and effective in space.	3	The role of this criterion is important in the sense that the longer the system is operational, the higher the amount of energy that it can generates. However, if assumptions on future technology developments are considered, in-orbit operations such as repairs, manufacturing, replacements, might mitigate the need for high component lifetime, since its duration might be extended by in-orbit services.

Table 4.7: Criteria description and scores

4.3.2. Launch segment

Orbit selection

The first trade-off to perform concerns the selection of the operational orbit. The options under consideration are Low Earth Orbit (LEO), Geostationary Orbit (GEO), and Highly Elliptical Orbit (HEO) such as Molniya. Medium-Earth Orbits have been excluded from this analysis based on a thorough review of existing literature and studies, which indicates that they are rarely considered for this type of mission.

It is essential to focus on the specific characteristics of the mission and how these are related to or affected by the parameters of the potential orbits, to assess which is the most suitable. In the case of a space solar power mission, the critical requirements to consider include maximizing the amount of solar power collected, thus the satellite's solar exposure; facilitating the transmission of this power to Earth; and optimizing the energy efficiency of the process. In the context of orbit selection, this means minimizing the energy expenditure to place and maintain the modules in orbit and manage in-orbit operations.

The level of station keeping maneuvers required is also an important factor to consider, given the size and footprint of a solar power satellite. Excessive orbital perturbations or stringent station-keeping requirements could lead to increased complexity and risk for the mission.

In the trade-off for orbit selection, the criteria have the following meanings/applications:

- **Cost**: Number of launches required, payload capacity, other services for satellites (e.g., station keeping, orbit maintenance).
- **Deployment complexity**: Challenges related to orbit insertion.
- **Operational complexity**: Required management of satellites in the selected orbit.
- **Mass**: Mass of the respective satellite(s).
- **Output Power**: Related to the satellite's exposure to the sun, and its ability to transmit power to Earth.
- **TRL**: Not applicable.
- **Failure tolerance**: Ease in implementing in-orbit services to act in case of failure.
- **Energy consumption**: Required energy to launch, deploy and maintain the satellite in the orbit, it is related to the cost criterion.

- **Lifetime**: Not applicable.

Criteria	Weight x Applicability	GEO		LEO		HEO	
		Value	Weighted	Value	Weighted	Value	Weighted
Cost	3	4	12	3	9	3	9
Deployment complexity	4	3	12	4	16	3	12
Operational complexity	4	5	20	2	8	3	12
Mass	4	2	8	3	12	2	8
Output Power	5	5	25	3	15	4	20
TRL	0						
Failure tolerance	4	2	8	4	16	3	12
Energy consumption	4	3	12	3	12	3	12
Lifetime	0						
SUM	28		97		88		85
Weighted TOTAL		-	3.46	-	3.14	-	3.06

Table 4.8: Trade-off results for orbit selection

GEO provides the advantage of continuous power transmission with a single satellite, minimizing station-keeping and operational complexities. Its stable positioning reduces the need for frequent orbital adjustments, while eclipse durations are limited to a maximum of 71 minutes per day during equinoxes. However, GEO requires a high ΔV for orbital insertion and larger antenna sizes for efficient transmission, leading to higher launch costs and complexity [123].

LEO offers lower launch costs and reduced transmission losses due to its proximity to Earth. However, continuous power delivery requires a constellation of satellites, significantly increasing system mass, energy consumption, and operational complexity. More frequent eclipses and the need for continuous attitude and power beam control further complicate the mission. Additionally, station-keeping is challenging due to strong orbital perturbations and decay of the semi-major axis [39]. On the other hand, LEO allows easier access for potential in-orbit servicing.

HEO reduces the number of satellites required compared to LEO while maintaining relatively continuous power delivery. However, these satellites require careful scheduling to ensure uninterrupted coverage, as each satellite passes over the target area three times per orbit for approximately four hours per pass. The ΔV required for orbit insertion is lower than GEO, reducing deployment costs. However, repeated passage through the Van Allen Radiation Belt accelerates degradation of solar panels and other critical components [34]. Station-keeping and pointing adjustments are also more demanding than in GEO.

As expected from the literature, and as result of a basic trade-off analysis performed following the criteria in Table 4.7, GEO is confirmed as the best orbit for a solar power satellite. Balancing operational efficiency, stability, and power output while reducing complexity in satellite constellations and beam management, it ensures continuous power transmission. While LEO has cost and launch advantages, its higher system complexity and environmental impact outweigh these benefits. HEO still involves multiple satellites and increased station-keeping efforts.

Launcher

In Chapter 2, Table 2.4 presents the technical specifications and performance metrics of the most suitable launchers, both currently in use and under development.

Selecting a launcher is a critical step, as it provides essential information regarding payload capacity and propellant requirements, which are fundamental for computing the energy needed for launches and orbital transport.

Given the significant advancements in launcher reusability and in-orbit refueling technologies (such as SpaceX's Starship), and considering the time required for the mission's preparation, design, and for most systems to achieve a sufficiently high Technology Readiness Level (TRL), the selection of a launcher can be based on future projections. Studies indicate that by 2040, it is realistic to expect fully reusable launchers capable of meeting market demands for frequent heavy payload launches at competitive prices, making this a reasonable assumption for mission design purposes [108].

Since the launcher's specifications influence the overall architecture of the mission—including the mass budget, deployment strategy, and orbital transfer requirements—it is reasonable to select, as a reference, the performance of a specific launching system. Thus, the launcher selection will be based on Starship's projected performance, which currently offers the highest payload capacity.

Nonetheless, a preliminary and simplified trade-off is performed among the most significant launchers available today (in terms of payload and/or reusability), including Starship. The criteria are adapted from Table 4.7 for this specific context as follows:

- **Cost**: Overall cost of launch services, including production, preparation, and launch operations.
- **Deployment complexity**: Practical feasibility and potential issues during deployment, especially for in-orbit refueling or modular delivery.
- **Operational complexity**: Difficulty in supporting the launcher through fueling, maintenance, and integration with infrastructure.
- **Mass**: Not applicable.
- **Output Power**: Not applicable.
- **TRL**: Maturity of the launch vehicle's architecture and systems.
- **Failure tolerance**: Not applicable.
- **Energy consumption**: Amount of energy (or propellant) needed per unit of payload delivered to the target orbit.
- **Lifetime**: Not applicable.

Criteria	Weight × App.	Starship		Ariane 5		Ariane 6		Falcon 9		Falcon Heavy	
		Value	Weighted	Value	Weighted	Value	Weighted	Value	Weighted	Value	Weighted
Cost	3	4	12	2	6	2	6	4	12	4	12
Deployment complexity	4	0	0	0	0	0	0	0	0	0	0
Operational complexity	4	0	0	0	0	0	0	0	0	0	0
Mass	0	0	0	0	0	0	0	0	0	0	0
Output Power	0	0	0	0	0	0	0	0	0	0	0
TRL	3	2	6	4	12	4	12	4	12	4	12
Failure tolerance	0	0	0	0	0	0	0	0	0	0	0
Energy consumption	4	5	20	1	4	1	4	2	8	3	12
Lifetime	0	0	0	0	0	0	0	0	0	0	0
Total	18		38		22		22		32		36
Total Weighted		2.11		1.22		1.22		1.78		2.00	

Table 4.9: Launcher trade-off matrix including all criteria and weighted scoring. The "Weight × Applicability" column reflects the actual importance used in the comparison.

The trade-off analysis, under the assumption that Starship will be fully operational and reusable, confirms it as the preferred launch vehicle. As previously stated, Starship will be used as the baseline for all main calculations throughout the study. Its superior payload capacity, combined with reusability and projected cost-efficiency, makes it the most favorable option among the launchers considered.

Nonetheless, in the next section dedicated to the Energy Analysis, calculations will also be performed for a currently operational and realistic alternative: Falcon Heavy, which ranked second in the trade-off evaluation. The results obtained with this launcher will be compared to those of Starship.

As expected, using Falcon Heavy would imply a significantly higher number of launches to deliver the same mass to GEO, leading to a lower energetic performance and overall efficiency. However, including this case provides a more grounded and realistic perspective on current technological capabilities and the challenges of launching such a massive structure to geostationary orbit.

Figure 4.3 illustrates the in-orbit refueling configuration, where two modules dock, allowing one to transfer fuel to the other, enabling it to continue its mission.

Figure 4.3: Starship modules during in-orbit refuel

Orbital transport

The trade-off analysis for selecting the operational orbit identified GEO as the most suitable option based on mission requirements and constraints. A critical aspect of mission planning is the transportation of the solar power satellite to its final orbit, as this directly influences the energy and propellant requirements. Various orbital transfer strategies are available, as outlined in Chapter 2, and the following section evaluates the most suitable option for transport to GEO:

1. Direct injection into GEO
2. Injection into LEO/GTO followed by transport via orbital transfer vehicles
3. Injection into LEO with orbit raising using onboard propulsion
4. Injection into GTO with orbit raising using onboard propulsion
5. Injection into LEO, in-orbit refueling of Starship, and orbit raising using refueled Starship

Direct injection into GEO (Option 1) is excluded due to its high propellant and ΔV demands. Instead, GEO is typically reached via an intermediate LEO or GTO. Options 2 and 5 rely on developing technologies, such as orbital tugs and in-orbit refueling, which, while promising, introduce uncertainties that hinder a detailed calculation method based on current technological maturity. Thus, the decision focuses on whether to inject into LEO or GTO and subsequently raise the orbit using onboard propulsion. Chemical propulsion is assumed when performing calculations for this subsystem. Although electric propulsion is an emerging technology offering high specific impulse (Isp) and requiring minimal propellant, it also comes with limitations. Specifically, electric thrusters have low thrust, resulting in prolonged transfer times [108]. This extended duration would expose the satellite to potential degradation of critical onboard systems, as the transfer would involve multiple passages through the Van Allen radiation belts. On the other hand, the high Isp of electric propulsion significantly reduces the required propellant mass, allowing most of the launcher's payload capacity to be allocated to the satellite module itself.

In this analysis, all launchers are assumed to operate from Cape Canaveral, Florida. This launch site imposes an initial orbital inclination of approximately $28.5°$. In contrast, European launch vehicles (such as Ariane 5 and Ariane 6), launched from the Guiana Space Centre in Kourou, benefit from a

near-equatorial location, allowing for a lower initial inclination. This geographic advantage reduces the ΔV required to reach geostationary orbit (GEO), which is equatorial by definition.

To reach GEO from higher-inclination orbits, an inclination change maneuver is required. This maneuver is typically performed at the apogee of the Geostationary Transfer Orbit (GTO), where the orbital velocity is at its minimum, thereby minimizing the propellant cost of the maneuver.

The ΔV required to perform this inclination change is given by:

$$\Delta V_{\text{inc}} = 2V \cdot \sin\left(\frac{\Delta i}{2}\right) \tag{4.1}$$

where:

- V is the orbital velocity at the maneuver point (usually at GTO apogee),
- Δi is the inclination change in radians.

This additional ΔV must be taken into account when comparing launcher performance, as it affects the amount of available payload mass and the overall mission feasibility.

Calculations

To determine the most energy-efficient approach, the required impulse velocities for the orbital maneuvers must be calculated. Two scenarios are analyzed:

1. Transfer from LEO to GTO, then to GEO.
2. Direct transfer from GTO to GEO.

A symbolic satellite mass of 1000 tons is assumed, with the necessary parameters summarized in Table 4.10.

Data	Value	Unit of Measure
Payload to LEO	100	ton
Payload to GTO	21	ton
Isp	350	s
g_0	9.80665	m/s^2
μ (gravitational parameter)	3.986×10^5	km^3/s^2
h_{LEO} (altitude LEO)	200	km
$h_{a,GTO}$ (altitude GTO apogee)	35786	km
$h_{p,GTO}$ (altitude GTO perigee)	200	km
Initial Inclination (Cape Canaveral)	28.5	degrees

Table 4.10: Data for Orbital Transfer

From the expression of orbital energy, the velocity at the point of interest of an orbit can be computed, see Equation 4.2.

$$\begin{aligned} E &= -\frac{\mu}{2a} = \frac{V^2}{2} - \frac{\mu}{r} \\ V &= \sqrt{\mu\left(\frac{2}{r} - \frac{1}{a}\right)} \end{aligned} \tag{4.2}$$

Where:

- E = orbital energy,
- r = radial distance of orbital point P from central body (Earth),
- a = semi-major axis
- V = the orbital velocity at point P,
- μ = the standard gravitational parameter, defined as $\mu = GM$, where G is the gravitational constant and M is the mass of the central body.

The total ΔV for each scenario includes the impulse needed to:

- raise the apogee from LEO to GTO,
- change the inclination at GTO apogee (where velocity is lowest and inclination maneuvers are most efficient),
- circularize the orbit at GEO.

$$\Delta V_{\text{tot}} = \Delta V_{\text{LEO}\to\text{GTO}} + \Delta V_{\text{GTO}\to\text{GEO}} + \Delta V_{\text{inc}} \tag{4.3}$$

Each of these terms is calculated as follows:

- $\Delta V_{\text{LEO}\to\text{GTO}} = V_{\text{GTO,p}} - V_{\text{LEO}}$
- $\Delta V_{\text{GTO}\to\text{GEO}} = V_{\text{GEO}} - V_{\text{GTO,a}}$
- $\Delta V_{\text{inc}} = 2V_{\text{GTO,a}} \cdot \sin\left(\frac{\Delta i}{2}\right)$

Where:

- V_{LEO} is the velocity in circular low Earth orbit,
- $V_{\text{GTO,p}}$ is the velocity at the perigee of the GTO,
- $V_{\text{GTO,a}}$ is the velocity at the apogee of the GTO,
- V_{GEO} is the velocity in circular geostationary orbit,
- Δi is the inclination change required to reach equatorial orbit.

The computed ΔV values for each transfer step allow estimation of the required propellant mass via the Tsiolkovsky equation (Eq. 4.4):

$$\Delta V = I_{SP} \cdot g_0 \cdot \ln\left(\frac{m_0}{m_f}\right) \tag{4.4}$$

Where:

- ΔV = Change in velocity (the total velocity increment).
- I_{SP} = Specific Impulse, which represents the efficiency of the propellant and is measured in seconds.
- g_0 = Standard gravitational acceleration at the Earth's surface.
- m_0 = Initial mass (including propellant).
- m_f = Final mass (dry mass).

Knowing the initial mass, which coincides with the payload capacity, and the other input data, and having computed the ΔVs, the actual transportable mass can be determined by solving for m_f. This represents the mass of the satellite module that can be transported per launch.

Dividing the total mass of the satellite by this value provides an estimate of the number of launches required.

In this computation, a key assumption is that the payload bay volume, or the allocatable volume in the fairing, is not considered as a limiting factor. This means that, given the appropriate mass, the satellite modules are assumed to fit within the available space.

All the results are summarized in Table 4.11, while Table 4.12 reports the assigned scores to the option for the present trade-off.

Data	Value	Unit of Measure
$\Delta V_{\text{LEO}\to\text{GTO}\to\text{GEO}}$	2.455	km/s
$\Delta V_{\text{GTO}\to\text{GEO}}$	1.477	km/s
ΔV_{inc}	0.786	km/s
$M_{P,\text{LEO}\to\text{GTO}\to\text{GEO}}$	74.7	ton
$M_{P,\text{GTO}\to\text{GEO}}$	10.14	ton
N. launches LEO	40	-
N. launches GTO	93	-

Table 4.11: Results of orbital transfer calculations

Criteria	Weight × Applicability	Injection into LEO		Injection into GTO	
		Value	Weighted	Value	Weighted
Cost	3	3	9	2	6
Deployment complexity	4	2	8	3	12
Operational complexity	4	2	8	2	8
Mass	0	–	–	–	–
Output Power	0	–	–	–	–
TRL	0	–	–	–	–
Failure tolerance	0	–	–	–	–
Energy consumption	4	3	12	2	8
Lifetime	0	–	–	–	–
SUM	15		37		34
Weighted TOTAL	–	–	2.47	–	2.27

Table 4.12: Trade-off results for injection strategy comparison

Injecting into LEO maximizes payload capacity per launch, reducing the number of launches required. However, onboard propulsion is necessary for orbit raising, meaning a portion of the payload capacity must be allocated for propellant rather than for the satellite modules.

Conversely, injecting into GTO requires fewer maneuvers, but the significantly lower payload capacity to GTO increases the total number of launches needed.

The choice between LEO and GTO injection impacts the total energy required for orbital transport. Since energy consumption depends on both the number of launches and the mass of expended propellant, these factors must be considered when assessing mission feasibility.

Given these considerations, LEO injection is selected as the preferred approach. This decision is driven by the higher payload capacity per launch, allowing for fewer overall launches, despite requiring additional onboard propulsion for orbit raising. While GTO injection simplifies the transfer, its lower payload capacity would result in an excessive number of launches, making it less efficient for this mission.

4.3.3. Tile components selection

The tile component design requires key selections regarding the solar cell technology, the device for converting direct current (DC) into radio frequency (RF) energy, and the antenna transmission design.

Solar Cell Technology

Given the high energy requirements and the extreme thermal challenges, solar cells with the highest efficiency are preferred, even if their specific power per unit mass is lower. Implementing the sandwich tile design introduces greater challenges in thermal management rather than mass constraints, making heat dissipation a critical factor in the technology selection.
Following the SPS-Alpha architecture, the selected solar cell technology is multijunction gallium arsenide (GaAs). Recent advancements in solar cell technology have led to the development of triple-junction solar cells with concentrators, achieving beginning-of-life (BOL) efficiencies of up to 45% [108, 74].
Given its compatibility with the concentration levels considered in this study, SPS-Alpha also serves as the primary conceptual foundation for the integrated tile concept adopted in this analysis.

The selected solar cell properties are summarized in Table 4.13.

Parameter	Value
BOL Efficiency	36% [122, 108]
Base Material	GaInP/GaAs/Ge on Ge substrate
Degradation Rate	0.1% per year
Power-to-Mass Ratio	805.9 W/kg [62]
Concentration Factor	3
Surface Density	0.5 kg/m^2 [108]

Table 4.13: Selected Solar Cell Properties

Furthermore, a thin layer (200 μm) of cover glass is included in the mass budget. This layer ensures an end-of-life efficiency of approximately 95% after 30 years of operation [108]. Given the continuous exposure of solar cells in geostationary orbit to ionizing radiation, the cover glass serves as a protective barrier, mitigating performance degradation.

Power Conversion

The selection of DC-to-RF conversion electronics is based on efficiency and availability considerations [51]. Three main technologies are typically considered for the conversion of direct current (DC) to radio frequency (RF) power in wireless power transmission systems: magnetrons, klystrons, and solid-state power amplifiers (SSPAs). Magnetrons are self-oscillating vacuum tubes that can achieve high efficiencies, typically in the range of 70–85%, and are relatively lightweight and cost-effective. However, they offer limited frequency and phase control, which reduces their suitability for phased-array applications [14]. Klystrons are linear-beam vacuum tubes that can also achieve high efficiencies and provide better frequency stability and control compared to magnetrons, but they are generally heavier, require high-voltage operation, and present integration challenges [14]. SSPAs, based on semiconductor technologies, are characterized by high modularity, ease of integration with phased arrays, and greater robustness. Although individual SSPAs exhibit lower power efficiency, recent developments have brought their efficiencies up to 70–80%, making them increasingly attractive for scalable SBSP applications [57].

The criteria for the trade-off described in Table 4.7 assume a specific meaning adapted to this selection.

- **Cost**: Overall cost of the complete group of DC-RF converters.
- **Deployment complexity**: Not applicable.

- **Operational complexity**: Level of integration difficulty within the satellite and phased array antenna, and thermal management requirements and antenna steering needs.
- **Mass**: Weight and number of components required to deliver the desired power.
- **Output Power**: Not applicable
- **TRL**: Maturity level of the technology.
- **Failure tolerance**: Degree of resilience to single-point failures in converters.
- **Modularity:** Capability of dividing the DC-RF conversion system into multiple independent modules with minimal dimensions.
- **Scalability:** Capability of adapting the technology to different power levels, including downscaling for lower-power applications such as prototypes or demonstrators.
- **Energy consumption**: Measure of the energy lost during the operation of the system, directly related to its conversion efficiency.
- **Lifetime**: Expected operational duration with minimal maintenance.

Table 4.14 outlines the evaluation criteria and provides a comparative analysis of how each power conversion technology performs with respect to these parameters. The outcome of the trade-off analysis is presented in Table 4.15.

Technical Criterion	Comment / Comparison of the Four Options
Cost	While the cost of a single DC-RF converter is not critical, industrial scalability makes a difference. SSPAs, based on semiconductor chips, are more cost-effective at scale compared to the other three technologies [6].
Mass	The required power conversion leads to very different total system masses. For instance, to transmit 2 GW at 5.8 GHz, Klystrons and Magnetrons require much larger mass than SSPAs. SSPA technology results in significantly reduced overall converter mass due to higher integration and miniaturization [70].
Design Complexity	Electron tube technologies (Klystron) require waveguides and centralized feeding structures. SSPA allows the placement of amplifiers and phase shifters at each radiating element, simplifying integration. Klystrons also suffer from frequency variability in mass production, affecting antenna signal coherence.
Operational Complexity	SSPA allows for electronically steerable antennas, while tube-based systems might require mechanical steering. Heat dissipation is more manageable with SSPA, which avoids concentrated hot spots characteristic of tubes.
Failure Tolerance	Failure of a single SSPA has minimal system impact due to redundancy. In contrast, failure in tube-based systems (with fewer converters) may cause substantial power loss.
TRL	SSPA are mature technologies with proven space heritage. Magnetron and Klystron are less common in space, used more in terrestrial applications like accelerators.
Lifetime	All four technologies show comparable lifetimes (15–25 years), but SSPA may offer better maintainability and slightly improved reliability.
Industrial Capability / Scalability	SSPA production is easier to industrialize due to chip-based manufacturing. Tube-based technologies are harder to mass-produce efficiently at large scales.

Table 4.14: Technical evaluation of DC-RF converter technologies

Criteria	Weight x Applicability	SSPA		TWTA		Magnetron		Klystron	
		Value	Value × Weight	Value	Value × Weight	Value	Value × Weight	Value	Value × Weight
Cost	3	4	12	3	9	3	9	2	6
Deployment complexity	0	3	12	4	16	3	12	2	8
Operational complexity	4	5	20	2	8	3	12	3	12
Mass	4	2	8	3	12	2	8	3	12
Output Power	0	5	25	3	15	4	20	2	10
TRL	0	–	–	–	–	–	–	–	–
Failure tolerance	4	2	8	4	16	3	12	3	12
Energy consumption	4	3	12	3	12	3	12	3	12
Lifetime	0	–	–	–	–	–	–	–	–
SUM	28		97		88		85		80
Weighted TOTAL	–	3.46		3.14		3.06		2.86	

Table 4.15: Trade-off results for orbit selection

For this study, SSPAs are selected as the preferred solution, in line with previously developed research [50]. Vacuum devices such as magnetrons and klystrons, while highly efficient, operate at high voltages and require specialized high-voltage power converters. These converters introduce additional source of inefficiencies, making them less suitable for space applications [52].

For SBSP applications, where the linearity of the transmitted signal is not a critical factor, Class E SSPAs provide an optimal trade-off. These amplifiers can achieve efficiencies of up to 80%, though at the cost of reduced linearity. The system operates with a continuous wave (CW) signal, with individual amplifiers integrated into a coherent array to maximize transmission efficiency [40].

Antenna Elements

Operating frequency
For the selection of the operating frequency, bands within the ISM spectrum between 1 and 24 GHz were considered. However, due to significant atmospheric attenuation above 10 GHz—especially under adverse weather conditions—only 2.45 GHz and 5.8 GHz remained viable for ensuring continuous 24/7 power delivery. The final choice of 5.8 GHz is based on their trade-off analysis, performed using the SBSP sizing tool developed at ESA. This trade-off highlighted that, although 5.8 GHz leads to a slight increase in solar panel area, it allows for a substantial reduction—up to one-third—in the onboard antenna area. This outcome is directly linked to the physical relationship connecting antenna aperture size and operating frequency: higher frequencies enable smaller apertures for the same beam performance. As a result, 5.8 GHz offers key advantages in terms of mass, volume, cost, and overall system complexity, making it the preferred operating frequency for the SBSP architecture.

Antenna elements
A key requirement for the antenna design is the implementation of a retrodirective phased array system. This system enables precise beam steering by responding to a reference beacon signal transmitted from the ground. The phased array technology ensures that the transmitted power remains accurately directed towards the designated receiving station, even in the presence of slight orbital perturbations or misalignments.

The integration of retrodirective technology is essential for the efficient operation of the SBSP system,

allowing for real-time adaptive beam pointing without requiring complex active control mechanisms. The antenna system consists of sub-panels, each comprising multiple ”bricks” that house the radiating elements (RE). These sub-panels, which are rigid structures designed for launch in a single piece, integrate power distribution networks and mechanical interfaces for in-orbit assembly. Each sub-panel is capable of transmitting electrical power to adjacent units [34]. At the core of the antenna architecture, the radiating element (RE) serves as the fundamental transmitting unit, ensuring the emission of RF power.
In this configuration, each sub-panel operates independently, containing its own solid-state power amplifier (SSPA) along with a phase and amplitude control device. The detailed design of the transmitting antenna is beyond the scope of this study. Figure 4.4 visually represents the structural organization of the antenna. Table 4.16 summarizes the selections made for each of the main systems of the mission.

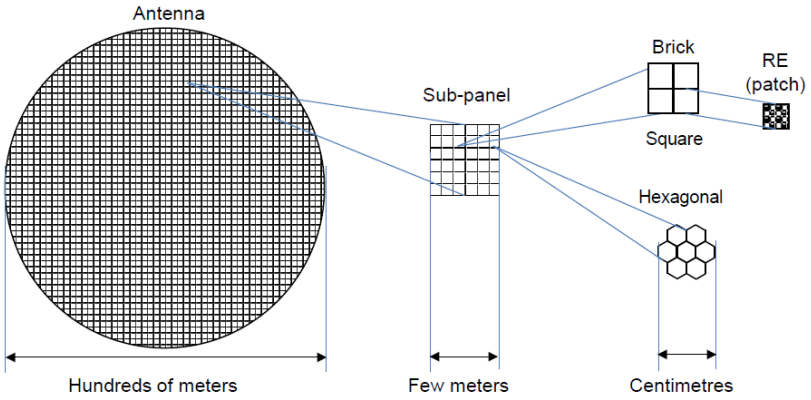

Figure 4.4: Transmitting antenna structural organization, [34]

System	Detail
Launch Segment	
Orbit	Geostationary
Transport	LEO $\rightarrow$ GTO $\rightarrow$ GEO
Launcher system	Starship
Space Segment	
Solar cells technology	Triple-junction Ga-As SCs
Power conversion	Solid-state power amplifiers
Power transmission	Retrodirective phased array @5.8GHz
Ground Segment	
Ground Power station	Rectifying Antenna

Table 4.16: Case study SBSP system specifications

4.3.4. Sizing

To perform the analyses, the full system must be appropriately sized. The sizing process begins with the mission requirement of delivering 1000 MW of power to the terrestrial power grid. Considering the efficiency chain of the energy conversion and transmission processes, the main components of the tile can be dimensioned accordingly. The various power levels throughout the system are computed using a backward approach: starting from the required power at the Ground Power Station, the necessary power at each preceding stage is obtained by sequentially dividing by the efficiency of the corresponding subsystem. This allows tracing back to the power that must be generated in orbit to meet the final demand on Earth. Table 4.17 reports the efficiencies of the main processes involved in the mission.

System	Efficiency
Power required : **5135.1 MW**	
Power collection (PV)	0.36
Power required : **1848.6 MW**	
DC-RF conversion	0.80 [34]
Transmitting antenna	0.98 [34]
Beam collection, atmospheric attenuation	0.83 [34]
Power required : **1202.9 MW**	
Ground (rectenna + grid)	0.8313
Power required : **1000 MW**	
Total efficiency	**0.198**

Table 4.17: Energy efficiency chain for the power transmission system

Efficiency chain

The chain of efficiencies reported in Table 4.17 serves as the central reference for sizing the system and represents an optimistic case, in which high-end values for subsystem efficiencies are considered, based on current technologies, existing literature, and demonstrations. However, given the very low Technology Readiness Level (TRL) of the mission and its key subsystems, and considering that no space mission with comparable specifications has ever been demonstrated, it is not only relevant but also necessary to explore less optimistic scenarios.

In particular, the efficiencies related to the photovoltaic subsystem and the wireless power transmission system are subject to a sensitivity analysis, presented later in section 5.3. These two subsystems are still at an early stage of development and rely on several performance assumptions. Therefore, it is important to consider a range of efficiency values, based on the current state-of-the-art, to understand how the system might behave if the actual performance is at the lower end of that range. This analysis helps evaluate how these variations impact satellite sizing and the overall energy performance of the system, offering a more realistic view of the mission's feasibility and highlighting potential design limitations under less ideal conditions.

The efficiency of the photovoltaic module, along with that of the power conversion components, has already been introduced. Additional contributions to the overall transmission system efficiency account for losses associated with wireless power transmission. These include both permanent and weather-dependent losses.
Permanent losses are independent of meteorological conditions and are primarily caused by gaseous absorption, due to molecular absorption bands of water vapor (H_2O) and oxygen (O_3). In contrast, weather-dependent losses are influenced by local atmospheric conditions above the Ground Power Station (GPS), such as precipitation and cloud coverage. These losses depend on various factors, including frequency, elevation angle, altitude, and the statistical occurrence and intensity of rain and cloud events at the specific location.

According to the International Telecommunication Union (ITU), for frequencies below 10 GHz, the impact of atmospheric attenuation remains minimal.

Photovoltaics

The first sizing step focuses on determining the solar cells' area required to generate sufficient power. Given the mission architecture, the sunlight incident on the surface is amplified by a factor of 3 [9], and the photovoltaic and transmitting array sides are assumed to have the same dimensions (integrated tile concept).

The power required at the PV side is 5135.1 MW; from this value, the needed solar cells area and the mass of the system are computed.
The power collection efficiency, combined with the incident solar flux, determines the total required PV area.
Considering an average incident power of 1361 W/m^2, multiplied by the concentration factor of 3, the required solar cell area is:

$$A_{PV} = \frac{E_{required}[W]}{E_{incident}[\frac{W}{m^2}]} = \frac{(1 \times 10^9 W)/\eta_{tot}}{3 \times 1361 \frac{W}{m^2}} \tag{4.5}$$

This results in an area of 1,236,949 m^2 (1112 meters sided square), corresponding to a mass of 618.47 tons. Specifications on the system are reported in Table 4.13.

Besides the solar cells, a layer of cover glass is included on top of them, serving the purpose of protecting against the space radiative environment and reducing the long-term degradation in efficiency and performance of the cells.

The thickness of the cover glass is 200 μm. A commercial study based on the architecture developed by J. Mankins et al. [108] reports that, for a solar power satellite in geostationary orbit, a cover glass with this thickness allows the solar cells to maintain 95% efficiency after 40 years of lifetime.

The surface density of the cover glass at 200 μm thickness is 0.52kg/m^2, from a volume density value derived from [108], and the resulting mass, based on the total area to be covered (area of solar cells), is 643.21 tons.

Transmitting array

Following the same methodology, the transmission system, which includes the retrodirective phased-array antennas and integrated circuits for RF generation, is dimensioned to match the photovoltaic module area.

For the density of the transmission system, the study from Caltech is taken as a reference, as it demonstrated a prototype integrated tile module with a density of 0.5 kg/m² on the transmission side [33]. However, to remain conservative, this exceptionally optimistic value, significantly lower than other estimations found in literature, is scaled up by a factor of three, resulting in a density of 1.5 kg/m². Applying this assumption, the total mass of the transmitting array is estimated to be 1855.42 tons.

Ground segment

There are two ways to size the transmitting and receiving antennas, which are related through the Friis transmission equation. The first approach, also followed in [108, 62], assumes that the entire surface of the tile facing Earth consists of transmitting arrays. The second approach considers a smaller transmitting aperture, with part of the available surface used for radiators and heat dissipation. This would require a larger aperture area for the ground receiving station.

At this stage of the analysis, there is no detailed assessment of whether a radiative surface will be necessary on the antenna side. However, given the architecture of the integrated tile, even if part of the surface is not used for transmitting arrays, it must still be structurally accounted for. Therefore, the first approach is adopted. As suggested in [108], imposing a 100% power transmission efficiency in

(4.6) ensures that the resulting ground power station (GPS) area is as conservative as possible.

The power transmission efficiency is governed by the Friis transmission equation, which in terms of aperture areas is given by:

$$P_r = P_t \left(\frac{A_t A_r}{\lambda^2 d^2} \right) \tag{4.6}$$

where:

- P_r = received power at the ground station [W]
- P_t = transmitted power from the satellite [W]
- A_t = effective aperture area of the transmitting antenna [m^2]
- A_r = effective aperture area of the receiving antenna [m^2]
- λ = wavelength of the transmitted signal [m], computed as $\lambda = \frac{c}{f}$, where c is the speed of light (3.0×10^8 m/s) and f is the transmission frequency
- d = distance between the transmitting and receiving antennas [m], which in this case corresponds to the geostationary orbit altitude

Assuming a 100% power transmission efficiency means that the entire transmitted power is received, i.e.,

$$\frac{P_\mathrm{r}}{P_\mathrm{t}} = 1 \tag{4.7}$$

which simplifies the Friis equation to:

$$A_\mathrm{r} = \frac{\lambda^2 d^2}{A_\mathrm{t}} \tag{4.8}$$

This expression determines the required receiving aperture area based on the chosen transmitting aperture, ensuring a conservative estimate for the ground power station (GPS) sizing.

$$A_\mathrm{GPS} = 2{,}766{,}000 \ \ \mathrm{m}^2 \tag{4.9}$$

The parameters used in the calculation are:

- Wavelength (λ): Computed for a transmission frequency of 5.8 GHz.
- Distance (d): Equal to 35,780,000 m, corresponding to the geostationary orbit altitude.

The total land requirement will be greater than the calculated aperture area, as it must also account for structural infrastructure, balance-of-system components, and other supporting facilities.
The mass allocated for the ground segment of the mission is computed taking as reference a density of 2 kg/m² from [34], yielding a total mass of 5532.1 tons.

Reflectors and Structure

For the solar reflectors to concentrate sunlight onto the main module, the mass is computed considering the building unit of the reference architecture from J. Mankins [62], [108]. Knowing the mass of one module (20 kg), and its area (1900 m^2), the resulting total mass for mirrors is 39 tonnes.

The structure of the system consists of connecting beams, a reflector support structure, and Hexbus modules(Figure 4.5), which serve as connectors between different system components.

Each Hexbus module has a unit area of 6.25 m^2 and a weight of 3.75 kg [108]. Based on the ratio of the total tile area to the unit module area, the total Hexbus mass is estimated at:

$$M_{\text{Hexbus}} = \frac{\text{Total Tile Area}}{\text{Unit Module Area}} \times \text{Unit Weight} = 742.2\,\text{tons}$$

This component ensures connectivity between the different layers of the tile.

The total structural mass, excluding the Hexbus modules and based on SPS Alpha data, is 1500 tons [62]. The primary materials used include aluminum for the reflector structure and beams, and CFRP (Carbon Fiber Reinforced Polymer) for the Hexbus modules in the power generation segment.

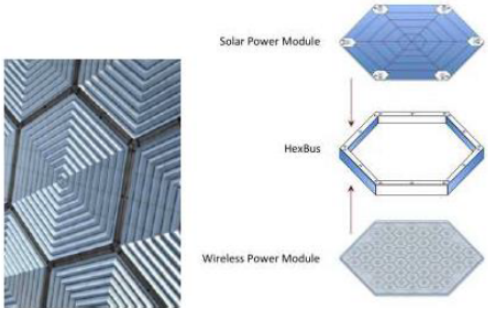

Figure 4.5: Hexbus connection modules [108]

The sizing results, area, and masses are summarized in Table 4.18.

System	Specification	Density [kg/m^2]	Mass [tons]
Photovoltaics	1.237 km^2	0.5	618.47
Cover Glass	1.237 km^2	0.52	643.21
Transmitting Antenna	1.237 km^2	1.5	1855.42
Hexbus	6.25 m^2 modules, 3.75 kg each	-	742.2
Structure	Based on SPS Alpha data [62]	-	1500
Reflectors	20 kg per 1900 m^2 unit	-	39
Total space segment mass			**5398.3**
Ground Power Station	2.77	2	5532.1

Table 4.18: Summary of tile concept sizing and mass budget

5

Energy Analysis

This chapter presents a Net Energy Analysis (NEA) to quantify the energetic performance of an SBSP system, assessing whether it provides a net energy surplus and how it compares to its terrestrial alternative, addressing the first set of research questions defined in chapter 3.

The need for this analysis arises from the fact that, while much research has focused on technical feasibility and economic viability, the energetic efficiency of SBSP remains an underexplored aspect.

To address this, the methodology is applied to a terrestrial PV power plant and the two SBSP architectures defined in Chapter 4, evaluating two key metrics:

- Energy Return on Energy Investment (EROEI): The ratio of total energy produced by the system over its lifetime to total energy demand required to build the system, indicating whether the system produces more energy than it consumes.
- Energy Payback Time (EPBT): The time required for the system to generate the same amount of energy that was invested in its production and deployment.

Beyond giving insights on feasibility, this study also introduces a method for estimating the energy efficiency of different SBSP architectures, which could serve as a new criterion in future trade-off studies for the selection of an architecture.

The following sections outline the methodology, define the system boundaries, and present the assumptions underlying the energy evaluation, along with the outcomes of the analysis. Subsequently, the results offer insights into the energy efficiency of SBSP and highlight the key parameters influencing its overall performance.
However, many of the input parameters used in the study, such as efficiencies, are based on future assumptions or limited to a single scenario (e.g., an optimistic case). To address this limitation, a sensitivity analysis of the most influential parameters is conducted to evaluate their impact on the system's overall performance. This provides valuable insights into potential improvements and allows for the exploration of alternative scenarios.

5.1. Analysis methodology

In this section, the methodological approach applied in the energy analysis is presented.
The first analytical choice is to define the boundaries of the analysis. As explained in Chapter 2, a life-cycle energy analysis can be conducted at various levels of detail, each yielding results with different degrees of accuracy.
For the scope of this study, which investigates space-based solar power from an energy perspective, focusing on computing key metrics and comparing SBSP with terrestrial solar power stations, the ”cradle-to-gate” approach is adopted [24]. According to this framework, the analysis considers energy inputs from the raw materials extraction phase up to the operational phase, while excluding decommissioning and disposal-related energy flows.

The rationale behind neglecting the decommissioning phase in this study is that, in the context of SBSP, this segment of the mission would be solely based on assumptions about future space operations and end-of-life disposal, introducing high uncertainty and limiting the accuracy and reliability of the results.

Hence, for each analysed scenario, the energy inputs will include:

- Energy embedded in raw materials
- Manufacturing and production energy
- Transport and launch energy required to reach the operational site (Earth orbit or ground station)

The energy output is defined as the total amount of energy produced by the system over its operational lifetime.

To address the research question related to the comparative analysis of SBSP and terrestrial solar power solutions, three case scenarios are defined in Chapter 4, and a section to compute energetic performance metrics for each case is included in the developed MATLAB script [22].
The input data for the script consists of system specifications (such as material densities, efficiencies, and thermo-optical properties) and operational requirements (e.g., maximum temperature constraints, power output to the grid). Through the implementation of parametric functions, applicable across different scenarios, the following energetic performance indicators are computed:

- Energy Return on Investment (EROI)
- Energy Payback Time (EPBT)

5.1.1. Energy output

The total energy delivered by the system throughout its lifetime is straightforward to compute. For the terrestrial case, the Global Horizontal Irradiance (GHI) [54] is required in kWh/m^2/year (or kWh/m^2/day multiplied by 365 days), along with the module efficiency and a yearly degradation factor, as explained in Chapter 4.

The total energy produced per square meter in a year can be calculated by multiplying the GHI by the module efficiency. The total energy output of the plant over its lifetime is then obtained by multiplying this value by the total surface area and applying the degradation factor over time. The energy output E_{total} can be expressed as:

$$E_{\text{total}} = A \cdot \eta_{\text{sys}} \cdot \sum_{t} GHI \times (1-d)^t \tag{5.1}$$

where:

- A is the total surface area of the PV plant (m^2),
- η_{sys} is the cumulative system efficiency,
- GHI is the Global Horizontal Irradiance (kWh/m^2/year),

- d is the annual degradation factor,
- N is the total number of operational years,
- t represents each year of operation.

This formula accounts for the gradual decrease in energy output due to panel degradation over time.

For the space-based case study, the design and sizing assumptions are based on the requirement to deliver 1 GW of continuous power to the grid. However, eclipse periods must be accounted for in the calculations; in GEO, there are approximately two eclipses per year, each lasting 71 minutes.

Given that the system is sized to produce 1 GW of power in its first operational year, the only additional factor to consider is the yearly degradation of system performance.

In space, exposure to the harsh environment (solar radiation, charged particles) leads to progressive performance deterioration in key satellite components, particularly in solar cells and other systems directly exposed to the external environment.

To account for this effect, a cumulative annual degradation factor of 1% is applied to the case study energy output delivered to the grid, as suggested in [108]. This factor reflects long-term efficiency losses due to the space environment. One mitigation strategy consists of applying a protective cover glass layer over the photovoltaic surface.

The thickness of the cover glass is 200 μm. The commercial study based on the architecture developed by J. Mankins et al. [108] taken as reference, reports that, for a solar power satellite in geostationary orbit, a cover glass with this thickness enables the solar cells to retain 95% of their initial efficiency after 40 years of operation.

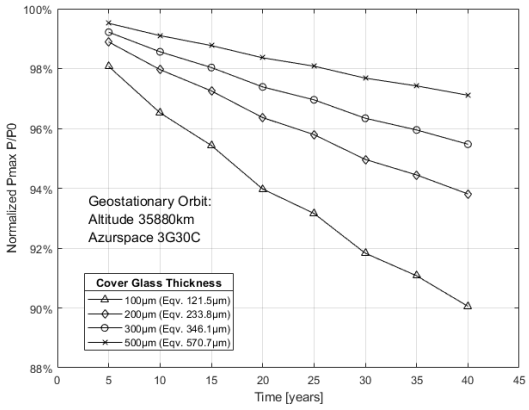

Figure 5.1: Protective cover glass for solar cells in SPS concept [108]

The total energy output (Equation (5.2)) over the system's lifetime is computed by summing the yearly outputs and multiplying the result by the number of operational hours per year. This provides the total energy in gigawatt-hours (GWh) instead of gigawatts (GW).

$$E_{\text{total}} = \left(\sum_{t=0}^{N} E_0 \cdot (1-d)^t \right) \cdot T \tag{5.2}$$

where:

- E_0 is the initial energy output (1000 MW),
- N is the total number of operational years,

- d is the annual degradation factor (0.01),
- T is the number of operational hours per year minus 1, accounting for eclipses ($\approx$ 8757.6 hours).

This approach ensures an accurate estimate of the total energy delivered to the grid over the system's lifetime, accounting for performance degradation.

For the baseline SBSP architecture referenced in external technical reports (e.g., Thales), the total energy output is not calculated here, as it is already provided in the source materials.

5.1.2. Energy Input

As already mentioned, computing the cumulative energy demand requires multiple considerations. In general, this demand can be divided into different contributing factors, each of which is accounted for through specific functions in the MATLAB script [22]. These functions are designed to calculate the energy demand associated with materials, photovoltaic cells, and transport, ensuring a structured approach to the estimation process.

The energy demand is categorized as follows:

Energy Demand for Materials Production

- The system requires various raw materials, such as composites, steel, aluminum, and concrete, which contribute to the total embedded energy.
- The energy required per kilogram of each material is obtained from offical databases, such as the World Economic Forum database [121].
- The total energy demand for materials is computed as:

$$E_{\text{materials}} = \sum_i (m_i \cdot e_i) \tag{5.3}$$

  where:
  - m_i is the total mass of material i needed (kg),
  - e_i is the specific energy demand per kg (J/kg or Wh/kg).
- The required material quantities are estimated during system sizing or taken from reference architectures when available.

Energy Demand for Photovoltaic Cell Production

- Photovoltaic cells have a specific energy demand per unit area (J/m^2) or per kilogram (J/kg), depending on the manufacturing process.
- This energy accounts for:
  - Material extraction (e.g., silicon, perovskites),
  - Cell production and fabrication processes.
- Since different PV technologies exhibit high variability in energy demand, special attention is given to selecting the correct energy input values based on the solar cell type employed.

Energy Demand for Transport

The energy demand associated with transport differs significantly between terrestrial solar plants and space-based solar power systems, requiring separate methodologies:

Terrestrial transport (ground-based solar power plant)

- Components must be transported via land or sea to the operational site.

- The transport energy demand is estimated using:

$$E_{\text{transport, ground}} = M \cdot d \cdot e_{\text{transport}} \tag{5.4}$$

  where:

  - M is the total transported mass (tons),
  - d is the transport distance (km),
  - $e_{\text{transport}}$ is the energy demand per ton-km (J/ton·km).

Space Transport (SBSP System Launch and Deployment)
Deploying a kilometer-scale solar power satellite in Earth orbit requires detailed calculations due to the high energy cost of launches and orbital transfers. The major energy contributions for space transport include:

- Launch Energy: The energy required to lift satellite modules and potential propellant for orbital transfer vehicles from Earth's surface into Low-Earth Orbit.
- Orbital Transfer Energy: The additional energy required to transfer modules from LEO to GEO (Geostationary Orbit).

This term represents one of the largest contributions to the total energy input in SBSP analysis. The primary factor influencing launch energy demand is the propellant consumption, which determines the total chemical energy expended for orbital insertion and maneuvering.

To compute the energy associated with burned and expelled propellant, the number of launches required to deploy all modules into orbit must first be determined. Additionally, if orbit raising or orbital transport is needed, the propellant required for these maneuvers must also be taken into account, reducing the available payload mass for each spacecraft module. Therefore, a dedicated section of the code is implemented to compute these parameters.

In Section 4.3.2, the methodology for computing the ΔV required for orbital transfer, the propellant mass needed, and the resulting payload mass constraints is outlined in detail. These calculations included:

- The LEO $\rightarrow$ GTO transfer via a Hohmann maneuver with an impulse to increase eccentricity.
- The GTO $\rightarrow$ GEO transfer, requiring an additional velocity impulse at apogee first to change the inclination and then circularize the orbit.
- Application of the vis-viva equation to determine orbital velocities at key points.
- Use of the Tsiolkovsky rocket equation to calculate the mass ratio and available payload after accounting for transfer propellant.
- The number of launches needed to deploy all the modules in orbot.

Section 4.3.2 applies the methodology to a reference satellite mass of 1000 tons, solely for the purpose of selecting the most efficient orbital transport method, as the system had not yet been sized. Here, however, the function is applied to compute the actual number of launches required to deploy the satellite to GEO, with injection into LEO using the computed values for the mass of the satellite.

For each Starship launch, the required energy is determined by evaluating the combustion energy of the propellant. The function `Energy_Input_Launches(n_launches)` computes the total energy expenditure for all launches based on:

- The total mass of propellant burned in both the Super Heavy (first stage) and Starship (second stage),
- The specific energy release per unit mass of methane,
- The conversion of energy from joules (J) to gigawatt-hours (GWh).

Propellant and Engine Details
The Super Heavy booster is powered by 33 Raptor engines, while the Starship second stage features

six engines—three standard Raptor engines and three Raptor Vacuum (RVac) engines, optimized for space operations.

The propulsion system operates on a cryogenic mixture of liquid methane (CH_4) and liquid oxygen (LOX) with an oxidizer-to-fuel ratio (O/F) of 3.6. This means that for every 3.6 parts of LOX, 1 part of methane is burned [118], [96], [59].

The total fuel load per launch is:

- Super Heavy: 3,600 tons of propellant,
- Starship: 1,200 tons of propellant.

From this, the total methane mass per launch is computed as:

$$M_{CH_4} = \frac{M_{\text{propellant}}}{\text{O/F ratio} + 1} \tag{5.5}$$

Applying equations (5.6) and (5.7), the energy required for propellant combustion is determined.

Mathematically, the energy per launch is computed as:

$$E_{\text{launch}} = M_{\text{propellant}} \times E_{\text{combustion}} \tag{5.6}$$

where:

- $M_{\text{propellant}}$ is the total propellant mass burned per launch,
- $E_{\text{combustion}}$ is the specific combustion energy of methane in joules per kilogram (J/kg).

The total energy required for n_{launches} launches is then computed as:

$$E_{\text{in, launch}} = \frac{E_{\text{launch}} \times n_{\text{launches}}}{3600 \times 10^9} \tag{5.7}$$

which gives the total launch energy in gigawatt-hours (GWh).

Energy Input for Orbital Transfers
Beyond the energy required for reaching orbit, additional fuel is needed for orbital maneuvers, which position the modules in their final orbits. The function `energy_in_orb_trans(num_launches, M_p)` accounts for this energy expenditure, where:

- M_p represents the propellant mass required per module transfer (computed through the Tsiolkovsky equation (4.4) from the total ΔV required for the maneuvers),
- The energy required for orbital maneuvers is computed using the same approach (specific energy per total mass of propellant), ensuring consistency in the overall mission energy budget.

A chemical bipropellant propulsion system is assumed in this analysis. According to the literature, one of the most commonly used propulsion systems for orbital transfers is the Nitrogen Tetroxide (N_2O_4) / Monomethylhydrazine (MMH) thruster [68].

This method ensures an accurate estimation of total energy costs, covering both launch and orbital positioning phases.

5.1.3. Energy metrics

Finally, based on the previously computed energy inputs and outputs, the methodology concludes with the evaluation of two key performance indicators: the Energy Return on Energy Invested (EROEI) and the Energy Payback Time (EPBT).

These metrics are defined as follows:

$$\text{EROEI} = \frac{E_{\text{out, total}}}{E_{\text{in, total}}} \tag{5.8}$$

where:

- $E_{\text{out, total}}$ is the total energy produced by the system over its entire operational lifetime,
- $E_{\text{in, total}}$ is the cumulative energy demand of the system, corresponding to the sum of all energy inputs detailed in subsection 5.1.2 (including materials production, solar cell manufacturing, ground and space segment construction, and transport logistics).

$$\text{EPBT} = \frac{E_{\text{in, total}}}{\overline{E}_{\text{out, yearly}}} \tag{5.9}$$

where:

- $\overline{E}_{\text{out, yearly}}$ represents the average annual energy output over the system's lifetime, accounting for the effects of performance degradation (e.g., solar cell efficiency loss over time).

5.2. Results

The results of the comparative energy analysis are presented and discussed in this section. Following the same order as in the section dedicated to the methodology, the results are presented first for the energy output, followed by the energy input.

5.2.1. Energy Output

For the terrestrial case, using as input the Global Horizontal Irradiance (GHI) value from Table 4.1, and considering a system lifetime of 30 years with a constant yearly degradation of 0.7% [83], as motivated in section 5.1 the total energy output for multijunction solar cell technology and system specifications listed in Table 4.2 is computed using Eq. (5.1). The results are summarized in Table 5.1.

Technology	η_{sys}	A [m²]	GHI [GWh/m²/year]	d	**Total Energy Output [GWh]** $E_{\text{total}} = A \cdot \eta_{\text{sys}} \cdot \sum_t \text{GHI} \cdot (1-d)^t$
Multi-junction	0.25	21,922,813	1598.2 x 10^{-6}	0.007	237,769

Table 5.1: Total energy output for ground-based solar stations over a 30-year lifetime, using the specified parameters and accounting for yearly degradation.

For the architecture derived from the trade-off and commercial study conducted by Thales and ESA, the total energy output is taken directly from that reference and amounts to 223.4 TWh. This value, slightly different from the one tht is computed for the case study, reflects the use of different assumptions specific to their analysis.

In contrast, for the case study space-based solution presented in this work, using Equation (5.2) to model a continuous 1 GW baseload power output and applying a yearly degradation factor of 1%, the resulting total energy output over the system's lifetime is 227,960.9 GWh.

System	E_0 [MW]	N [years]	d	T [hours/year]	Total Energy Output [GWh] $E_{\text{total}} = \left(\sum_{t=0}^{N} E_0 \cdot (1-d)^t\right) \cdot T$
Space-based (case study)	1000	30	0.01	8757.6	227,961

Table 5.2: Total energy output over a 30-year lifetime for the space-based system, accounting for a 1% yearly degradation and eclipse-related downtime.

5.2.2. Energy Input

The energy inputs required for the system are assessed for three different cases: the terrestrial photovoltaic power station, the ESA trade-off case, and the main space-based power system (SPS) case. The results account for the embedded energy in materials, transportation, launch operations, and orbital transfer energy requirements.

Terrestrial Case

For the ground-based photovoltaic power station, the total embedded energy investment is calculated by considering both the structural materials and the photovoltaic (PV) modules. The support structure requires approximately 6,700 tons of steel and 40,000 tons of concrete, both of which contribute substantially to the overall energy input. According to [35], the embedded energy is estimated at 30 GWh per kiloton of steel and 2.5 GWh per kiloton of concrete.

The multi-junction PV array covers an area of 21,922,813 m², with an associated embedded energy of 3072 MJ/m². In addition, the energy required for transporting materials over a distance of 300 km is included, based on a transport energy intensity of 2.26 MJ per ton per kilometer [47].

All energy contributions are converted to gigawatt-hours (GWh) using the relation 1Wh=3600J, and summed to obtain the total embedded energy. The total energy input for the terrestrial multi-junction PV station is thus computed to be 18,799.9 GWh. Table 5.3 summarizes the individual contributions and the overall total energy input for the terrestrial case.

With the computed total energy output reported in Table 5.1, the energy metrics can be evaluated:

$$\text{EROEI} = \frac{E_{\text{out, total}}}{E_{\text{in, total}}} = \frac{237{,}769\,\text{GWh}}{18{,}799.9\,\text{GWh}} \approx 12.65 \tag{5.10}$$

$$\text{EPBT} = \frac{E_{\text{in, total}}}{\overline{E}_{\text{out, yearly}}} = \frac{18{,}799.9\,\text{GWh}}{7{,}925.6\,\text{GWh/year}} \approx 2.37\,\text{years} \approx 866\,\text{days} \tag{5.11}$$

These results are consistent and in line with the main findings in literature [84], [10].

Component	Quantity	Specific Energy Input	Energy Input (GWh)
Steel	6,700 t	30 GWh/kt	55.833
Concrete	40,000 t	2.5 GWh/kt	27.778
Multi-junction PV	21,922,813 m²	3072 MJ/m² [47]	18,707
Transport (land)	300 km (materials)	2.26 MJ/ton·km [47]	8.795
Total Energy Input:			**18,799.9**

Table 5.3: Energy input for the terrestrial photovoltaic power station, including specific energy inputs per unit of material or distance.

Baseline SBSP Case

In the trade-off scenario developed by ESA and Thales Alenia Space, the energy investment for the entire SBSP system is evaluated by dividing it into four main segments:

1. Solar Power Satellite (SPS)
2. Launch
3. In-orbit Transport
4. Ground Power Station (GPS)

This framework serves as a reference methodology and is partially adopted in this work for consistency and comparability.

The total satellite mass is estimated at 6,640 tons, distributed as follows:

- 1,870 tons for photovoltaics
- 250 tons for wireless power transmission
- 3,370 tons for structural components
- 1,150 tons for other subsystems

The study assumes the following material composition for the satellite:

- 60% composites, aluminum, or other easily processed materials
- 17% steel or steel-like materials
- 3% silicon or similar materials
- 20% perovskite for PV cells

Using material-specific energy intensities, the total embedded energy for satellite construction is estimated to be 789 GWh [34].

The Ground Power Station is sized based on a surface area of 34 km^2, resulting in an estimated mass of 70,000 tons assuming a density of 2 kg/m^2. The assumed material composition is:

- 80% steel or similar materials
- 19% aluminum or other easily processed materials
- 1% silicon or similar materials

Using average energy intensities, the total embedded energy for the GPS is estimated at 3,209 GWh.

The study used as a reference for this architecture does not provide an explicit number of launches, but includes energy investments for both launch and orbital transport. These are based on assumptions regarding launcher performance, and transfer maneuvers:

- Launch energy investment: 3,179 GWh
- In-orbit transport energy investment: 62 GWh
- Total combined energy investment: 3,241 GWh

Considering the total input energy for this scenario, and the reported energy output, the EROEI and EPBT are computed as follows:

$$E_{\text{in, total}} = E_{\text{in, SPS}} + E_{\text{in, launch}} + E_{\text{in, orb}} + E_{\text{in, GND}} = 789 + 3179 + 62 + 3209 = 7239 \text{ GWh} \quad (5.12)$$

$$\text{EROEI} = \frac{E_{\text{out, total}}}{E_{\text{in, total}}} = \frac{223400 \text{ GWh}}{7239 \text{ GWh}} \approx 30.87 \quad (5.13)$$

$$\overline{E}_{\text{out, yearly}} = \frac{E_{\text{out, total}}}{30} = \frac{223400 \text{ GWh}}{30} = 7446.7 \text{ GWh/year} \quad (5.14)$$

$$\text{EPBT} = \frac{E_{\text{in, total}}}{\overline{E}_{\text{out, yearly}}} = \frac{7239 \text{ GWh}}{7446.7 \text{ GWh/year}} \approx 0.97 \text{ years} \approx 354 \text{ days} \tag{5.15}$$

Integrated tile SPS Case

In the primary case study of the space-based power system (SPS), the energy investment in the solar power satellite accounts for various components, including:

- the photovoltaic system,
- transmission array materials,
- CFRP for hexbus structures,
- Aluminum, composite and steel for structures and reflectors.

The total system mass is computed as M_{tot} = 5,398.3 tons, distributed as shown in Table 4.18.
The structural components, including reflectors and the backbone structure, are mainly composed of aluminum and steel, with embedded energy intensities of 300 GJ/kg and 100 GJ/kg, respectively. Carbon fiber reinforced polymer (CFRP) is used for the Hexbus modules connecting different tile layers, with a specific energy intensity of 800 GJ/kg. These values are first converted to GWh/kg and then applied to their respective subsystem masses to compute the total material-related energy input.

For the photovoltaic segment, a surface area of approximately 1.237 km² is required to generate the upstream power, considering a 1 GW delivery to Earth and the full chain of subsystem efficiencies. The solar cell technology assumed is multi-junction, with a manufacturing energy demand of 3072 MJ/m² [47], applied over the full cell area. A cover glass layer with a thickness of 200 µm is also included, and its mass is calculated from volume and density data, contributing to the material energy demand.

Transport-related energy inputs are divided into launch and orbital transfer phases. Based on a total system mass of 5,398.3 tons and launcher assumptions aligned with SpaceX Starship performance (100 tons payload to LEO, specific impulse of 350 s), the total number of launches is estimated at 214. The energy required for methane combustion during launch is computed assuming standard combustion values and propellant mass per flight. In addition, the energy required for propellant used during the orbital transfer from LEO to GEO is included, based on the Tsiolkovsky rocket equation and total required ΔV. All contributions are summed and converted into GWh to obtain the final total energy input associated with the deployment and construction of the integrated space-based solar power system. Particularly,

- Launches energy: 3442.61 GWh,
- Orbital maneuvers: 125.68 GWh.

The embedded energy associated with the ground power station is calculated based on its total mass and material composition. Assuming a surface density of 2 kg/m^2 [34] and a total area of 2.77 km^2, the ground station mass is estimated at 5532 tons. The material breakdown follows the same assumptions used in the reference architecture: 80% steel, 19% aluminum, and 1% silicon. By applying specific energy intensities of 100 MJ/kg for steel, 300 MJ/kg for aluminum, and 2000 MJ/kg for silicon, the total embedded energy required for the construction of the ground segment is estimated to be 241.3 GWh. This value accounts for the production of the materials composing the ground power station. Additional contribution, such as infrastructure, transport, rectifiers, and electrical systems, are included by referencing the total ground station energy input from the baseline architecture, leading to an estimated overall energy investment of approximately 2000 GWh [34].
All these contributes are then included in the total energy input accounting for the full life-cycle investment of the integrated SPS system.

Considering the total input energy for this scenario, and the computed energy output, the EROEI and EPBT for the integrated tile SPS system are evaluated as follows:

$$E_{\text{in, total}} = E_{\text{in, SPS}} + E_{\text{in, launch}} + E_{\text{in, orb}} + E_{\text{in, GND}} = 2327.7 + 3442.6 + 125.7 + 2241.2 = 8137.2 \text{ GWh} \tag{5.16}$$

$$\text{EROEI} = \frac{E_{\text{out, total}}}{E_{\text{in, total}}} = \frac{227960.9\ \text{GWh}}{8137.2\ \text{GWh}} \approx 28.02 \tag{5.17}$$

$$\overline{E}_{\text{out, yearly}} = \frac{E_{\text{out, total}}}{30} = \frac{227960.9\ \text{GWh}}{30} = 7598.7\ \text{GWh/year} \tag{5.18}$$

$$\text{EPBT} = \frac{E_{\text{in, total}}}{\overline{E}_{\text{out, yearly}}} = \frac{8137.2\ \text{GWh}}{7598.7\ \text{GWh/year}} \approx 1.07\ \text{years} \approx 391\ \text{days} \tag{5.19}$$

Table 5.4 reports the breakdown of energy input contributions for the case study of space based solar power.

Component	Quantity	Specific Energy Input	Energy Input (GWh)
Multi-junction PV	1.237 km^2	0.000853 GWh/m^2 [47]	1055.5
Steel	1079.7 t	0.028 GWh/t	29.91
Silicon	1,546.2 t	0.556 GWh/t	859
Aluminum	2,618.7 t	0.083 GWh/t	218.2
CFRP (Hexbus structure)	742.2 t	0.222 GWh/t	164.7
Total SPS Embedded Energy			**2327.7**
Launch Operations	214 launches	Estimated (methane combustion)	3442.6
Orbital Transfer	-	Based on Δv and I_{sp}	125.7
Ground Power Station	5532 t	-	2241.2
Total Energy Input (SPS + Launch + GPS)			**8137.2**

Table 5.4: Complete breakdown of energy input for the Integrated Tile SPS architecture, including satellite subsystems, launch, orbital transport, and ground segment.

5.2.3. Comparison of the three cases

Here, the results of the three analysed cases are compared in Table 5.5. As expected, the energy outputs are very similar among the three architectures, since all systems are sized to deliver approximately 24 GWh of energy per day. However, due to differences in degradation factors and minor system specifications, the total energy output over the lifetime of each system slightly varies. In particular, the ground-based system exhibits a higher value of produced energy, linked to a lower degradation factor, thanks to the more stable environmental conditions and the potential for maintenance.

The energy input, on the other hand, shows a significantly higher value for the ground-based concept. This is mainly due to the much larger area of PV modules required when sizing a system on Earth, where solar input is intermittent and affected by atmospheric and seasonal factors. The production of high-efficiency solar cells is extremely energy-intensive, and when scaled up to the needed surface, this becomes the dominant contributor to the total energy investment.

The space-based systems, by contrast, benefit from continuous solar exposure and higher system-level efficiencies, which allow for a reduced PV surface and hence lower embedded energy in the materials. This advantage compensates for the high energy cost associated with launching and deploying the infrastructure in space. Despite the additional energy input from launch and orbital maneuvers, the total energy investment remains significantly lower than in the terrestrial case.

The EROEI and EPBT results clearly show that, from an energetic perspective, the space-based options offer more promising returns. Nonetheless, it is important to note that several assumptions are made throughout the analysis, such as launcher performance, in-orbit assembly requirements, and

subsystem efficiencies, and some contributions (e.g., energy to build the launch vehicle) are not included. Therefore, sensitivity analyses are conducted to explore how these uncertainties affect the overall energy performance of the system.

In particular, the ESA/Thales baseline case shows an even more favorable EROEI compared to the case study architecture. However, the methodology behind this reference case lacks specific details on material quantities and their associated energy intensities. Therefore, while it provides a useful benchmark, its direct comparison must be approached with caution.

Case	E_{out} [GWh]	E_{in} [GWh]	EROEI	EPBT
Ground-based Station	237,769	18,799.9	12.6	2.4 years (876 days)
First SBSP Architecture	223,400	7,239	30.87	0.97 years (354)
Integrated Tile Architecture	227,960.9	8,137.2	28.02	1.07 years (391 days)

Table 5.5: Energy Return and Payback Time, comparison of the three cases

5.2.4. Conclusions

This chapter aimed to evaluate the energy performance of various solar power architectures, comparing ground-based photovoltaic plants with space-based power systems (SBSP), using key metrics such as Energy Return on Energy Invested (EROEI) and Energy Payback Time (EPBT). The analysis highlights the potential of SBSP to offer substantially higher energy returns over its operational lifetime when compared to terrestrial systems. These results suggest that, under certain conditions, SBSP may represent a viable and more efficient long-term alternative for clean baseload energy generation, though only if key technological and operational challenges can be addressed.

The analysis, however, is built on several assumptions and simplifications which, while necessary for computational feasibility, introduce uncertainty into the results. To ensure high transparency and interpretability, the following assumptions are outlined:

Key Assumptions

- **Launcher Selection and Performance**: The study assumes that SpaceX's Starship will be fully operational and capable of delivering 100 tons to Low Earth Orbit (LEO). The payload mass constraints are considered, but volume constraints are not explicitly evaluated, as this would require a detailed design of the modular satellite architecture and deployment system. Instead, it is assumed that the payload fits within the available fairing volume.
- **Tsiolkovsky Rocket Equation Simplifications**: The orbital transfer calculations assume ideal conditions, including constant exhaust velocity, no external forces acting on the rocket, and negligible atmospheric drag and gravity losses. These factors could slightly alter the actual ΔV requirements and propellant mass in a real mission.
- **Structural and Material Composition Approximations**: The mass distribution among photovoltaic modules, wireless power transmission arrays, and support structures is based on reference architectures and literature estimates. While the study accounts for primary structural materials such as CFRP, aluminum, steel, and composites, other components and detailed considerations on their composition are not included.
- **Decommissioning and End-of-Life Considerations**: The analysis excludes decommissioning energy costs, as end-of-life disposal strategies for space-based solar power satellites remain speculative. However, However, given the large size of the space structure, these factors are expected to have a significant impact on the final results.

Limitations and Open Considerations

- **Launcher Materials and Reusability**: The energy required to produce all materials for the launcher is not included, as there is limited data on its full material breakdown. Similarly, the

impact of reusability is not considered, as there is uncertainty about the number of flights each vehicle can withstand. These are expected to havenon-negligible impact on overall performance.

- **Alternative Transportation Methods**: The study does not consider alternative orbital transfer methods, such as low-thrust electric propulsion, which could reduce propellant consumption at the cost of longer transfer times, or the use of orbital tugs or in-orbit Starshi refuel.
- **Sensitivity to Launcher Performance Estimates**: The results are based on projected Starship performance, which may change as the system is developed and tested. However, the model is parametric, so it can be updated with new launcher specifications.
- **Neglecting In-Orbit Assembly Complexity**: While the SPS concept has a modular deployment, the energy required for robotic assembly, maintenance, or station-keeping operations in orbit is not included in the estimates.

Overall, the results provide useful indications and help to understand key differences between the examined SBSP architectures. While based on simplified assumptions, the methodology offers a practical framework for early-stage comparison. Further work could focus on refining subsystem models and incorporating uncertainty to improve the robustness of the analysis.

To assess the robustness of the findings, a sensitivity analysis is carried out. Parameters such as photovoltaic efficiency, WPT efficiency, degradation factor, system lifetime, and launcher performance are varied within reasonable limits. The resulting variations in EROEI are tracked.

5.3. Sensitivity Analysis

Finally, the effect of relevant parameters on the energetic performance of the case study is assessed through a sensitivity analysis. By varying one single parameter at a time while keeping all others constant, this method allows us to isolate the individual effects. This final step of the energy analysis is particularly valuable, as it provides preliminary insights into the most critical aspects to focus on in order to improve the energy efficiency of the system. In particular, parameters related to developing technologies have been analyzed to evaluate their potential impact.

This analysis also connects to the previous chapter, where the energy analysis and system sizing were based on assumptions and limitations. In this context, adopting more realistic values allows for an exploration of how different scenarios would affect overall performance.

By studying how variations in system characteristics influence the Energy Return On Investment (EROEI), this analysis highlights the parameters that most significantly affect the sustainability of the mission.

5.3.1. Selection of Parameters for Sensitivity Analysis

The parameters selected for the sensitivity analysis are presented, underlining their relevance and the rationale behind their selection.

Specific Impulse of the Orbital Transfer Vehicle (I_{sp})

Defined as the thrust generated per unit of propellant consumed, the specific impulse is a key indicator of propulsion system efficiency. Investigating its effect on overall energy performance is particularly relevant as it relates to one of the in-development technologies of the mission: the orbital transfer system.
Given recent advancements in orbital tugs and electric propulsion, analyzing the effect of varying I_{sp} helps in understanding how different propulsion technologies might impact the overall system. This parameter is expected to affect the required propellant mass for the transfer, and consequently, the allocatable mass of the module as a launch payload for each launch.

Photovoltaic Efficiency (η_{PV})

As the main energy generation system of the mission, the photovoltaic (PV) subsystem plays a crucial role in energy performance. The efficiency of the PV system directly impacts the size of the solar cells, their mass, and the structural mass of the spacecraft.
Given that current research focuses on new materials and lighter, high-efficiency PV cells, this parameter is highly relevant for future system improvements. Considering technologies operating at lower efficiencies, this analysis explores how performance would degrade if these currently available systems were used.

Wireless Power Transmission Efficiency (η_{WPT})

As in any space mission, efficiency is critical since every loss translates into additional mass or performance penalties. In the case of Space-Based Solar Power , the wireless power transmission system represents a particularly challenging technology due to its low technology readiness level.
Investigating how future higher efficiencies for retrodirective phased array transmission of gigawatts of power over long distances could impact the system is therefore crucial. This parameter is particularly interesting to study because of its highly uncertain nature and the unknown potential future developments in SBSP systems.

System Lifetime

The longer the system operates, the more energy it produces over its life, allowing the energy investment (launch, construction, manufacturing) to be amortized over more output. However, in current space operations, long lifetimes are limited due to the lack of in-orbit repair or replacement.

The baseline assumes a 30-year lifetime. The analysis explores both more conservative lifespans and extended missions under the assumption that operational and environmental conditions allow prolonged functionality, without full system repair.

Degradation Factor (d)

This factor indicates the annual decline in performance of key components such as PV panels and transmission systems. A lower degradation rate may reflect future improvements in component reliability or partial in-orbit servicing capabilities.

Its influence is cumulative over the mission life: even small changes significantly affect the total energy output and, consequently, the EROEI.

Launcher Performance

The launcher is a key contributor to the energy investment required for deploying the system. While the baseline design assumes an advanced launcher under development with high payload capacity and efficiency, this analysis also considers the implications of relying on currently operational launch systems. Particularly, as explained in chapter 4, the use of Falcon Heavy as launcher system for the mission is simulated.

Table 5.6 summarizes the rationales behind the selection of parameters and the expected impact on the energetic performance of the system.

Parameter	Justification	Impact on System Performance
Specific Impulse (I_{sp})	Indicator of propulsion system efficiency, linked to propellant mass	Affects required energy for orbital transfers and launch payload allocation
Photovoltaic Efficiency (η_{PV})	Determines the efficiency of power collection	Impacts array size, structural mass, and energy payback
Wireless Power Transmission Efficiency (η_{WPT})	Determines energy delivery from orbit to Earth	Affects net delivered energy and system viability
System Lifetime	Duration of productive operation	Impacts total energy output and amortization of energy investments
Degradation Factor (d)	Annual performance decay of components	Influences total energy output and long-term sustainability
Launcher Performance	Allows assessment of system performance using current high-TRL launchers.	Affects launch energy demand, number of launches, and EROEI

Table 5.6: Parameter Selection Justification for Sensitivity Analysis

5.3.2. Results

Visual Analysis of EROEI Trends

Figure 5.2 shows the EROEI response to five different parameters, and indicates the base values of the case study:

- In Figure 5.2(a), increasing photovoltaic efficiency (η_{PV}) consistently improves EROEI. The curve grows non-linearly, showing enhanced gains at higher efficiencies.
- In Figure 5.2(b), a similar behavior is observed for the wireless power transmission efficiency (η_{WPT}), which strongly influences net output energy.
- In Figure 5.2(c), EROEI increases with higher specific impulse (I_{sp}), although the effect gradually saturates.
- In Figure 5.2(d), longer system lifetime leads to nearly linear improvements in EROEI, as the energy investment is amortized over a greater output period.
- In Figure 5.2(e), a higher degradation factor reduces EROEI significantly. The curve declines with increasing slope, indicating that small increases in degradation strongly affect output energy

over time.

Discussion of results

- *Photovoltaic Efficiency (η_{PV})*: This parameter directly affects the required area of solar panels. Higher efficiency leads to a smaller area, which reduces the mass of PV modules, reflectors, structural support, and cover glass. Since η_{PV} appears in the denominator of the power requirement equation ($P_{pv} = P_{wpt}/\eta_{pv}$), its impact is amplified due to its inverse proportionality. As a result, improvements in PV efficiency propagate through several mass-related variables in the system.
- *Wireless Power Transmission Efficiency (η_{WPT})*: An increase in η_{WPT} reduces the power required at the transmitting end (P_{wpt}), which also reduces PV system size and WPT array area. This affects both the energy output (via total efficiency η_{tot}) and energy investment (through mass and material requirements).
- *Specific Impulse (I_{sp})*: Higher I_{sp} improves propulsion efficiency, lowering the propellant mass required for orbital transfer according to the Tsiolkovsky rocket equation:

$$M_{\text{final}} = M_0 \cdot \exp\left(-\frac{\Delta V}{I_{sp} \cdot g_0}\right)$$

  A lower propellant mass reduces the number of launches and their associated energy cost. However, the effect saturates at higher values, as diminishing returns become evident once transfer mass becomes a smaller fraction of the total. This is especially relevant when considering electric propulsion systems, which can achieve I_{sp} values above 1000–3000 s. These systems are more mass-efficient but offer lower thrust and longer transfer durations. In this study, transfer time is not modeled, but it remains a potential future extension.
- *System Lifetime*: A longer operational duration increases the cumulative energy output. Since the energy investment remains constant, EROEI improves almost linearly. This result highlights the importance of ensuring long-term reliability of space systems, even in the absence of in-orbit servicing.
- *Degradation Factor*: Higher degradation reduces the yearly energy output, especially over longer missions. Since degradation accumulates year over year, its effect on total energy output is exponential. Small increases in this parameter lead to strong EROEI penalties.

Normalized Sensitivity Analysis

To compare the impact of these parameters quantitatively, a normalized sensitivity coefficient is computed for each one. This coefficient evaluates the relative change in EROEI in response to a relative change in the parameter, defined by:

$$S = \frac{\Delta \text{EROEI}/\text{EROEI}_{\text{base}}}{\Delta x / x_{\text{base}}} \tag{5.20}$$

The EROEI variation is calculated using central difference approximation, applying a $\pm 10\%$ variation around each baseline value. Figure 5.3 shows the sensitivity results.

- System lifetime shows the highest sensitivity. A 10% change causes nearly a 9% variation in EROEI.
- Photovoltaic efficiency and WPT efficiency follow closely, with similar coefficients. Their dual effect on both energy output and component sizing amplifies their impact.
- Specific impulse also contributes significantly but with diminishing returns at high values.
- The degradation factor has a negative sensitivity, as expected, and its effect is smaller in normalized terms due to its low baseline.

These results help prioritize future research and technology improvements by identifying which parameters most critically affect the energy return of the system.

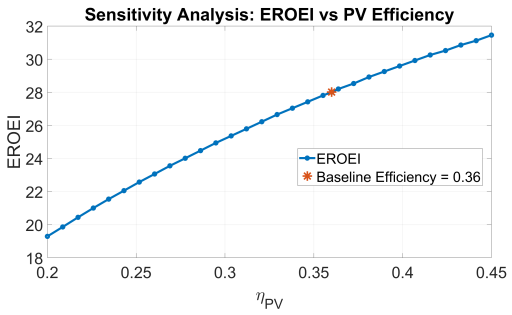

(a) PV Efficiency (η_{PV})

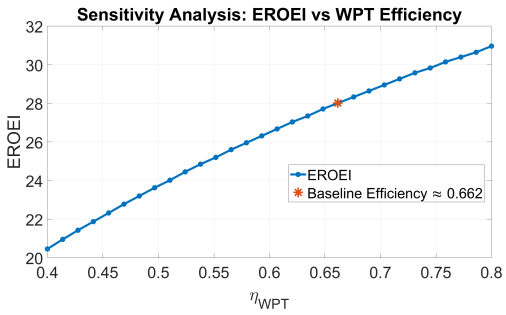

(b) WPT Efficiency (η_{WPT})

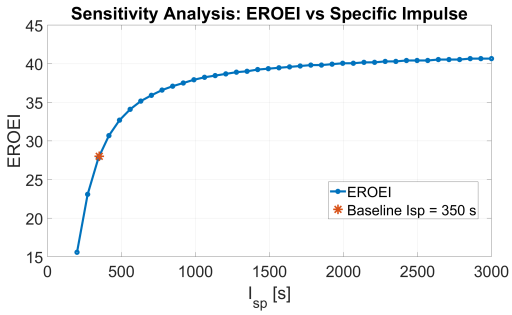

(c) Specific Impulse (I_{sp})

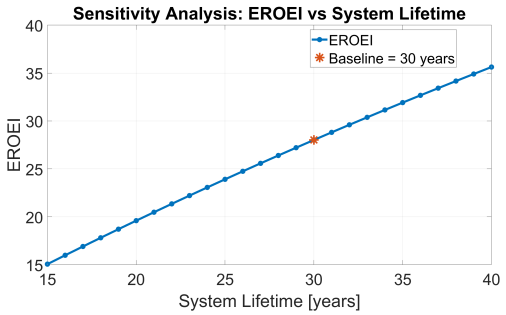

(d) System Lifetime

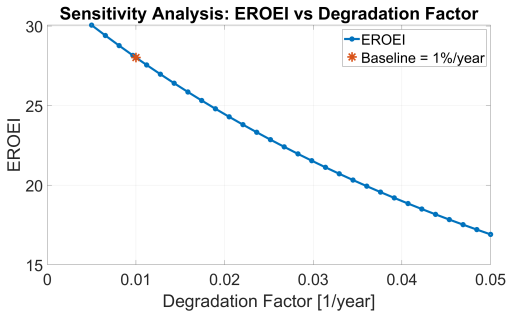

(e) Degradation Factor

Figure 5.2: EROEI sensitivity analysis with respect to 5 key system parameters.

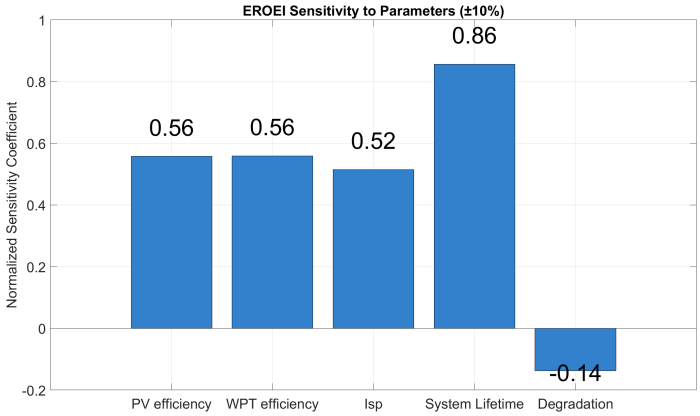

Figure 5.3: Normalized sensitivity coefficients of EROEI to system parameters (±10%).

Parameter	Base	Range	Effect on EROEI
Specific Impulse I_{sp}	350 s	200–3000 s	$I_{sp} \uparrow \Rightarrow$ propellant $\downarrow$, EROEI $\uparrow$
PV Efficiency η_{PV}	0.36	0.20–0.45	$\eta_{PV} \uparrow \Rightarrow$ area, mass $\downarrow$, EROEI $\uparrow$
WPT Efficiency η_{WPT}	0.64	0.40–0.80	$\eta_{WPT} \uparrow \Rightarrow$ system size $\downarrow$, EROEI $\uparrow$
System Lifetime	30 years	15–40 years	Lifetime $\uparrow \Rightarrow$ output $\uparrow$, EROEI $\uparrow$ (linear)
Degradation Factor d	0.01	0.005–0.05	$d \uparrow \Rightarrow$ output $\downarrow$, EROEI $\downarrow$ (nonlinear)
Launcher	Starship	Falcon Heavy	Launches $\uparrow$, energy cost $\uparrow$, EROEI $\downarrow$

Table 5.7: Summary of parameters tested in the sensitivity analysis, including base case, variation range, and qualitative effects on EROEI.

Launcher performance

As anticipated, the analysis is also conducted considering a currently operating launch vehicle—Falcon Heavy—to assess how the energetic performance of the system varies with current launch capabilities. The main changes implemented in the model are:

- Payload to Low Earth Orbit (LEO): $m_0 = 63.8$ tons
- Specific Impulse: $I_{sp} = 285$ s
- Total propellant per launch: 1330 tons (RP-1/LOX)

As a consequence, the number of required launches increases substantially due to the reduced payload capacity. This significantly raises the contributions of launch-related energy inputs, both for the launch phase and for the orbital transfer.

The results of the simulation using Falcon Heavy parameters are reported in Table 5.8.

The results are summarized in Table 5.8.

Parameter	Value
Number of Launches (n_{launch})	721
Launch Energy ($E_{\text{in, launch}}$) [GWh]	7367.8
Orbital Transfer Energy ($E_{\text{in, orb}}$) [GWh]	187.24
Total Energy Input ($E_{\text{in, total}}$) [GWh]	12124
Total Energy Output (E_{out}) [GWh]	227960
EROEI	18.80
EPBT [years]	1.60

Table 5.8: Energy results for the scenario using Falcon Heavy as launcher.

The resulting EROEI is significantly lower than that obtained using Starship (approximately 28), already suggesting that current launch technology is probably incompatible with the energy sustainability requirements of such a project.

Moreover, it is important to note that the energy embedded in the production and reusability of the launcher itself is not accounted for in this analysis—if included, this would further reduce the EROEI. Similarly, the inclusion of thermal control systems would increase the system mass and energy input, further lowering the performance (see Table 6.9.

These findings confirm the critical dependence of Space-Based Solar Power (SBSP) concepts on the availability of high-capacity, fully reusable launch systems such as Starship, which are essential to achieve favorable energetic returns.

5.3.3. Conclusions

The sensitivity analysis complements the energy assessment presented in the previous sections by quantifying how variations in key parameters influence the overall energetic performance of the SBSP system. While the main energy analysis offers a first-order estimate of system feasibility, this section demonstrates that many of the results are highly dependent on assumed values—particularly those related to subsystem efficiencies and lifetime performance.

The results confirm that system lifetime and degradation factor are among the most influential parameters. Given the long-term nature of SBSP operations, even small changes in degradation rates or lifespan have a significant cumulative impact on the total energy returned. Similarly, the analysis shows that the system is particularly sensitive to variations in PV and wireless power transmission (WPT) efficiency. Because these factors influence both the size and mass of major subsystems, as well as the net energy delivered to the ground, their impact on EROEI is amplified throughout the model.

Although the analysis shows that SBSP could still be energetically competitive with terrestrial alternatives under more conservative efficiency assumptions, these findings should be interpreted with caution. The current framework relies on a number of simplifications and idealized assumptions, such as aggregated energy coefficients, perfect subsystem integration, and the absence of some critical functions like thermal management, in-orbit assembly, or maintenance.

To move beyond preliminary estimates, it is necessary to progressively include more realistic modeling of each subsystem and their interactions. In this context, the next chapter focuses on the thermal control system, which plays a fundamental role in space system design but is not yet reflected in the energy balance. This step marks the beginning of a more granular implementation of physical models within the NEA, allowing for a better understanding of how real-world design constraints might shift the conclusions drawn so far.

6

Thermal Analysis

The final phase of this study focuses on analyzing the thermal behavior of the integrated tile architecture. While the energy analysis has demonstrated promising results in terms of efficiency, it assumes ideal thermal conditions and does not account for the complexities of the thermal environment. However, the thermal system directly influences energy performance by affecting the efficiency and reliability of key components such as solar cells, power transmission systems, and electronics. For instance, elevated temperatures can degrade solar cell efficiency and may lead to the need for active thermal regulation, which would consume additional power and reduce the net energy output. Therefore, to ensure a degree of reliability in the energy results, it is crucial to analyze the thermal system of the integrated tile case study under realistic orbital conditions. The analysis and design are primarily driven by the requirement to maintain passive control techniques. In fact, if active control techniques become necessary, the energy performance, system complexity, and overall feasibility will be negatively affected.

In general, analyzing the integrated tile concept without addressing the thermal aspect would be unreliable, as, given the extreme thermal conditions and the constraints on heat dissipation, neglecting it would undermine the credibility of the overall analysis.

The thermal analysis is based on a modular unit of the system, operating in geostationary orbit (GEO) and delivering 1 GW of baseload power—the same configuration considered in the energy analysis—with the SPS-Alpha reference architecture serving as the primary data source.

This chapter presents the thermal analysis conducted on a prototype satellite module for the defined scenario. It begins by outlining the thermal challenges, system requirements, and analysis objectives. The methodology is then described, including the rationale behind it and the development of progressive thermal models. Finally, the results are presented and discussed, offering insights and points for reflection on the subject.

6.1. Methodology

To address the research question on the thermal aspects of the integrated tile, the following approach is adopted.

First, the thermal challenge that motivates this analysis is outlined, along with the objective it defines; this provides the necessary context for the study.

Next, the thermal requirements of the system are defined, as they guide both the development of the analysis and the interpretation of the results.

The modular unit selected for the study is then described, highlighting the key parameters relevant to the thermal analysis. The analysis is conducted using ESATAN-TMS, beginning with the characterization of the thermal environment in which the system operates. A radiative case is developed to compute

the external thermal loads, defining the thermal conditions that the system must withstand and the heat fluxes acting on it.

Following this, the thermal model is constructed in ESATAN, with detailed components defined and mapped to their corresponding physical geometries.

The results of the thermal case in ESATAN-TMS yield the temperatures of the defined nodes.First, they are first analyzed without any thermal control measures, enabling the identification of thermal zones and components that require thermal management.

A preliminary thermal control design is then developed. Specific control techniques are selected based on defined criteria, appropriately sized, and applied to the model. Their effects on the overall thermal behavior are evaluated.

Finally, conclusions are drawn, with particular emphasis on the connection between thermal and energy analyses, assessing the impact of thermal constraints on the system's energy performance.

6.1.1. Thermal challenge and objective

While the integrated tile architecture demonstrates promising energy performance, it presents a critical thermal challenge that must be addressed to validate the energy analysis results.

The main thermal issue arises from the system's ability to handle several gigawatts of power while having limited radiative surfaces for heat dissipation (for the compactness of the tile architecture). This study aims to determine whether passive thermal control can maintain the system within operational temperature limits or if active thermal management is required.

The objective is to analyze the thermal behavior of the integrated tile and quantify the impact of thermal constraints on system performance.

6.1.2. Thermal Requirements

The thermal analysis studies the behavior and response of the satellite to the aforementioned thermal loads. The thermal control system has the scope of ensuring that the components of the satellite stay within the defined temperature boundaries. To do that, thermal requirements need to be defined. Usually, these depend on the functioning and specifics of the components, such as solar cells and electronics, and their operating temperature limits. Beyond defining operating temperature limits, additional thermal constraints must be considered, and among these, a key factor is temperature gradient uniformity, which ensures thermal consistency across components and prevents localized overheating or mechanical deformation due to uneven thermal expansion. Table 6.1 summarizes the operating temperature limits for the analyzed components, and allowed thermal gradients.

Component	Operating Temperature Range [°C]	Temperature gradient
Solar Cells	[-140, +150]	$\Delta T_{\text{solar panels}} < 20 - 30°C$
Antenna	[-50, 70]	$\Delta T_{\text{Antenna}} < 5°C$
SSPAs (and Conversion)	[-20, 150]	$\Delta T_{\text{SSPAs}} < 10 - 15°C$

Table 6.1: Temperature Requirements of Components

The compliance with the thermal requirements is verified through post-processing of the thermal model simulation results. The verification approach is as follows:

For each component and across the entire orbit, the minimum and maximum temperature across all mesh nodes must fall within the defined range:

$$T_{\text{min}}^{\text{component}} \leq T_{\text{node}_i} \leq T_{\text{max}}^{\text{component}}, \quad \forall i \tag{6.1}$$

If any node exceeds the specified limits, the component is considered out of compliance and may require additional thermal control measures.

The maximum temperature difference ΔT across all nodes of each component must not exceed the defined threshold:

$$\max(T_{\text{node}_i}) - \min(T_{\text{node}_j}) < \Delta T_{\text{allowed}}, \quad \forall i, j \tag{6.2}$$

where $\Delta T_{\text{allowed}}$ is the maximum allowable gradient defined for each component.

If this condition is violated, adjustments in thermal management (e.g., heat distribution) may be necessary.

By applying this verification method, the thermal control strategy can be refined to ensure that all components operate within safe and optimal conditions.

These requirements will form the foundation for a robust thermal analysis of the spacecraft.

6.2. Thermal model

Here, the thermal model built in ESATAN is presented. Initially, the model is analyzed without any thermal control methods to assess its thermal behavior and determine the need for thermal management. The results are then presented step by step, with each implementation of a control method followed by an evaluation. If further thermal management is required, additional control measures are applied, and the results are analyzed accordingly.

6.2.1. Model setup

The modeled component consists of three main elements: the solar cells, the conversion system (specifically the solid-state power amplifiers), and the transmitting array.

The thermal model used in this analysis is based on a modular unit of the tile, under the assumption that each module behaves as thermally independent. This does not imply that thermal control is implemented at this stage, but rather serves as a simplifying assumption for the analysis. Nonetheless, the overall thermal system design takes into account that these modules will eventually be assembled in orbit.

Since this is an idealized model, the temperature effects on the efficiency of key layers—particularly the photovoltaic and DC-to-RF conversion layers—are not accounted for. These efficiencies tend to decrease as temperature rises, generating additional heat that must be dissipated, further increasing the module temperature. A study conducted by Jaffe et al. [52] shows that while preliminary thermal vacuum tests on the RF electronics revealed only limited efficiency variation (within 2%) between –20°C and +95°C, the complete module was not tested under the more extreme thermal conditions predicted by simulation. Notably, their thermal model suggests that under three suns of solar concentration, module temperatures can exceed 150°C, levels at which efficiency degradation in both photovoltaic and DC-to-RF layers becomes significantly more critical [52]. Even though multijunction solar cells are more suitable for concentrating systems, thanks to their relatively lower sensitivity to temperature increases compared to other technologies [16], a study has shown a 5% reduction in the efficiency of a PV module based on triple-junction technology for a temperature increase from 5°C to 170°C and concentration ratios (C) ranging from 1 to 3000 [43].

The total tile architecture, summarized in Table 4.18, follows a modular structure composed of multiple independently functioning units. The thermal analysis is conducted on a demonstrator prototype with the dimensions of a single module, specifically 2.5m x 2.5m, consisting of three layers (PV, Conversion board, Transmission array).
These layers are connected via the Hexbus structure, and each module is assumed to be equipped with an electronic interface for integration with adjacent modules.

The key parameters relevant to the thermal analysis, scaled to a single module, are summarized in Table 6.2.

Parameter	Value
Module Dimensions	2.5 m × 2.5 m
Number of Layers	3 (PV, DC-RF Conversion, Transmission)
Structural Connection	Hexbus Framework
Functionality	Independently Operating Unit
Fraction of incoming solar power at PV	25,518 W

Table 6.2: Key Parameters of the Analyzed Module

A geometry for the modular unit is defined and implemented in ESATAN.

6.2.2. Geometry definition

Layers

The first step in defining the model is to incorporate the three layers of the tile: one for the solar cells, one for the integrated circuit board with electronic components, and the last for transmission. Each layer is represented as a rectangular geometry with a defined thickness and is further divided into a 10 × 10 mesh of nodes for detailed thermal analysis.

The materials and properties associated with each layer are summarized in Table 6.3.

Property	PV Layer	Conversion Layer	Antenna
Material	Gallium-Arsenide	Copper	Aluminum
Density [kg/m^3]	5320	8960	2700
Conductivity [W/(m K)]	55	380	237
Specific Heat [J/(kg K)]	330	385	870
Thermo-optical Properties			
Solar Absorptivity	0.91	-	0.5
IR Emissivity	0.81	-	0.5

Table 6.3: Material Properties of Different Layers

Each layer has two surfaces: front and rear. The external surfaces of the PV and Antenna layers are classified as active, meaning both radiative and conductive heat fluxes are considered. Conversely, the conversion layer surfaces and the internal surfaces of the PV and Antenna layers are treated as purely conductive, as no radiation occurs at the internal interfaces within the tile structure. This is why the conversion layer does not have any thermo-optical properties defined in Table 6.3.

Interaction between layers

Each layer is connected to the next within the tile. As defined in Chapter 4, this architecture achieves employs Hexbus structures made of CFRP to achieve connection between layers.

To model these connections in ESATAN, user-defined conductors are introduced between the corner nodes of each layer. In ESATAN, a user-defined conductor is a thermal connection explicitly specified by the user, allowing for customized properties such as conductivity and shape factor rather than relying on default material-based conduction. Specifically, these contact conductors are defined with a conductivity of 100 W/(m·K) ([62]) and a shape factor[1] of 0.06. In Figure 6.1, the model geometry is shown, including the three layers and the conduction paths, which are represented as red lines connecting the layers.

[1] Ratio between the cross-sectional area of the conductor and its length.

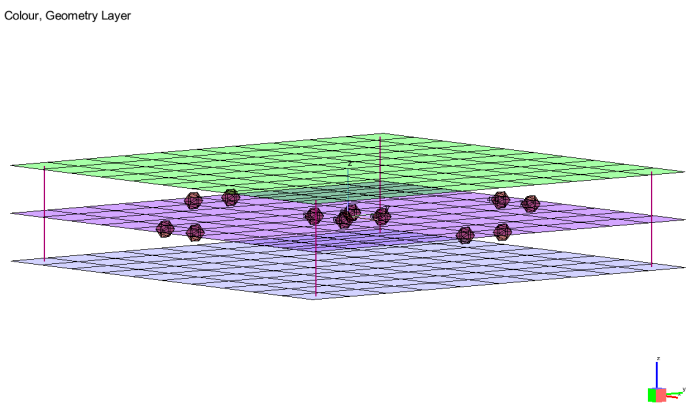

Figure 6.1: Geometry of ESATAN model

Internal Heat Sources

To model internal heat dissipation from electronic components, the focus is on the solid-state power amplifiers (SSPAs), as they are the primary sources of internal heat generation. Their thermal behavior is represented using non-geometrical nodes in ESATAN. These nodes are typically used to model thermal capacities, couplings, and energy exchanges that do not correspond to physical surfaces or structural elements of the spacecraft. As the geometry or structural aspect of the SSPAs are not relevant for the analysis, these are modeled as non-geometrical nodes.

A total of twelve SSPAs are incorporated into the model.

The heat dissipated by these components is modeled by applying a boundary condition defined as 'total heat' to the entire group of SSPAs. This ensures that the heat is distributed appropriately among them. Performing basic calculations, the total heat dissipated by the SSPAs can be computed based on the incoming solar radiation on the PV surface as follows.

$$H_{\text{SSPA}} = (1 - \eta_{\text{SSPA}}) \cdot \text{A}_{\text{SC}} \cdot S \cdot c \cdot \alpha_{\text{sc}} \cdot \eta_{\text{sc}} \tag{6.3}$$

Where:

- S is the incoming solar radiation per unit area,
- A_{SC} is the area of the solar cells,
- $c = 3$ is the solar concentration factor,
- α_{sc} is the absorptivity of the solar cells,
- η_{sc} is the efficiency of the solar cells,
- η_{SSPA} is the efficiency of the SSPAs.

The value of incoming solar radiation per unit area, S, is set to 1361 W/m^2, which is the average solar flux received by a spacecraft in geostationary orbit. This is amplified by a factor of 3 (c) to account for the use of solar reflectors that concentrate sunlight onto the tile; the value of 3 is based on the SPS-Alpha design [61].

To obtain the total power incident on the PV area, the area of the solar cells must be considered. In this study, as discussed in chapter 4, this corresponds to a value of 1236949.6 m^2.

The product $S \cdot A_{\text{SC}} \cdot c \cdot \alpha_{\text{sc}} \cdot \eta_{\text{sc}}$ represents the power incident on the PV side of the tile. Here, the absorptivity of the solar cells is assumed to be 0.91, while the efficiency η_{sc} is 0.36. This means that a portion of the incoming radiation is absorbed and converted into electricity, which is assumed to reach

the SSPAs without losses. Multiplying by the solar absorptivity and efficiency of the solar cells yields the power transferred from the concentrated sunlight through the PV layer to the SSPAs.

The final term, $(1-\eta_{\text{SSPA}})$, accounts for the fraction of power arriving at the SSPAs that is not converted into RF power and is instead lost as heat. A conservative assumption is made that all of this lost energy is dissipated as heat.

Using these values, and considering a 2.5 m $\times$ 2.5 m prototype with 12 non-geometric nodes representing the SSPAs, the total heat dissipated by the SSPAs is:

$$H_{\text{total}} = (1-0.8) \cdot 1361 \text{ W/m}^2 \cdot 3 \cdot 0.91 \cdot 0.36 = 1837.35 \text{ W},$$

which corresponds to approximately 153.1 W per SSPA.

Finally, to model the circuit contacts, accounting for the fact that these SSPAs are connected to both the solar cells and the phased array elements, each non-geometrical node is linked to:

1. One node on the solar cell side
2. One node on the antenna surface

This connection is implemented using a user-defined conductor, which has the thermal properties of copper, as copper is the primary material of the circuit. Figure 6.2 highligthhs the non-geometrical nodes in the model and the boundary condition applied to them.

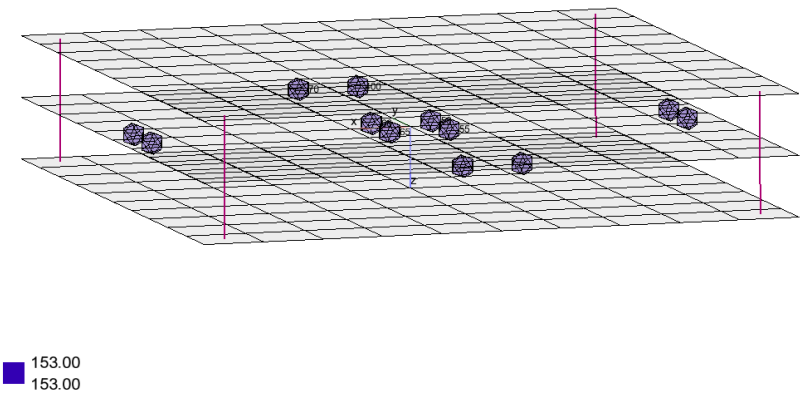

Figure 6.2: Boundary condition of heat dissipation of solid-state power amplifiers

6.2.3. Pointing Settings and Requirements

The following point to address and model is the system's pointing or attitude. The mission is subject to a dual pointing requirement:

- The antenna shall always point toward Earth, ensuring continuous RF power transmission to the ground.
- The solar cells shall continuously receive sunlight, except during eclipse periods. This is achieved through the rotation of dedicated solar reflectors.

These requirements are directly derived from the mission requirement of uninterrupted power beaming.

However, the complex geometry of these rotating reflectors is not included in the thermal model, as it would significantly complicate the analysis without offering additional insight relevant to this study. Therefore, to model the continuous sunlight incident either si mette un pointing req on the thermal model for the pv side to always face sun or a fixed heat input on it.

The model focuses solely on the modular tile component, represented as a flat, layered structure. Naturally, a single tile cannot simultaneously satisfy both pointing requirements across its two opposite faces: if one always faces the Earth, the opposite side cannot always be pointed towards the Sun. This limitation must be accounted for in the thermal modeling process.

To overcome this, the first step of computing the thermal loads on the model through the radiative environment is defined through two separate analyses, each isolating one side of the tile as a standalone surface in orbit, exposed to the relevant external fluxes:

- A first radiative case simulates the solar cell side, modeled as a flat plate continuously facing the Sun in geostationary orbit. The front side is assigned the thermo-optical properties of the solar cells, while the back side is considered inactive, as it does not contribute meaningfully to the analysis.
- A second radiative case simulates the antenna side, modeled as a flat plate continuously facing Earth. The front side uses the thermo-optical properties of the antenna surface, and the back side is again treated as inactive.

These two simplified cases allow for an accurate estimation of the external thermal loads acting on each surface independently.

In the step of the actual thermal analysis, the integrated layered geometry described in subsection 6.2.2 includes both sides of the tile.

To fulfill the solar pointing requirement in the analysis, the continuous solar flux on the solar cells is modeled as a uniform heat flux boundary condition applied directly to the PV surface. This represents the effect of the concentrating reflectors, even though they are not explicitly modeled.

However, care must be taken when defining this heat load. Since the boundary condition must represent the absorbed heat per unit area, not the total incident solar flux, several factors must be included. The heat flux per unit area applied as a boundary condition is therefore:

$$H_{\text{SC}} = S \cdot c \cdot (1 - \eta_{\text{sc}}) \cdot \alpha_{\text{sc}} \tag{6.4}$$

Where:

- S is the solar flux in GEO ($1361\,\mathrm{W/m^2}$),
- c is the concentration factor due to mirrors (assumed to be 3)
- α_{sc} is the absorptivity of the solar cells (assumed 0.91)
- η_{sc} is the efficiency of the solar cells (assumed 0.36)

This equation calculates the actual thermal load absorbed by the solar cell layer, accounting for the portion of the solar flux that is not converted into electricity and is instead dissipated as heat.

The first two terms, $S \cdot c$, represent the concentrated solar radiation incident on the photovoltaic surface per unit area. Multiplying by the absorptivity α_{sc} gives the portion of that radiation which is absorbed by the surface. Finally, the term $(1 - \eta_{\text{sc}})$ accounts for the fraction of absorbed energy that is not converted into electrical power and is therefore dissipated as heat.

By inserting numerical values,

$$H_{\text{SC}} = 1361 \cdot 3 \cdot (1 - 0.36) \cdot 0.91 = 2377.9 \text{W/m}^2 \tag{6.5}$$

This, together with the heat dissipated by the SSPAs, constitutes the main internal source of heat and must be taken into account when performing the thermal analysis.

6.3. Radiative case: Thermal loads

The first step in the analysis is to assess the external thermal loads acting on the system. To do so, the orbital environment is defined. In this study, the orbit is geostationary, and the primary sources of external heat are:

- Solar radiation and planetary albedo in the visible-to-near-infrared spectrum (except during eclipses).
- Earth's infrared emission, which contributes to the thermal balance.

Table 6.4 summarizes the expected results from running the radiative case in ESATAN.

Thermal Loads	Details
External Loads	
Solar Flux	- Constant on solar cell side, with a concentration factor of 3 - Predominant contribution on antenna side - Absent during eclipses
Albedo Flux	- Always zero for solar cell side (always opposed to Earth) - Always present for antenna except during eclipses
Planet IR Flux	- Always zero for solar cell side (always opposed to Earth) - Constant for antenna side, always facing Earth
Internal Loads	
Conversion Components (SSPAs)	- Heat dissipation $\approx$ 20% of handled power (efficiency) - Constant except during eclipses

Table 6.4: Thermal Loads Breakdown

The radiative case in ESATAN focuses on modeling the radiative interactions between the system and its environment. This analysis allows for the computation of external thermal contributions by determining the incoming heat fluxes on the modeled geometry once the orbital environment is defined.

To achieve this, key orbital parameters, pointing requirements, and simulation details are specified. Since the orbit remains unchanged throughout all thermal simulations, the radiative case remains consistent. The main parameters used for this analysis are summarized in Table 6.5.

Additionally, the simulation date influences the results, as different thermal conditions can occur based on solar exposure. In this case, the hot and cold cases are investigated and selected for the analysis.

6.3.1. Radiative case results

The radiative case run for this model is straightforward, computing the fluxes on the surfaces. As previously explained, the concentration factor on the solar cells is accounted for in the boundary conditions of the thermal case. Therefore, the results from the radiative case must be multiplied by this factor for the solar cells.

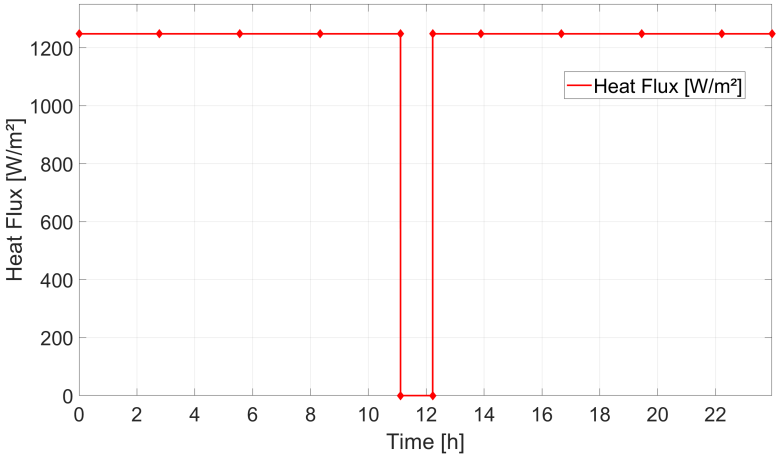

Figure 6.3: Solar flux on PV side

As expected, the solar flux remains constant on the solar cells throughout the orbit, except during an eclipse period, where it abruptly drops to zero. The value indicated in the graph (output from ESATAN expressed in $, \mathrm{W/m^2}$) must be multiplied by the concentration factor (3) and the area of the solar cells, yielding:

$$H_{\text{solar}} = 1254\,\mathrm{W/m^2} \times 3 \times 6.25\,\mathrm{m^2} = 23,512\,\mathrm{W}$$

Both the albedo and infrared (IR) flux remain zero throughout the orbit on the solar cell side, as expected.

On the antenna side, the planetary IR flux is constant because the antenna is always facing Earth. The albedo flux exhibits slight variations, particularly following the eclipse. During this period, the Sun is on the opposite side of Earth, meaning no radiation is reflected back as albedo.

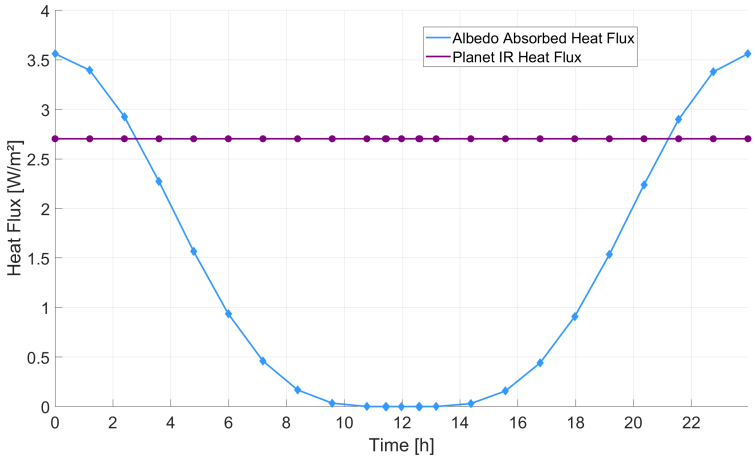

Figure 6.4: IR and Albedo absorbed flux on the antenna side

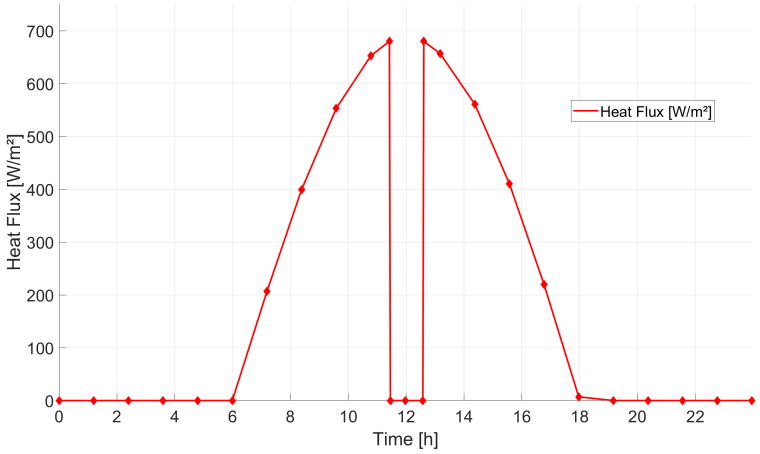

Figure 6.5: Solar absorbed flux on the antenna side

Parameter	Value
Orbit parameters	
Mission Type	ORBITAL
Orbit Centre	PLANET (Earth)
Date of Simulation	21/03/2025
Planet Radius [m]	6,371,000
Gravitational Constant [m/s²]	9.798
Perigee Altitude [m]	35,786,000
Apogee Altitude [m]	35,786,000
Final Anomaly [°]	360.0 (one full orbit)
Pointing	
Primary Vector	Z_{BODY} [0.0, 0.0, 1.0] (ZENITH)
Secondary Vector	Y_{BODY} [0.0, 1.0, 0.0] (NORMAL TO ORBIT)
Planet details	
Planet Temperature [K]	254.3
Planet Infrared Emissivity	1.0
Planet Albedo	0.306

Table 6.5: Radiative Case Definition: GEO

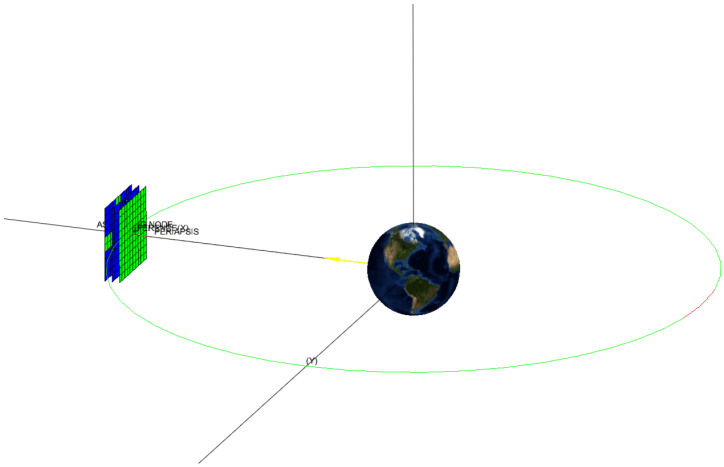

Figure 6.6: Radiative case implementation, ESATAN

6.4. Definition of the thermal case

To define the thermal case in ESATAN-TMS, the geometric model is first uploaded, followed by the selection of a radiative case. In this analysis, the GEO (Geostationary Orbit) case, already simulated and presented in section 6.3 is chosen, ensuring that the spacecraft's thermal interactions with the space environment are accurately modeled.

Next, conductors are included in the model, both generated and user-defined. These elements define the conductive heat transfer pathways between different components. Boundary conditions are also specified, including the environment temperature, which is set to 3K, representing the deep-space background temperature.

Finally, the type of solution method is selected. In this case, a steady-state thermal analysis is performed, ensuring that the simulation captures the equilibrium thermal behavior of the spacecraft.

6.4.1. Thermal case results

The thermal case results are first presented for the spacecraft model described in section 6.2, with no thermal control strategies applied.

Operating temperature requirement

Figure 6.7 shows the temperature profiles for the four key components throughout one orbital revolution. For each component, maximum, average, and minimum node-based temperatures are plotted to display temporal evolution.

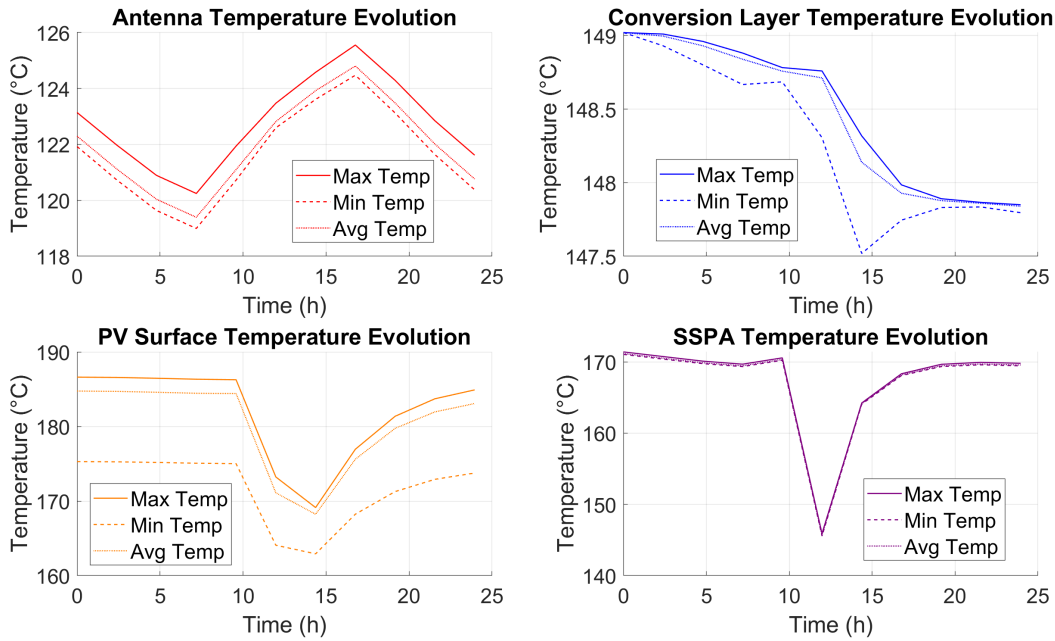

Figure 6.7: Temperature results from thermal case with no control

One of the first observations is the sharp temperature drop occurring around t ~9.4 hours. This coincides with the event of a total eclipse, during which the spacecraft exits solar exposure. The effect is immediate: temperatures for most components drop due to the sudden loss of radiative heating.

In the case of the SSPAs, the eclipse also marks a cessation of internal heat generation, as these amplifiers are inactive when not powered by the solar array. In practice, the inclusion of a battery or energy storage system to supply power during eclipse phases could be considered in the overall spacecraft design to maintain the operability of critical systems such as the SSPAs. However, since an auxiliary power source has not been modeled or included in the current thermal sizing or system architecture, the amplifiers remain unpowered during the eclipse. Consequently, their temperatures exhibit a rapid decline due to the lack of internal dissipation.

In contrast, the antenna demonstrates a different thermal response. This is attributable to its consistent exposure to planetary infrared (IR) radiation throughout the orbit, for its attitude requirement of continuous pointing towards Earth. Unlike the solar input, the IR flux from the planet remains uninterrupted during the eclipse, providing a continuous, even if limited, source of thermal input.

However, the most significant observation from the plotted results is that none of the components maintain temperatures within their specified operational limits, as summarized in Table 6.6. The table shows a comparison between:

- the minimum and maximum simulated temperatures
- the acceptable operating temperature limits defined by component specifications

To provide a clear overview of the thermal performance, Figure 6.8 presents a bar chart where each shaded bar corresponds to the allowed operating temperature range for each component. Plotted on these bars are markers indicating the simulated maximum and minimum temperatures obtained from the thermal analysis.
These results clearly confirm that the thermal requirements concerning the allowable temperature limits are not satisfied under the current configuration.

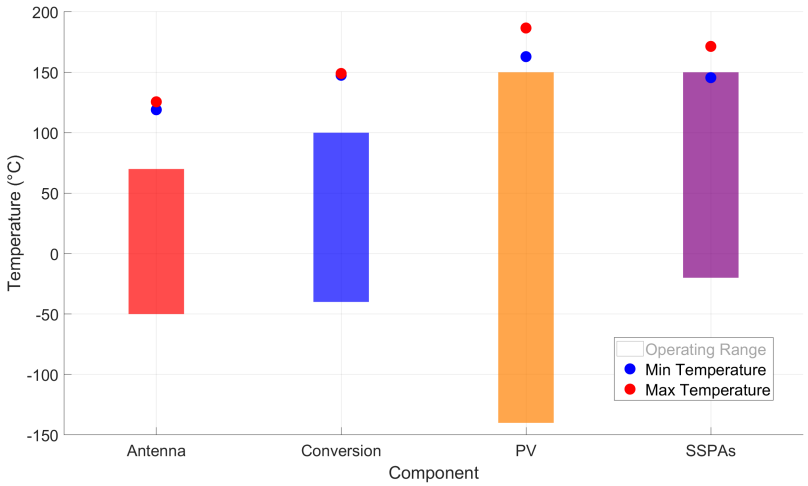

Figure 6.8: Comparison of simulated vs. operating temperature ranges without thermal control

Component	Min Simulated (°C)	Max Simulated (°C)	Min Limit (°C)	Max Limit (°C)
Antenna	118.99	125.55	-50	70
Conversion	147.52	149.02	-40	100
PV	162.92	186.62	-140	150
SSPAs	145.56	171.40	-20	150

Table 6.6: Operating and simulated temperature ranges for each component

It is evident from both Table 6.6 and Figure 6.8 that all components exceed the allowable temperature limits at various points in the orbit. While the SSPAs marginally stay within their limits on the lower end, all others clearly operate outside their required thermal envelopes.

Thermal gradient requirement

In addition to meeting the absolute temperature range limits, the spacecraft components must also satisfy thermal gradient constraints, which ensure that no component experiences excessive internal temperature differences. These gradients are critical in preventing mechanical stress, material fatigue, or failure due to differential thermal expansion between materials.

As shown in Figure 6.9, the temperature difference (defined as the maximum minus the minimum node temperature within each component) is computed at every time step for all components. The resulting trends for each component are plotted against their respective maximum allowable gradients. The results demonstrate total compliance with the requirement for all components. The antenna, conversion electronics, and SSPAs maintain low internal gradients, well below their respective thresholds of 5°C and 15°C. Even the PV surface, which operates at the highest absolute temperatures, exhibits a maximum gradient of approximately 12°C, significantly under the allowed 30°C limit.

This behavior indicates that temperature is quite uniform within each component. This is likely due to good conductive paths and the thermal properties of the materials used. So, even though the components go well outside their operational temperature limits, internally they maintain uniform temperatures.

In conclusion, the thermal analysis case confirms that, despite meeting the thermal gradient requirement, thermal control is still necessary, as the absolute temperature levels remain outside the acceptable operational range.

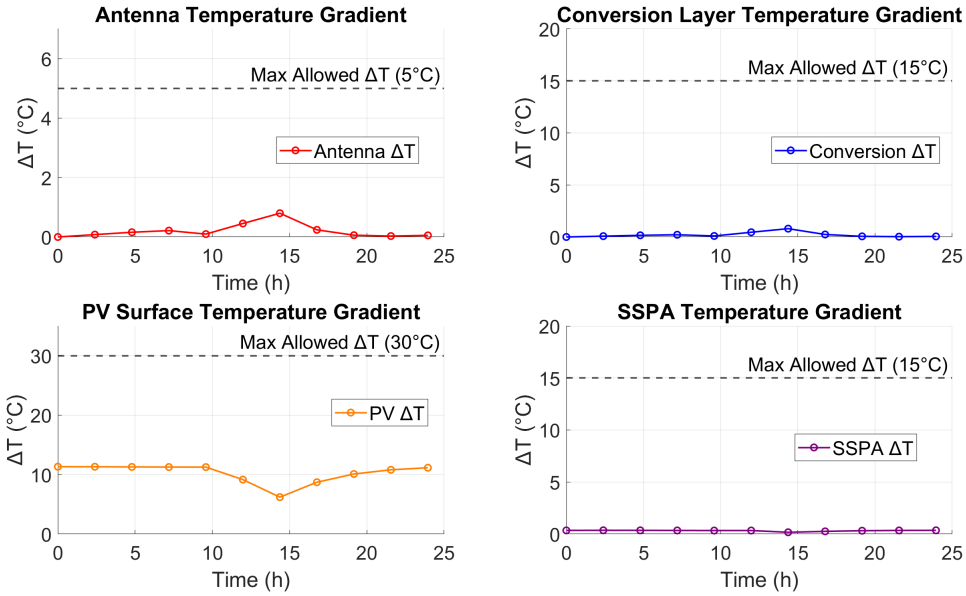

Figure 6.9: Temperature gradient for each component, without thermal control

6.5. Thermal control implementation

Since the results from the first iteration of the thermal case show that none of the components maintain their temperature within the allowed limits, thermal control techniques are implemented.

This part of the study addresses the final research question: whether passive control techniques are sufficient to maintain the operational temperature ranges.

The preliminary design of thermal control systems first considers basic methods, starting with the simplest ones. Additionally, it identifies the critical areas where thermal management is most necessary.

6.5.1. White paint for Antenna

One of the first thermal control strategies implemented is the application of a passive thermal control coating on the active side of the phased array antenna. This approach is especially advantageous when low-mass, low-complexity solutions are preferred. The primary selection criteria for the coating include low solar absorptivity, high infrared emissivity, proven space heritage, mechanical durability, and, crucially, transparency to radiofrequency signals at the operating frequency of the antenna (5.8 GHz).

Applying a thermal control paint allows for modification of the antenna's thermo-optical properties to reduce the absorbed solar flux, which is the dominant source of heat on this surface. Unlike active thermal systems, which increase system mass and power demands, this passive solution simplifies integration and reliability.

Among the various coatings considered, AZ-93, developed by AZ Technology and widely used in the aerospace industry, is selected. AZ-93 is a white inorganic thermal control coating with a low solar absorptivity ($\alpha \approx 0.13$–0.17) and high infrared emissivity ($\epsilon \approx 0.89$–0.93), offering effective passive cooling for sun-facing components on spacecraft. AZ-93 has been validated for use on RF-sensitive surfaces thanks to its compatibility with MLP-300-AZ, a dedicated RF-transparent primer that maintains electromagnetic transparency when paired with top coatings like AZ-93 [46], [45].

This ensures that, even when applied directly to radiating elements of antennas, the coating does not interfere with transmission efficiency. It should be noted, however, that not all thermal control coatings are compatible with RF applications — many standard white paints and OSRs contain dielectric or metallic particles that can scatter or absorb radiofrequency signals, compromising antenna efficiency.

For this analysis, the following thermo-optical properties are used in the thermal model to characterize the coated surface:

- Solar absorptivity: $\alpha = 0.13$
- Infrared emissivity: $\epsilon = 0.91$

These values are used to update the model of the antenna-facing surface in ESATAN-TMS. A new thermal simulation is conducted to quantify the impact of the coating on the antenna's equilibrium temperature profile. The resulting thermal behavior of the components of the tile is displayed in Figure 6.10, and it is compared against the uncoated configuration to assess the effectiveness of the solution in Figure 6.11.
Figure 6.12 shows the compliance with the thermal requirement on gradients throughout the nodes of each component.

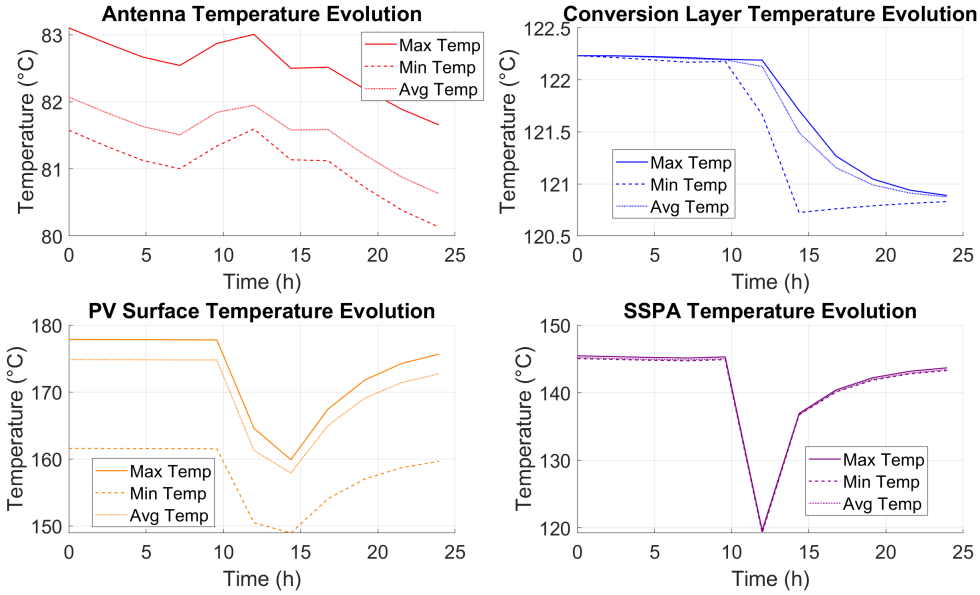

Figure 6.10: Temperature results from thermal case with coating on antenna side

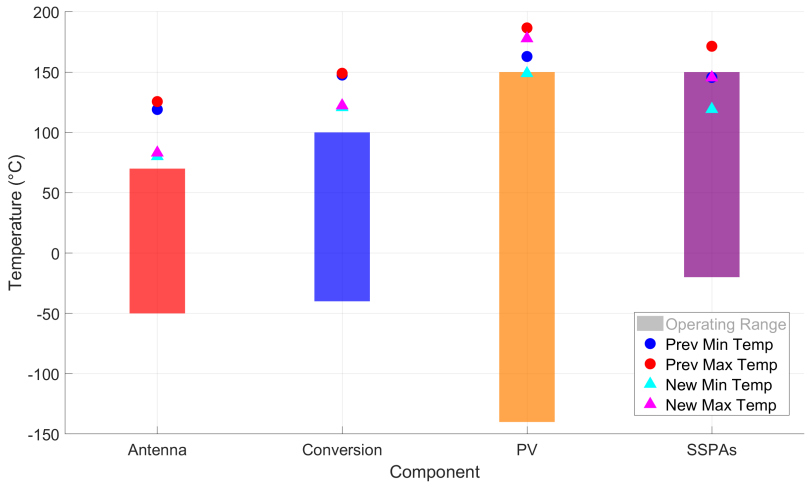

Figure 6.11: Comparison of actual vs. operating temperature ranges with wait paint on antenna

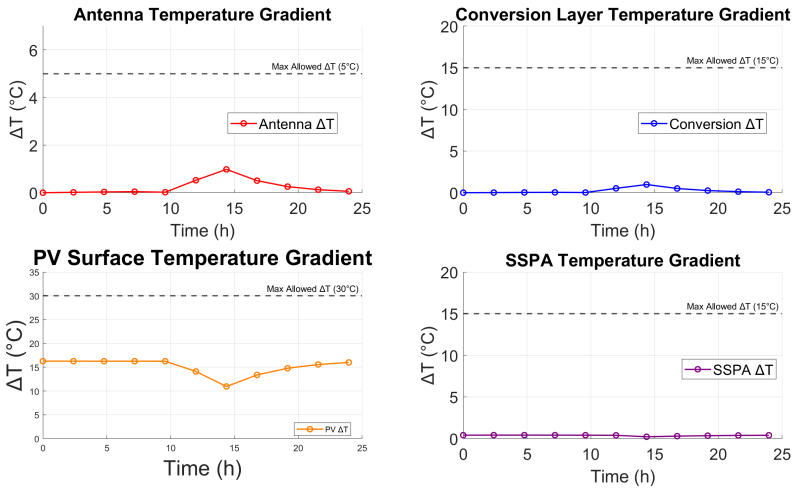

Figure 6.12: Temperature gradient for each component, with white paint

- **Reduction in Antenna Temperature:** The maximum temperature of the antenna decreases from 123.14°C to 83.10°C, showing a notable improvement. However, it still does not fully meet the operational range requirements. This indicates that while First-Flex effectively reduces heat absorption, additional thermal control measures are needed.
- **Temperature Reduction in Other Components:** The application of the coating leads to a significant reduction in temperatures for other components as well. The PV cells experience a decrease of approximately 10°C, the conversion layer sees a reduction of around 20°C, and the SSPAs cool down by more than 25°C. Despite these improvements, none of the components fully reach their operational limits, highlighting the need for further thermal management.
- **Overall Effectiveness of paint:** Although this control system alone is not sufficient to bring all components within the required temperature range, it contributes to a meaningful temperature reduction, particularly for the antenna. Its ability to lower heat absorption while maintaining RF transparency demonstrates its potential; however, additional measures are necessary to fully stabilize the thermal environment.

6.5.2. Radiators and CCHPs

The second thermal control method implemented consists of radiator surfaces that passively radiate excess heat. The first thermal control method, the white paint coating on the active antenna side, remains in use.

From the results of the first iteration of thermal control methods implementation, critical thermal zones are identified. Specifically, the SSPAs are characterized by concentrated heat dissipation, requiring a thermal management technique to distribute the accumulated heat. Furthermore, the solar cells are the most critical component, as they constantly receive high power fluxes and are conductively connected to the SSPAs, which also dissipate heat.

Although radiators on the solar cell side are not common in spacecraft thermal control designs, because their efficacy would be reduced by the fact that they absorb solar radiation, they are sized to be positioned in this area. This choice is due to the fact that this is the most thermally critical part of the system, requiring urgent cooling.

The radiators are preliminarily sized for a single module, considering the amount of heat to dissipate and their properties. To estimate the required area of radiators to be placed on a modular unit of the tile, the total heat that needs to be dissipated (from the solar cells and SSPAs, which are the components considered) is first computed. Then, a heat balance is imposed by equating this with the heat that would be radiated by the radiators. Even if preliminary, this methodology allows for a first sizing of the radiative area on the module.

This computation is implemented in the analysis script developed for this study.

The variable to be sized is the radiator area A_{rad}. Consequently, the area available for the solar cells is reduced, since part of the total module area is allocated to radiators.

For a $2.5\,\text{m} \times 2.5\,\text{m}$ module, the total heat to be dissipated from the solar cells is estimated as:

$$Q_{\text{sc}} = S \cdot c \cdot (\mathsf{A}_{\text{tot}} - A_{\text{rad}}) \cdot \alpha_{\text{sc}} \cdot (1 - \eta_{\text{sc}}) \tag{6.6}$$

where

- S is the solar flux in GEO ($1361\,\text{W/m}^2$),
- c is the concentration factor due to mirrors (assumed to be 3),
- α_{sc} is the absorptivity of the solar cells (assumed to be 0.91),
- η_{sc} is the efficiency of the solar cells (assumed to be 0.36).

A detailed explanation of these terms is already provided in subsection 6.2.3; here, the expression is simply multiplied by the effective solar cell area $A_{\text{tot}} - A_{\text{rad}}$.

Additionally, heat is dissipated by the SSPAs, which is conservatively estimated as 20% of the incoming energy directed to them:

$$Q_{\text{SSPA}} = S \cdot c \cdot (\mathsf{A}_{\text{tot}} - A_{\text{rad}}) \cdot \alpha_{\text{sc}} \cdot \eta_{\text{sc}} \cdot (1 - \eta_{\text{SSPA}}) \tag{6.7}$$

where

- η_{SSPA} is the efficiency of the solid-state power amplifiers (assumed to be 0.80).

The other parameters remain the same. These expressions are further detailed in subsection 6.2.2, and again, the used area is $A_{\text{tot}} - A_{\text{rad}}$.

By substituting the known values and summing the two contributions, the required radiator area A_{rad} is obtained by imposing a heat balance:

$$Q_{\text{diss}} = Q_{\text{sc}} + Q_{\text{SSPA}} = A_{\text{rad}} \cdot \epsilon_{\text{rad}} \cdot \sigma \cdot T_{\text{rad}}^4 \tag{6.8}$$

where

- T_{rad} is the radiator temperature limit in K. Higher temperatures may be considered for specific extreme applications, such as propulsion systems,
- ϵ_{rad} is the emissivity of the radiator surface,
- σ is the Stefan–Boltzmann constant ($\sigma = 5.670374419 \times 10^{-8}\ \text{W m}^{-2}\,\text{K}^{-4}$).

The properties of the radiator are summarized in Table 6.7.

Property	Symbol	Value	Unit
IR emissivity	ϵ_{rad}	0.85	–
Solar absorptivity	α_{rad}	0.10	–
Temperature limit	T_{rad}	300 [48]	°C

Table 6.7: Radiator properties

Solving equation (6.8) with the substituted values yields a radiator area of

$$A_{\text{rad}} = 1.815\,\text{m}^2$$

This corresponds to approximately 29% of the total module area.

This implies a reduction in the area available for solar cells, and thus in the total area available for energy collection. One might question why the radiators are placed on the same tile surface instead of being deployed on a separate, external surface. This configuration would maintain the full area for solar power collection.

However, in an in-orbit assembled system, adding deployable radiators to each module would make it harder to connect the modules together. It would also complicate the mechanical design and make the overall assembly less practical.

An alternative configuration was considered, where radiators are placed at the outer edge of the full tile, with well-structured conductive paths between modules. This setup would allow accumulated heat to be transported outward and dissipated via external radiators. However, due to the preliminary nature and limitations of the current thermal analysis, this concept was not implemented.

To support heat transfer from internal sources to the radiators, constant conductivity heat pipes (CCHPs) are modeled and thermally connected to the radiative surfaces. Heat pipes are passive thermal control devices capable of transporting heat from hot sources to cold sinks with very high thermal conductivity.

In this study, off-the-shelf CCHPs from Advanced Cooling Technologies (ACT) are selected. These feature a 6063 aluminum wick and ammonia as the working fluid. The operating temperature range of ammonia, from 195.4 K to 405.5 K, corresponds to a Celsius range that encompasses the expected thermal environment of the system.

Their implementation in the thermal model is illustrated in Figure 6.13.

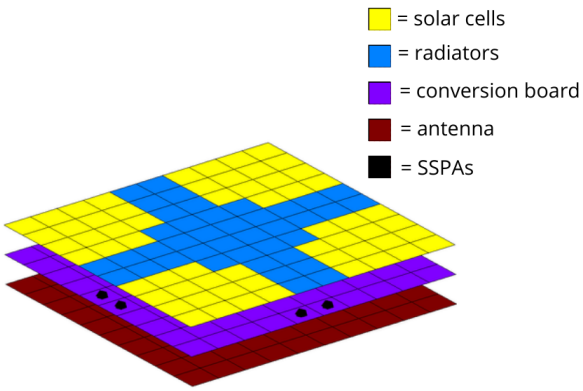

Figure 6.13: Radiators model

The color coding used in the layout is clarified in the legend in Figure 6.13: yellow areas correspond

to solar cells, blue regions to radiator surfaces, purple to power conversion units, black dots to SSPAs, and the bordeaux area to the antenna.

The cross-shaped arrangement of the radiator surfaces is motivated by the following considerations:

- It is consistent with the modular assembly strategy envisioned for the system. Heat pipes, used to transfer heat from internal sources to the radiators, are placed directly beneath the radiator regions. The cross-shaped layout enables a simple and uniform thermal connection scheme among adjacent modules. This facilitates scalable thermal integration without requiring deployable elements and ensures compatibility with structural interfaces in all directions.
- Structurally, the cross shape avoids interference with other key subsystems, such as the antenna and conversion electronics. This enables a clean separation between thermal management and functional payload areas within the module.

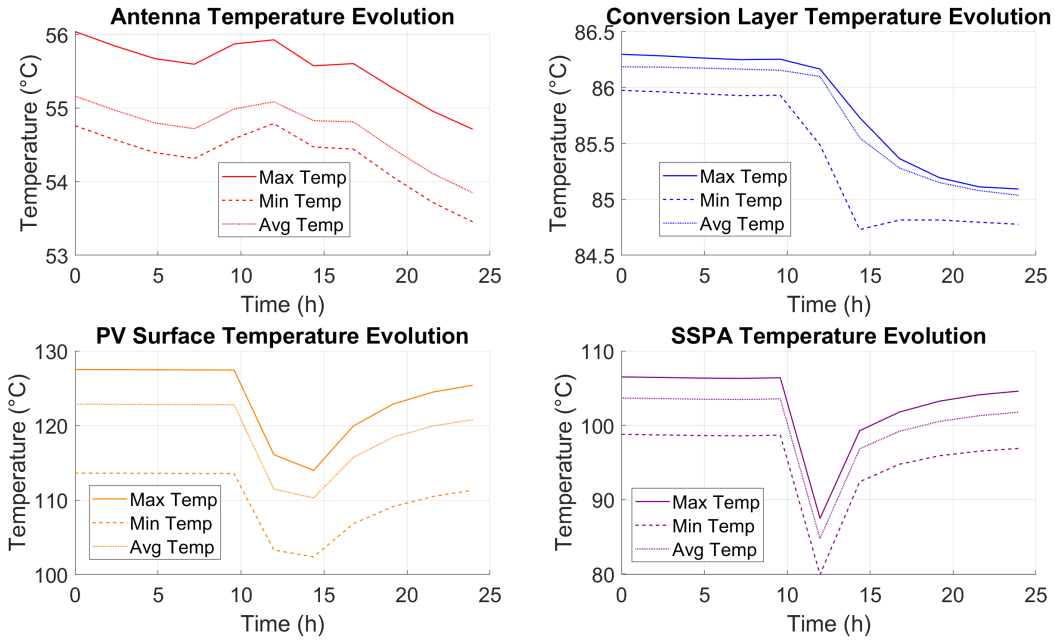

Figure 6.14: Temperature results from thermal case with coating + radiators + heat pipes

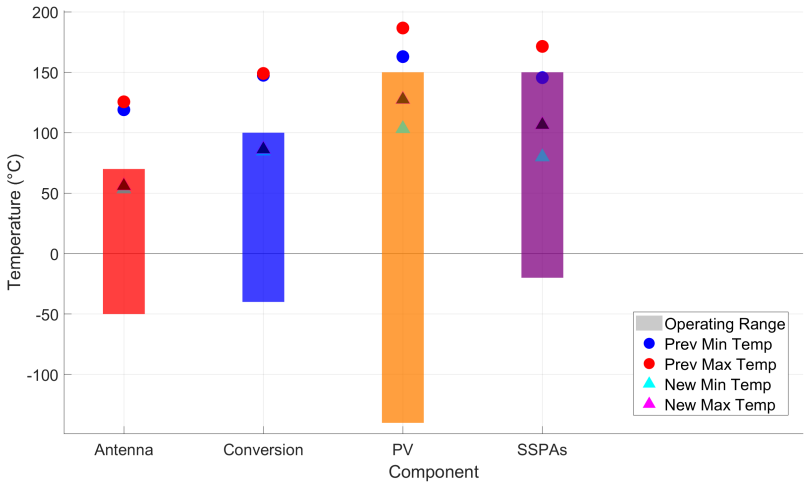

Figure 6.15: Comparison of actual vs. operating temperature ranges with thermal control

Component	Min Simulated (°C)	Max Simulated (°C)	Min Limit (°C)	Max Limit (°C)
Antenna	53.45	56.04	-50	70
Conversion	84.78	86.30	-40	100
PV	103.29	127.50	-140	150
SSPAs	79.94	106.51	-20	150

Table 6.8: Operating and actual temperature ranges (real absolute values) for each component

The results shown in Figure 6.14 and Figure 6.15 demonstrate that all components now remain within their operational temperature ranges, confirming the effectiveness of the implemented thermal control strategy.

Previously, the system struggled with excessive temperatures, especially in the solar cells and SSPAs, which are critical areas due to high heat fluxes and power dissipation. By distributing the heat effectively using radiators and constant conductivity heat pipes (CCHPs), the temperature profiles have significantly improved. The PV cells exhibit a significant temperature reduction of approximately 59.1°C compared to the uncontrolled case, demonstrating the effectiveness of the thermal regulation system in mitigating overheating. The conversion layer experiences a 62.7°C drop; the SSPAs undergo the most significant improvement, with a temperature decrease of 64.9°C compared to the uncontrolled scenario, ensuring safer operation and prolonged component lifespan. The antenna, which previously exceeded its operational limits, now remains within the required thermal range, with a temperature reduction of 69.5°C, highlighting the crucial role of thermal management in maintaining system reliability.

Compliance with Thermal Requirements:
The operating temperature ranges of all components now fall within the defined limits in Table 6.1.
In addition to staying within the minimum and maximum temperature limits, the system now meets the second key requirement: temperature gradients across each component are within the specified constraints.
Specifically, the solar panels' temperature difference satisfies the condition:

$$\Delta T_{\text{solar panels}} < 20 - 30^{\circ}C$$

The antenna maintains:

$$\Delta T_{\text{Antenna}} < 5^{\circ}C$$

The SSPAs meet the required thermal gradient:

$$\Delta T_{\text{SSPAs}} < 10 - 15^{\circ}C$$

This is illustrated more clearly in the graphs presented in Figure 6.16, which show the maximum temperature differences observed across the mesh nodes for each component. The dashed line indicates the maximum allowable temperature gradient. As can be observed, all components satisfy this requirement.

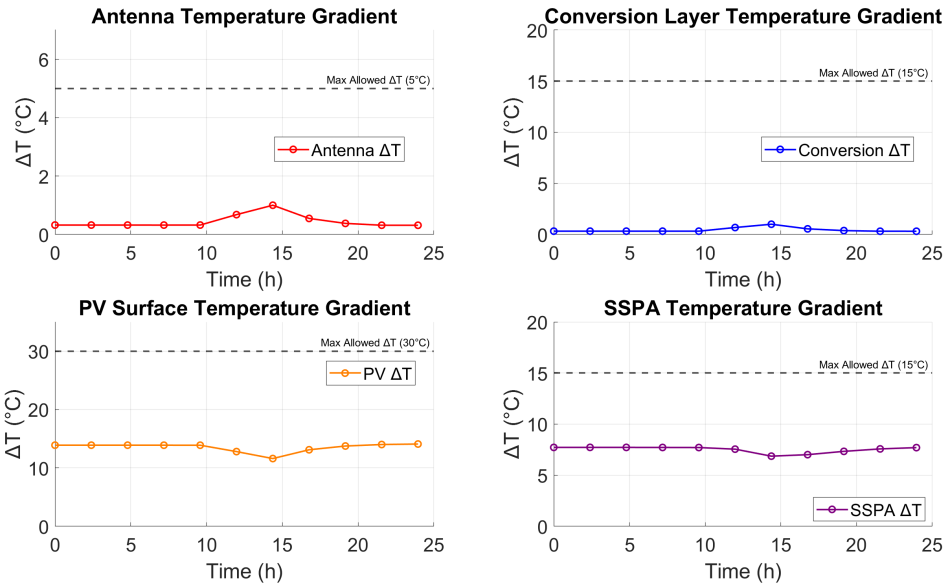

Figure 6.16: Temperature gradient for each component, with thermal control

This confirms that the combination of radiators and heat pipes has successfully distributed excess heat, preventing localized overheating while maintaining overall thermal stability. The verification process, including post-processing of the thermal simulation, supports these conclusions.

Overall, this final thermal control strategy is effective, ensuring safe and optimal operating conditions for all system components.

However, a significant limitation of the analysis is that it does not consider requirements regarding temperature stability over time. This is particularly important in cases where significant temperature fluctuations occur due to eclipse events. Future work should therefore include an in-depth analysis and modeling that explicitly addresses this requirement.

6.6. Link with Energy Analysis

An important final consideration is the connection between the thermal analysis results and the previously conducted energy analysis. The primary reason for performing the thermal assessment was to enhance the evaluation of energy efficiency by incorporating a crucial aspect that should not be overlooked: the contribution of the thermal control system.
In this way, the study contributes to enriching the research on the topic and advancing our understanding of whether it makes sense to continue investing in this concept, as well as where to focus future efforts for improvement.

Even though the thermal case analysis demonstrates that it is possible to maintain the module's temperature within operational limits using only passive techniques, this has significant implications for the overall energy computation. While no active control is required, meeting the thermal requirements necessitates the introduction of an extensive radiator surface area. This, in turn, reduces the available area for solar cells within the tile, lowering the harvested power.

This represents the trade-off for avoiding the use of active thermal control methods.

To account for this impact, the energy analysis is re-evaluated using updated input data, incorporating the revised radiator sizing as a key parameter.

Particularly, as explained in subsection 6.5.2 and expressed in Equation (6.8), the required radiator area to dissipate the heat was preliminarily sized for a modular unit prototype of 2.5 m × 2.5 m. The same methodology is extended to the entire satellite, under the assumption that the calculations scale proportionally. The ratio between the radiator area and total area remains the same (29%). Therefore, by calculating the heat dissipated by both solar cells (Eq. (6.6)) and the SSPAs (Eq. (6.7)), the required total radiator area is estimated as:

$$\mathrm{A}_{\mathrm{rad,\ total}} = 359{,}188.87\ \mathrm{m}^2$$

From here, the mass of the PV system is updated by applying the appropriate density to the reduced PV area, and the radiator mass is computed using a reference density of 4 kg/m^2 [48].

This results in an updated total mass of the system:

$$m_{\mathrm{tot,new}} = 6{,}655.5\ \mathrm{tons}$$

The new PV mass becomes:

$$m_{\mathrm{pv,new}} = 438.9\ \mathrm{tons}$$

Since radiators are primarily composed of aluminum, their material contribution is included in both the mass and energy input computations. The increase in mass leads to a corresponding increase in the number of launches required, and thus a higher energy input related to both launch and orbital transfer phases.

The updated energy inputs are as follows:

- Energy input from SPS construction: $E_{\mathrm{in,SPS,new}} = 2{,}069.1\ \mathrm{GWh}$
- Energy input for launches: $E_{\mathrm{in,launch,new}} = 4{,}247\ \mathrm{GWh}$
- Energy input for orbital transfer: $E_{\mathrm{in,orb,new}} = 155.04\ \mathrm{GWh}$
- Energy input from ground operations (assumed constant): $E_{\mathrm{in,GND}} = 2{,}000\ \mathrm{GWh}$

Thus, the total energy input becomes:

$$E_{\mathrm{in,\ total}} = 2069.1 + 4247 + 155.04 + 2000 = 8{,}471.1\ \mathrm{GWh}$$

Due to the reduced available surface area for solar cells (as part is now covered by radiators), the energy output is also revised. The updated total energy output over the system's lifetime is:

$$E_{\text{out, total}} = 147{,}210 \text{ GWh}$$

The average annual output is calculated based on a 30-year operational lifetime:

$$\overline{E}_{\text{out, yearly}} = \frac{147{,}210}{30} = 4{,}906.9 \text{ GWh/year}$$

The updated energy performance indicators are calculated as follows:

- EROEI (Energy Return on Energy Invested):

$$\text{EROEI} = \frac{E_{\text{out, total}}}{E_{\text{in, total}}} = \frac{147{,}210}{8{,}471.1} \approx 17.38$$

- EPBT (Energy Payback Time):

$$\text{EPBT} = \frac{E_{\text{in, total}}}{\overline{E}_{\text{out, yearly}}} = \frac{8{,}471.1}{4{,}906.9} \approx 1.66 \text{ years} \approx 606 \text{ days}$$

The results of this updated energy analysis are summarized in Table 6.9. The updated values of EROEI and EPBT are computed also in the case of using Falcon Heavy as launching system.

Case	EROEI	EPBT
Without thermal system	28.01	1.07 years (344 days)
Updated	17.38	1.66 years (606 days)
Falcon Heavy	10.99	2.47 (902 days)
Terrestrial PV plant	12.6	2.4 years (876 days)

Table 6.9: Comparison of energy performance metrics with and without integration of the thermal control system.

The EROI index is significantly lower after the implementation of thermal control in the energy analysis. However, it remains promising compared to the defined terrestrial case. As already specified in the initial energy results, several limitations and assumptions were considered, and many energy inputs were not accounted for in the analysis.

The integration of thermal analysis into the energy assessment plays a critical role in refining the evaluation of SBSP performance. While the original energy analysis provided a promising outlook, it overlooked the contribution of the thermal control system, a necessary component for maintaining operability in space. By introducing this subsystem into the assessment, a more comprehensive and realistic picture emerges.

Although the inclusion of thermal control leads to a significant reduction in key performance metrics (EROEI and EPBT), the updated results remain favorable when compared to terrestrial renewable systems. This demonstrates that SBSP can still offer competitive energy returns, even under more constrained and realistic conditions. More importantly, this step highlights that any robust analysis of SBSP must move beyond idealized scenarios and progressively incorporate the impact of subsystem-level requirements.

This work shows that energy performance is highly sensitive to architectural and technological assumptions. For instance, when launch operations are based on currently available vehicles such as Falcon Heavy, and thermal control is considered, rather than future ultra-heavy launchers, the system's EROEI

falls below that of ground-based photovoltaic plants. This finding confirms that SBSP viability is closely tied to developments in launch infrastructure and overall mission design.

Ultimately, the integration of thermal constraints not only improves the robustness of the energy analysis, but also points toward a necessary direction for future research: energy assessments must be grounded in realistic subsystem modeling to support credible feasibility studies. The thermal model presented here constitutes a first step in that direction and lays the foundation for expanding the evaluation studies to other critical systems, such as power conversion, structural support, and in-orbit assembly.

7

Conclusions

This chapter presents the conclusions of the study by summarizing the main findings and linking them to the research questions outlined in Chapter 3.
This thesis evaluated the energetic feasibility and thermal constraints of a modular space-based solar power (SBSP) system based on the integrated tile architecture. The comprehensive energy and thermal analyses addressed the core objectives and research questions outlined in the research plan, delivering insightful findings and highlighting important trade-offs and critical considerations for future development.

The research questions guiding this study were:

RQ1: How does the life-cycle energy performance of space-based solar power systems compare to terrestrial solar power systems in terms of lifetime energy efficiency, considering variations in architecture?

RQ1.1: What are the differences in energy performance between terrestrial solar power systems and space-based systems, for a defined baseline architecture?

RQ1.2: How does the integrated tile architecture affect the net energy performance compared to the baseline?

RQ2: What are the main thermal challenges of the tile component in an SBSP system, and how do they impact the system's overall energy performance?

RQ2.1: How does heat accumulation in the integrated tile affect system efficiency, and what are the consequences for its energetic performance?

RQ2.2: What thermal management strategies can be implemented to meet thermal requirements, and what is their impact on the energy performance of the system?

The energy analysis established that under optimized conditions, the integrated tile architecture demonstrates superior energy performance compared to terrestrial photovoltaic (PV) plants. Addressing RQ1.1, the baseline SBSP system outperformed terrestrial PV, achieving significantly higher values for Energy Return on Energy Invested (EROEI) and shorter Energy Payback Time (EPBT). Addressing RQ1.2, the integrated tile concept exhibited an initial EROEI of 28.01 and an EPBT of 1.07 years, substantially outperforming ground-based PV systems (EROEI of 12.6 and EPBT of 2.4 years). These results highlight the promising potential of SBSP for sustainable large-scale power generation, contingent on advancements in launch technologies and efficiency optimization.

However, realistic constraints, especially thermal management systems, significantly impacted overall system performance.
In response to RQ2.1, the analysis identified significant heat accumulation issues due to the compact design and high power density of the integrated tile architecture. Without appropriate thermal control, temperatures exceeded operational limits, substantially reducing efficiency and risking component

failure.

In addressing RQ2.2, essential thermal control measures were evaluated, including passive radiative panels and specialized surface coatings. Implementing these measures reduced the EROEI to 17.38 and increased the EPBT to 1.66 years. Despite the decline in performance, SBSP maintained competitive viability against terrestrial alternatives when thermal constraints were realistically considered.

Sensitivity analysis further reinforced these conclusions, identifying system lifetime, degradation rates, photovoltaic efficiency, and wireless power transmission efficiency as crucial parameters. Small variations in these parameters could substantially affect long-term energy yields.

The thermal analysis highlighted the importance of effective thermal management strategies. Future development should optimize these techniques to balance thermal management efficiency against structural complexity and associated energy penalties.

Moreover, reliance on existing launch vehicles, such as Falcon Heavy, proved significantly less energy-efficient compared to projected ultra-heavy launch systems like Starship, highlighting the critical dependency of SBSP energetic feasibility on advanced launch capabilities.

7.1. Future Work

Future research should address the critical areas identified through this study and the limitations inherent in the current analyses:

- Enhanced thermal management solutions, investigating active thermal control methods and their energetic impacts to improve energy balance.
- Detailed subsystem-level analyses (e.g., power conversion units, structural components) to improve overall energy efficiency and reduce system mass.
- Advanced launch systems, evaluating developments in reusable launch vehicles essential for energetically viable large-scale SBSP deployment.
- Experimental validation, undertaking practical demonstrations of integrated tile prototypes under realistic operational conditions to validate theoretical findings and guide iterative improvements.
- Addressing analysis limitations, including:
  - Detailed modeling of launcher energy costs, including production energy and comprehensive launch campaign energy expenditures.
  - Improved modeling of subsystem-level energy inputs to enhance accuracy.
  - Extended thermal analysis of modularity impacts, covering full modules rather than single tiles.
  - Detailed analysis of temperature-dependent efficiency variations for system components to refine energy performance predictions.

By addressing these recommendations and limitations, future research can significantly advance the practical feasibility of SBSP, reinforcing its potential role in global renewable energy infrastructure.

References

[1] European Space Agency (ESA). *SBSP in support of Net Zero*. URL: https://www.esa.int/Enabling_Support/Space_Engineering_Technology/SOLARIS/SBSP_in_support_of_Net_Zero (visited on 05/29/2024).

[2] European Space Agency (ESA). *The Case for an ESA preparatory programme for Space-Based Solar Power for terrestrial energy needs*. Technical Report. European Space Agency, 2022.

[3] European Space Agency. *SOLARIS web page*. URL: https://www.esa.int/Enabling_Support/Space_Engineering_Technology/SOLARIS/SOLARIS2.

[4] European Space Agency. *Technology Readiness Levels (TRL)*. URL: https://www.esa.int/Enabling_Support/Space_Engineering_Technology/Shaping_the_Future/Technology_Readiness_Levels_TRL.

[5] Khandoker Alam et al. "Towards Net Zero: A Technological Review on the Potential of Space-Based Solar Power and Wireless Power Transmission". In: (Jan. 2023). DOI: 10.2139/ssrn.4628408.

[6] *Architecture Selection Report*. Tech. rep. TASI-SD-SBSP-TNO-0637. Thales Alenia Space, Nov. 2023.

[7] Regan Arndt and Robert Puto. "Basic understanding of IEC standard testing for photovoltaic panels". In: *TÜV SÜD Prod. Serv* (2010).

[8] Dale Arney et al. *In-space Servicing, Assembly, and Manufacturing (ISAM) State of Play*. Tech. rep. NASA, 2023.

[9] *Assessment of strategic, economic, environmental, and societal benefits, costs, and risks*. Technical Note. Roland Berger, OHB System, Aug. 2022.

[10] Kodami Badza, Y. Soro, and Marie Sawadogo. "Life cycle assessment of a 33.7 MW solar photovoltaic power plant in the context of a developing country". In: *Sustainable Environment Research* 33 (Nov. 2023). DOI: 10.1186/s42834-023-00201-x.

[11] Udayan Banik et al. "Enhancing passive radiative cooling properties of flexible CIGS solar cells for space applications using single layer silicon oxycarbonitride films". In: *Solar Energy Materials and Solar Cells* 209 (2020), p. 110456. ISSN: 0927-0248. DOI: https://doi.org/10.1016/j.solmat.2020.110456. URL: https://www.sciencedirect.com/science/article/pii/S0927024820300623.

[12] Aditya Baraskar et al. "Space solar power satellite for the Moon and Mars mission". In: *Journal of Space Safety Engineering* 9.1 (2022), pp. 96–105. ISSN: 2468-8967. DOI: https://doi.org/10.1016/j.jsse.2021.10.008. URL: https://www.sciencedirect.com/science/article/pii/S2468896721001026.

[13] Robin Biesbroek et al. "The ClearSpace-1 mission: ESA and ClearSpace team up to remove debris". In: *8th European Conference on Space Debris*. Apr. 2021, 228, p. 228.

[14] William C Brown. "Wireless Power Transmission Options for Space Solar Power". In: *Proceedings of the IEEE*. Vol. 101. 6. IEEE. 2013, pp. 1434–1447. DOI: 10.1109/JPROC.2013.2255312.

[15] William C. Brown. "THE HISTORY OF THE DEVE1,OPMENT OF THE RECTENNA". In: (1980).

[16] Maria Browne, Brian Norton, and S.J. McCormack. "Phase change materials for photovoltaic thermal management". In: *Renewable and Sustainable Energy Reviews* 47 (July 2015), pp. 762–782. DOI: 10.1016/j.rser.2015.03.050.

[17] John Bucknell. *Survey of Space Based Solar Power (SBSP)*. Feb. 2024.

[18] Caltech. *Space Solar Power Project*. 2023. URL: https://www.spacesolar.caltech.edu/ (visited on 06/20/2024).

[19] Andrea Capannolo et al. “Chapter Four - Orbital dynamics”. In: *Modern Spacecraft Guidance, Navigation, and Control*. Ed. by Vincenzo Pesce, Andrea Colagrossi, and Stefano Silvestrini. Elsevier, 2023, pp. 131–206. ISBN: 978-0-323-90916-7. DOI: https://doi.org/10.1016/B978-0-323-90916-7.00004-4. URL: https://www.sciencedirect.com/science/article/pii/B9780323909167000044.

[20] Ian Cash. “CASSIOPeiA – A new paradigm for space solar power”. In: *Acta Astronautica* 159 (2019), pp. 170–178. ISSN: 0094-5765. DOI: https://doi.org/10.1016/j.actaastro.2019.03.063. URL: https://www.sciencedirect.com/science/article/pii/S0094576518320708.

[21] Ian Cash. “CASSIOPeiA solar power satellite”. In: *2017 IEEE International Conference on Wireless for Space and Extreme Environments (WiSEE)*. 2017, pp. 144–149. DOI: 10.1109/WiSEE.2017.8124908.

[22] Ludovica Castronovo. *TUDelft_MSc_Thesis*. https://github.com/ludovicastronovo/TUDelft_MSc_Thesis. Accessed: 2025-04-02. 2025.

[23] *Concept for a European SBSP development program*. Final Report. Roland Berger, OHB System, Aug. 2022.

[24] Jasmin Cooper and Adam Hawkes. “Life cycle environmental trade-off of decarbonising UK industrial clusters — A cradle to gate approach”. In: *Science of The Total Environment* 954 (2024), p. 176101. ISSN: 0048-9697. DOI: https://doi.org/10.1016/j.scitotenv.2024.176101. URL: https://www.sciencedirect.com/science/article/pii/S0048969724062570.

[25] Sáde K. Cromratie Clemons et al. “Life cycle assessment of a floating photovoltaic system and feasibility for application in Thailand”. In: *Renewable Energy* 168 (2021), pp. 448–462. ISSN: 0960-1481. DOI: https://doi.org/10.1016/j.renene.2020.12.082. URL: https://www.sciencedirect.com/science/article/pii/S096014812032022X.

[26] Paul Denholm and Robert M. Margolis. *Evaluating the Limits of Solar Photovoltaics (PV) in Traditional Electric Power Systems*. Tech. rep. NREL/TP-6A20-51664. Accessed: 2025-03-30. National Renewable Energy Laboratory (NREL), 2012. URL: https://www.nrel.gov/docs/fy12osti/51664.pdf.

[27] Mathieu Deremetz et al. “MIRROR -A Modular and Relocatable Multi-arm Robot Demonstrator for On-orbit Large Telescope Assembly”. In: Oct. 2023.

[28] DOE/NASA. *Program Assessment Report Statement of Finding—Satellite Power Systems*. 1980.

[29] *European OTVs vehicles*. URL: https://europeanspaceflight.com/european-otvs-index/ (visited on 06/27/2024).

[30] European Space Agency. *ESA Nebula: The Open Dissemination Platform for Future Studies*. URL: https://nebula.esa.int/.

[31] *European Space Agency*. URL: https://www.esa.int/.

[32] *Executive Summary Report*. Tech. rep. TASI-SD-SBSP-ORP-0293. Thales Alenia Space, Dec. 2023.

[33] A. Fikes et al. “The Caltech Space Solar Power Demonstration One Mission”. In: *2022 IEEE International Conference on Wireless for Space and Extreme Environments (WiSEE)*. 2022, pp. 18–22. DOI: 10.1109/WiSEE49342.2022.9926883.

[34] *Final Report*. Tech. rep. TASI-SD-SBSP-ORP-0292. Thales Alenia Space, Dec. 2023.

[35] World Economic Forum. *Net-Zero Industry Tracker 2023 Edition*. Accessed: 2023-11. In collaboration with Accenture: World Economic Forum, Nov. 2023. URL: https://www.weforum.org/reports/net-zero-industry-tracker-2023-edition.

[36] Giorgio Franceschetti et al. “Innovative rectenna design for space solar power systems”. In: (May 2012). DOI: 10.1109/IMWS.2012.6215773.

[37] P. Friedlingstein et al. “Global Carbon Budget 2021”. In: *Earth System Science Data* 14.4 (2022), pp. 1917–2005. DOI: 10.5194/essd-14-1917-2022. URL: https://essd.copernicus.org/articles/14/1917/2022/.

[38] Jaime Garnica, Raul Chinga, and Jenshan Lin. “Wireless Power Transmission: From Far Field to Near Field”. In: *Proceedings of the IEEE* 101 (June 2013), pp. 1321–1331. DOI: 10.1109/JPROC.2013.2251411.

[39] Andrea Garulli et al. “Autonomous Low-Earth-Orbit Station-Keeping with Electric Propulsion”. In: *Journal of Guidance Control and Dynamics* 34 (Nov. 2011), pp. 1683–1693. DOI: 10.2514/1.52985.

[40] Habib Ghasemizadeh Tamar, Abdolreza Nabavi, and Mohsen Haghighat. “Analysis and design procedure of a mm-Wave Class-E power amplifier”. In: *Microelectronics Journal* 111 (2021), p. 105036. ISSN: 1879-2391. DOI: https://doi.org/10.1016/j.mejo.2021.105036. URL: https://www.sciencedirect.com/science/article/pii/S0026269221000471.

[41] Peter E. Glaser. “Power from the Sun: Its Future”. In: *Science* 162.3856 (1968), pp. 857–861. DOI: 10.1126/science.162.3856.857. eprint: https://www.science.org/doi/pdf/10.1126/science.162.3856.857. URL: https://www.science.org/doi/abs/10.1126/science.162.3856.857.

[42] *Global Carbon Project*. URL: https://www.globalcarbonproject.org/ (visited on 05/27/2024).

[43] Henning Helmers, Michael Schachtner, and Andreas W. Bett. “Influence of temperature and irradiance on triple-junction solar subcells”. In: *Solar Energy Materials and Solar Cells* 116 (2013), pp. 144–152. ISSN: 0927-0248. DOI: https://doi.org/10.1016/j.solmat.2013.03.039. URL: https://www.sciencedirect.com/science/article/pii/S0927024813001529.

[44] Aloysius F. Hepp, Ryne P. Raffaelle, and Ina T. Martin. “Chapter Nineteen - Space photovoltaics: New technologies, environmental challenges, and missions”. In: *Photovoltaics Beyond Silicon*. Ed. by Senthilarasu Sundaram et al. Solar Cell Engineering. Elsevier, 2024, pp. 675–766. ISBN: 978-0-323-90188-8. DOI: https://doi.org/10.1016/B978-0-323-90188-8.00014-2. URL: https://www.sciencedirect.com/science/article/pii/B9780323901888000142.

[45] AZ Technology Inc. *AZ-93 Safety Data Sheet (SDS)*. Tech. rep. CPS-C-001 Rev. F. Retrieved from internal documentation. AZ Technology Inc., 2016.

[46] AZ Technology Inc. *AZ-93 White Inorganic Thermal Control Coating*. Accessed: 2025-04-02. 2024. URL: https://www.aztechnology.com/product/1/az-93.

[47] Masakazu Ito et al. “Life cycle assessment and cost analysis of very large-scale PV systems and suitable locations in the world”. In: *Progress in Photovoltaics: Research and Applications* 24.2 (2016), pp. 159–174. DOI: https://doi.org/10.1002/pip.2650. eprint: https://onlinelibrary.wiley.com/doi/pdf/10.1002/pip.2650. URL: https://onlinelibrary.wiley.com/doi/abs/10.1002/pip.2650.

[48] Naoko Iwata et al. “Thermal Performance Evaluation of Space Radiator for Single-Phase Mechanically Pumped Fluid Loop”. In: *Journal of Spacecraft and Rockets* 59.1 (2022), pp. 225–235. DOI: 10.2514/1.A35030. eprint: https://doi.org/10.2514/1.A35030. URL: https://doi.org/10.2514/1.A35030.

[49] Paul Jaffe. “Sandwich module testing for space solar power”. In: *2013 IEEE Aerospace Conference*. 2013, pp. 1–12. DOI: 10.1109/AERO.2013.6497366.

[50] Paul Jaffe, Jason Hodkin, and Forest Harrington. “Development of a sandwich module prototype for Space Solar Power”. In: *2012 IEEE Aerospace Conference*. 2012, pp. 1–9. DOI: 10.1109/AERO.2012.6187077.

[51] Paul Jaffe et al. “Sandwich Module Development for Space Solar Power”. In: 2011. URL: https://api.semanticscholar.org/CorpusID:46913410.

[52] Paul Jaffe et al. “Sandwich module prototype progress for space solar power”. In: *Acta Astronautica* 94.2 (2014), pp. 662–671. ISSN: 0094-5765. DOI: https://doi.org/10.1016/j.actaastro.2013.08.012. URL: https://www.sciencedirect.com/science/article/pii/S0094576513003214.

[53] Zhihong Jiang et al. “Progress and Development Trend of Space Intelligent Robot Technology”. In: *Space: Science & Technology* 2022 (Jan. 2022), pp. 1–11. DOI: 10.34133/2022/9832053.

[54] Panagiotis Kosmopoulos. “Chapter 1 - Solar irradiance and exploitation of the Sun’s power”. In: *Planning and Management of Solar Power from Space*. Ed. by Panagiotis Kosmopoulos. Academic Press, 2024, pp. 1–20. ISBN: 978-0-12-823390-0. DOI: https://doi.org/10.1016/B978-0-12-823390-0.00006-5. URL: https://www.sciencedirect.com/science/article/pii/B9780128233900000065.

[55] Air Force Research Laboratory. *ARACHNE*. URL: https://afresearchlab.com/technology/arachne/.

[56] Delun Li et al. “A Survey of Space Robotic Technologies for On-Orbit Assembly”. In: *Space: Science & Technology* 2022 (2022). DOI: 10.34133/2022/9849170. eprint: https://spj.science.org/doi/pdf/10.34133/2022/9849170. URL: https://spj.science.org/doi/abs/10.34133/2022/9849170.

[57] Xiaofan Li et al. “Wireless laser power transmission: Recent progress and future challenges”. In: *Optics and Lasers in Engineering* 165 (2023), p. 107428. DOI: 10.1016/j.optlaseng.2023.107428.

[58] Zhe Liu et al. “Advancements and challenges in wireless power transfer: A comprehensive review”. In: *Nexus* 1.2 (2024), p. 100014. ISSN: 2950-1601. DOI: https://doi.org/10.1016/j.ynexs.2024.100014. URL: https://www.sciencedirect.com/science/article/pii/S2950160124000123.

[59] Volker Maiwald et al. “About feasibility of SpaceX’s human exploration Mars mission scenario with Starship”. In: *Scientific Reports* 14.1 (2024), p. 11804. ISSN: 2045-2322. DOI: 10.1038/s41598-024-54012-0. URL: https://doi.org/10.1038/s41598-024-54012-0.

[60] John Mankins. “A technical overview of the ”SunTower” solar power satellite concept”. In: *Acta Astronautica* 50 (Mar. 2002), pp. 369–377. DOI: 10.1016/S0094-5765(01)00167-9.

[61] John Mankins. *SPS-ALPHA: The First Practical Solar Power Satellite via Arbitrarily Large Phased Array*. NASA Innovative Advanced Concepts (NIAC) Program supported a Phase 1 “SPS-ALPHA” project. Artemis Innovation Management Solutions, LLC, Sept. 2012.

[62] John Mankins, Nobuyuki Kaya, and Massimiliano Vasile. “SPS-ALPHA: The First Practical Solar Power Satellite via Arbitrarily Large Phased Array (A 2011-2012 NIAC Project)”. In: July 2012. ISBN: 978-1-62410-190-8. DOI: 10.2514/6.2012-3978.

[63] John C. Mankins. “A fresh look at space solar power: New architectures, concepts and technologies”. In: *Acta Astronautica* 41.4 (1997). Developing Business, pp. 347–359. ISSN: 0094-5765. DOI: https://doi.org/10.1016/S0094-5765(98)00075-7. URL: https://www.sciencedirect.com/science/article/pii/S0094576598000757.

[64] Hiroshi Matsumoto. “Research on solar power satellites and microwave power transmission in Japan”. In: *IEEE Microwave Magazine* 3 (2002), pp. 36–45. URL: https://api.semanticscholar.org/CorpusID:110113614.

[65] I. G. Mitrofanov et al. “Hydrogen Mapping of the Lunar South Pole Using the LRO Neutron Detector Experiment LEND”. In: *Science* 330.6003 (2010), pp. 483–486. DOI: 10.1126/science.1185696. eprint: https://www.science.org/doi/pdf/10.1126/science.1185696. URL: https://www.science.org/doi/abs/10.1126/science.1185696.

[66] *Mobile Servicing System*. 2023. URL: https://www.nasa.gov/international-space-station/mobile-servicing-system/ (visited on 06/27/2024).

[67] Sarah Moran. *We have lift-off: a history of space-based solar power*. URL: https://edblogs.columbia.edu/scppx3335-001-2014-1/2014/03/12/we-have-lift-off-a-history-of-space-based-solar-power/ (visited on 05/29/2024).

[68] Noor Muhammad Feizal Muhalim and Subramaniam Krishnan. “DESIGN OF NITROGEN-TETROXIDE / MONOMETHYL- HYDRAZINE THRUSTER FOR UPPER STAGE APPLICATION”. In: 2013. URL: https://api.semanticscholar.org/CorpusID:52905413.

[69] NASA. *NASA’s Dragonfly Project Demonstrates Robotic Satellite Assembly Critical to Future Space Infrastructure Development*. 2017. URL: https://www.nasa.gov/technology/nasas-dragonfly-project-demonstrates-robotic-satellite-assembly-critical-to-future-space-infrastructure-development/ (visited on 06/25/2024).

[70] NASA. *Wireless Power Transmission for Space Solar Power*. Tech. rep. SSP Exploratory Research and Technology Program (SERT). National Aeronautics and Space Administration (NASA), 2002. URL: https://ntrs.nasa.gov/api/citations/20030022668/downloads/20030022668.pdf.

[71] *NASA Power state-of-the-art*. 2021. URL: https://www.nasa.gov/wp-content/uploads/2021/10/3.soa_power_2021.pdf (visited on 07/01/2024).

[72] *Net Zero by 2050*. IEA, 2021. URL: https://www.iea.org/reports/net-zero-by-2050.

[73] *Northrop Grumman*. URL: https://www.northropgrumman.com/space/space-logistics-services (visited on 06/25/2024).

[74] NREL. *Photovoltaic Research: Best Research-Cell Efficiency Chart*. URL: https://www.nrel.gov/pv/cell-efficiency.html#:~:text=NREL%20maintains%20a%20chart%20of%20the%20highest%20confirmed,certified%20efficiency%20measurements.%20Access%20our%20research-cell%20efficiency%20data..

[75] Victor U.J. Nwankwo, Sandip K. Chakrabarti, and Robert S. Weigel. "Effects of plasma drag on low Earth orbiting satellites due to solar forcing induced perturbations and heating". In: *Advances in Space Research* 56.1 (2015), pp. 47–56. ISSN: 0273-1177. DOI: https://doi.org/10.1016/j.asr.2015.03.044. URL: https://www.sciencedirect.com/science/article/pii/S0273117715002562.

[76] Mark J. O'Neill. "Chapter fifteen - Space photovoltaic concentrators for outer planet and near-Sun missions using ultralight Fresnel lenses". In: *Photovoltaics for Space*. Ed. by Sheila G. Bailey et al. Elsevier, 2023, pp. 411–432. ISBN: 978-0-12-823300-9. DOI: https://doi.org/10.1016/B978-0-12-823300-9.00007-8. URL: https://www.sciencedirect.com/science/article/pii/B9780128233009000078.

[77] Roberto Opromolla et al. "Future in-orbit servicing operations in the space traffic management context". In: *Acta Astronautica* 220 (2024), pp. 469–477. ISSN: 0094-5765. DOI: https://doi.org/10.1016/j.actaastro.2024.05.007. URL: https://www.sciencedirect.com/science/article/pii/S0094576524002510.

[78] Jacob Paul. *Energy crisis lifeline as space power station 'makes more sense than nuclear'*. 2022. URL: https://www.express.co.uk/news/science/1676623/energy-crisis-solar-power-space-energy-initiative-nuclear (visited on 06/10/2024).

[79] Joseph N. Pelton. "Space-Based Solar Power Satellite Systems". In: *Space 2.0: Revolutionary Advances in the Space Industry*. Cham: Springer International Publishing, 2019, pp. 103–114. ISBN: 978-3-030-15281-9. DOI: 10.1007/978-3-030-15281-9_8. URL: https://doi.org/10.1007/978-3-030-15281-9_8.

[80] C. M. Pieters et al. "Character and Spatial Distribution of OH/H₂O on the Surface of the Moon Seen by M³ on Chandrayaan-1". In: *Science* 326.5952 (2009), pp. 568–572. DOI: 10.1126/science.1178658. eprint: https://www.science.org/doi/pdf/10.1126/science.1178658. URL: https://www.science.org/doi/abs/10.1126/science.1178658.

[81] Seth Potter et al. *Wireless Power Transmission Options for Space Solar Power*. Presented at the International Space Development Conference, Washington, DC. 2008. URL: https://www.nss.org/wp-content/uploads/2008/06/WPT-Options.pdf.

[82] RatedPower. *Lifecycle analysis of a photovoltaic (PV) plant*. Accessed: 2025-03-30. 2024. URL: https://ratedpower.com/blog/lifecycle-analysis-pv-plant/.

[83] Marco Raugei. *Methodological guidelines on Net Energy Analysis of Photovoltaic Electricity*. Jan. 2016.

[84] Marco Raugei et al. *Methodological Guidelines on Net Energy Analysis of Photovoltaic Electricity*. Tech. rep. T12-07: 2016. IEA-PVPS Task 12, Subtask 2.0 LCA. International Energy Agency (IEA) - Photovoltaic Power Systems Programme (IEA-PVPS), 2016. URL: https://www.iea-pvps.org/.

[85] Hannah Ritchie and Pablo Rosado. "Energy Mix". In: *Our World in Data* (2020). URL: https://ourworldindata.org/energy-mix.

[86] Hannah Ritchie and Pablo Rosado. “Fossil fuels”. In: *Our World in Data* (2017). URL: https://ourworldindata.org/fossil-fuels.

[87] Hannah Ritchie, Max Roser, and Pablo Rosado. “Renewable Energy”. In: *Our World in Data* (2020). URL: https://ourworldindata.org/renewable-energy.

[88] Christopher T. Rodenbeck et al. “Microwave and Millimeter Wave Power Beaming”. In: *IEEE Journal of Microwaves* 1.1 (2021), pp. 229–259. DOI: 10.1109/JMW.2020.3033992.

[89] Erica Rodgers et al. *Space-Based Solar Power*. Tech. rep. Office of Technology, Policy, and Strategy, Washington, DC: NASA, Jan. 2024.

[90] s. *Orbitfab*. URL: https://www.orbitfab.com/rafti/ (visited on 07/18/2024).

[91] Susumu Sasaki et al. “A new concept of solar power satellite: Tethered-SPS”. In: *Acta Astronautica* 60.3 (2007), pp. 153–165. ISSN: 0094-5765. DOI: https://doi.org/10.1016/j.actaastro.2006.07.010. URL: https://www.sciencedirect.com/science/article/pii/S0094576506002815.

[92] *SBSP Design Assumptions and Constraints Report*. Tech. rep. TASI-SD-SBSP-TNO-0636. Thales Alenia Space, Nov. 2023.

[93] *SBSP Study Review*. Technical Note. Roland Berger, OHB System, Feb. 2022.

[94] Wolfgang Seboldt et al. “European sail tower SPS concept”. In: vol. 48. Mar. 2001. DOI: 10.1016/S0094-5765(01)00046-7.

[95] *Shijian-21 Satellite*. 2022. URL: https://www.eoportal.org/satellite-missions/shijian-21#mission-status (visited on 06/25/2024).

[96] Martin Sippel, Sven Stappert, and Aaron Koch. “Assessment of multiple mission reusable launch vehicles”. In: *Journal of Space Safety Engineering* 6.3 (2019), pp. 165–180. ISSN: 2468-8967. DOI: https://doi.org/10.1016/j.jsse.2019.09.001. URL: https://www.sciencedirect.com/science/article/pii/S2468896719300886.

[97] David V. Smitherman. “A Comparison Of A Solar Power Satellite Concept To A Concentrating Solar Power System”. In: *AIAA SPACE 2013 Conference and Exposition*. DOI: 10.2514/6.2013-5344. eprint: https://arc.aiaa.org/doi/pdf/10.2514/6.2013-5344. URL: https://arc.aiaa.org/doi/abs/10.2514/6.2013-5344.

[98] Solargis. *Solargis – Solar Data and PV Performance*. Accessed: 2025-03-30. 2024. URL: https://solargis.com.

[99] *Space Based Solar Power De-risking the pathway to Net Zero*. Tech. rep. 004456-52265R Issue 1B. Frazer-Nash Consultancy Ltd., Sept. 2021, pp. 1–26.

[100] *Space Solar Power Info: Limitless clean energy from space*. URL: https://nss.org/space-solar-power-info/ (visited on 06/10/2024).

[101] *Space-based solar power: could beaming sunlight back to Earth meet our energy needs?* 2022. URL: https://physicsworld.com/a/space-based-solar-power-could-beaming-sunlight-back-to-earth-meet-our-energy-needs/ (visited on 06/12/2024).

[102] P.J. Staritz et al. “Skyworker: a robot for assembly, inspection and maintenance of large scale orbital facilities”. In: *Proceedings 2001 ICRA. IEEE International Conference on Robotics and Automation (Cat. No.01CH37164)*. Vol. 4. 2001, 4180–4185 vol.4. DOI: 10.1109/ROBOT.2001.933271.

[103] *Statistical Review of World Energy*. Energy Institute - with major processing by Our World in Data. 2023. URL: https://ourworldindata.org/grapher/years-of-fossil-fuel-reserves-left.

[104] Bernd Strassner and Kai Chang. “Microwave Power Transmission: Historical Milestones and System Components”. In: *Proceedings of the IEEE* 101 (June 2013), pp. 1379–1396. DOI: 10.1109/JPROC.2013.2246132.

[105] *Study on Cost-Benefit Analysis of Space-Based Solar Power (SBSP) Generation for Terrestrial Energy Needs*. Final Report 014843-101 53886R Issue: 1.0. Frazer-Nash Consultancy Ltd., LE London Economics, July 2022.

[106] Leopold Summerer and Oisin Purcell. “Concepts for wireless energy transmission via laser”. In: Jan. 2009.

[107] *System Breakdown, Costs and Technical Feasibility*. Technical Note FNC 014843-100 53334R Issue: 1.3. Frazer-Nash Consultancy Ltd., LE London Economics, Aug. 2022.

[108] *System Breakdown, Costs and Technical Feasibility of a SPS*. Technical Note. Roland Berger, OHB System, July 2022.

[109] Hideya Takahashi et al. “Wireless laser power transmission: Recent progress and future challenges”. In: *Optical Engineering* 62.2 (2023), p. 022207. DOI: 10.1117/1.OE.62.2.022207.

[110] Kürşat Tekbıyık et al. *Wireless Power Transmission on Martian Surface for Zero-Energy Devices*. 2021. DOI: 10.48550/ARXIV.2112.02154. URL: https://arxiv.org/abs/2112.02154.

[111] Brian Tierney et al. “Scalable, High-Sensitivity X-Band Rectenna Array for the Demonstration of Space-to-Earth Power Beaming”. In: *IEEE Access* PP (Feb. 2021), pp. 1–1. DOI: 10.1109/ACCESS.2021.3057020.

[112] Diego Urbina et al. “Skybeam: In-Orbit Assembly for Space-Based Solar Power with European technologies”. In: Oct. 2023.

[113] Christopher Valenta and Gregory Durgin. “Harvesting Wireless Power: Survey of Energy-Harvester Conversion Efficiency in Far-Field, Wireless Power Transfer Systems”. In: *Microwave Magazine, IEEE* 15 (June 2014), pp. 108–120. DOI: 10.1109/MMM.2014.2309499.

[114] Rosaria Verduci et al. “Solar Energy in Space Applications: Review and Technology Perspectives”. In: *Advanced Energy Materials* 12 (June 2022). DOI: 10.1002/aenm.202200125.

[115] Emily C. Warmann et al. “An ultralight concentrator photovoltaic system for space solar power harvesting”. In: *Acta Astronautica* 170 (2020), pp. 443–451. ISSN: 0094-5765. DOI: https://doi.org/10.1016/j.actaastro.2019.12.032. URL: https://www.sciencedirect.com/science/article/pii/S0094576519314651.

[116] *What’s EROSS*. URL: https://eross-h2020.eu/eross/ (visited on 06/25/2024).

[117] Wikipedia. *Solar Irradiance*. URL: https://en.wikipedia.org/wiki/Solar_irradiance.

[118] Jascha Wilken, Martin Sippel, and Michael Berger. “Critical Analysis of SpaceX’s Next Generation Space Transportation System: Starship and Super Heavy”. In: *2nd International Conference on High-Speed Vehicle Science Technology (HiSST)*. Sept. 2022. URL: https://elib.dlr.de/188531/.

[119] James R. Woodyard and Geoffrey A. Landis. “Radiation resistance of thin-film solar cells for space photovoltaic power”. In: *Solar Cells* 31.4 (1991). Special Issue: Radiation Effects on Solar Cells, pp. 297–329. ISSN: 0379-6787. DOI: https://doi.org/10.1016/0379-6787(91)90103-V. URL: https://www.sciencedirect.com/science/article/pii/037967879190103V.

[120] World Bank Group and ESMAP. *Global Solar Atlas*. Accessed: 2025-03-30. 2024. URL: https://globalsolaratlas.info.

[121] *world Economic Forum*. URL: https://www.weforum.org/.

[122] Masafumi Yamaguchi et al. “Multi-junction solar cells paving the way for super high-efficiency”. In: *Journal of Applied Physics* 129.24 (June 2021), p. 240901. ISSN: 0021-8979. DOI: 10.1063/5.0048653. eprint: https://pubs.aip.org/aip/jap/article-pdf/doi/10.1063/5.0048653/20022196/240901_1_5.0048653.pdf. URL: https://doi.org/10.1063/5.0048653.

[123] Wenbo Yang and Shaoyuan Li. “A station-keeping control method for GEO spacecraft based on autonomous control architecture”. In: *Aerospace Science and Technology* 45 (2015), pp. 462–475. ISSN: 1270-9638. DOI: https://doi.org/10.1016/j.ast.2015.06.020. URL: https://www.sciencedirect.com/science/article/pii/S1270963815001972.

[124] Tao Zhang et al. “Review on space energy”. In: *Applied Energy* 292 (2021), p. 116896. ISSN: 0306-2619. DOI: https://doi.org/10.1016/j.apenergy.2021.116896. URL: https://www.sciencedirect.com/science/article/pii/S0306261921003810.

[125] Yifan Zheng et al. “Wireless laser power transmission: Recent progress and future challenges”. In: *Space Solar Power and Wireless Transmission* 1.1 (2024), pp. 17–26. ISSN: 2950-1040. DOI: https://doi.org/10.1016/j.sspwt.2023.12.001. URL: https://www.sciencedirect.com/science/article/pii/S2950104023000020.

[126] Xirui Zhu et al. “Long-Range Wireless Microwave Power Transmission: A Review of Recent Progress”. In: *IEEE Journal of Emerging and Selected Topics in Power Electronics* PP (Nov. 2020), pp. 1–1. DOI: 10.1109/JESTPE.2020.3038166.